Saskatchewan
Agriculture
and Food

ADF

AGRICULTURE DEVELOPMENT FUND

FINAL REPORT

20020021

USE OF THE CANADIAN LIGHT SOURCE (SYNCHROTRON) TO UNDERSTAND AND IMPROVE THE NUTRITIVE VALUE OF HIGH FIBRE PLANT MATERIALS FOR LIVESTOCK

Funded by: The Agriculture Development Fund

January 2007

Prepared by: University of Saskatchewan

2007-04622/

Use of Canadian Light Source (National Synchrotron Facility) to Understand and Improve the Nutritive Value of High Fibre Plant Materials for Livestock

ADF Project # 20020021

Final Report

September, 2006

By

P.Yu*, H. C. Block*, D. A. Christensen*, and C. R. Christensen & J.J. McKinnon*[1]**

*Department of Animal & Poultry Science

University of Saskatchewan

&

**Canadian Light Source Inc. & Veterinary Biomedical Sciences, WCVM.

Saskatoon, Sk.

[1]Corresponding author

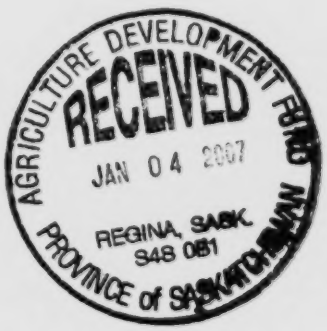

Table of Contents

Abstract 8

Executive Summary 8

Research Progress 12

Introduction 12

Overall Project Objectives 13

Completed Projects 14

Project 1: Use of Synchrotron Infrared Microspectroscopy (SR-FTIR) to Determine Chemical Differences in the Matrix of Micro-Endosperm Tissue of Two Barley (Harrington vs. Valier) Varieties in Relation to Rumen Degradation Characteristics 14

Project Summary 14

Project Details 15

Introduction 15

Objective 15

Materials and Methods 16

Harrington and Valier Barley 16

In situ Rumen Incubations 16

Chemical Analysis 16

The Synchrotron IR Slide Preparation 16

Photomicrograph of Cross-Section of Endosperm Tissue 17

Synchrotron Fourier Transform Infrared Microspectroscopy (SR-FTIR) 17

Experimental Design and Data Analysis 17

Statistical Analysis 17

Results and Discussion 18

In situ Rumen Degradation Characteristics 18

Photomicrograph of Barley Endosperm 18

The SR-FTIR Spectral Analysis 18

Conclusion 19

Literature Cited 20

Tables 22
Table 1 22
Figures 23
Figure 1 23
Figure 2 23
Figure 3 24
Figure 4 24
Figure 5 25
Figure 6 25
Project 2: Chemical Imaging of Micro-Structures of Plant Tissues within Cellular Dimension Using Synchrotron Infrared Microspectroscopy 26
Project Summary 26
Project Details 26
Introduction 26
Objective 27
Materials and Methods 27
Plant Tissue 27
SR-FTIR Microspectroscopic Window Preparation 28
Photomicrograph of Plant Tissue Cross-Sections 28
Synchrotron Light Source and SR-FTIR 28
Data Analysis and Chemical Imaging 28
Results and Discussion 29
Traditional Chemical Analysis vs. Advanced Analytical Technique (SR-FTIR) 29
Ultra-Spatially Resolved Chemical Mapping of Plant Tissue 30
Conclusion 32
Literature Cited 33
Figures 35
Figure 1. 35
Figure 2. 36
Figure 3. 37

Figure 4. 38

Project 3: Using Synchrotron-Based FTIR Microspectroscopy to Examine Protein Secondary Structure of Feather and Other Feed Protein Sources in Relation to Digestibility. 39

Project Summary 39

Project Details 40

Introduction 40

Objective 42

Materials and Methods 42

Feed Protein Sources - Feather, Wheat, Oat and Barley 42

Synchrotron IR Slide Preparation 42

Photomicrograph of Feather Tissue Cross-Sections 42

Synchrotron Light Source and FTIR Microspectroscopy 43

Chemical Imaging 43

Quantify the Percentage of α-helix and β-sheet in Feed Protein Secondary Structures 43

Result and Discussion 44

Feather Photomicrograph 44

Unique Secondary Structures of Feather Protein Indicated by Amide I Infrared Band, Compared with Other Feed Protein Sources 44

Ultra-Spatially Resolved Chemical Mapping of Protein Amide I β-Sheet to α-Helix Ratio 45

Modeling of Protein Amide I Peaks to Quantify the Percentage of Protein Secondary Structures (α-Helix, β-Sheet) 46

Conclusions 47

Literature Cited 48

Figures 50

Figure 1. 50

Figure 2(a). 51

Figure 2(b). 52

Figure 2(c).....53
Figure 3.....54
Figure 3. (Continued).....55
Project 4: Use of Synchrotron-Based FTIR Microspectroscopy to Determine the Effect of Heat Treatment on Protein Secondary Structures of Brown and Golden Flaxseeds at a Cellular Level in Relation to Nutritive Value of Protein.....56
Project Summary.....56
Project Details.....57
Introduction.....57
Objective.....59
Materials and Methods.....59
Flaxseeds and Heating Processing.....59
Synchrotron IR Slide Preparation.....59
Photomicrograph of Cross-Sections of Feather Tissues.....59
Synchrotron Light Source and FTIR Microspectroscopy.....60
Data Analysis and Chemical Images.....60
Quantifying the Proportion of α-Helix and β-Sheet in Feed Protein Secondary Structures.....61
Statistical Analysis.....61
Result and Discussion.....62
Photomicrograph of Flaxseed Tissues.....62
Ultra-Spatially Resolved Chemical Mapping of Protein and Protein to Starch Ratio in Flaxseeds.....62
Characteristics of Protein Secondary Structures of Flaxseed Tissue Indicated by Amide I.....63
Modeling of Protein Amide I Peaks to Quantify Percentage of Protein Secondary Structures (α-Helix, β-Sheet and the Ratio of α-Helix to β-Sheet).....64
Conclusions.....65
Literature Cited.....67

Tables 71
Table 1. 71
Table 2. 71
Figures 72
Figure 1. 72
Figure 2. 73
Figure 3. 74
Figure 4. 75
Figure 5. 76
Figure 6. 77
Figure 7. 78
Figure 8. 79
Project 5: Evaluation of the ability of SR-FTIR in reflectance mode to characterize lignin in brown midrib millet forage leaf and stem material. 80
Project Summary 80
Project Details 80
Introduction 80
Objective 81
Materials and Methods 81
Brown Midrib Millet 81
Synchrotron IR Slide Preparation 82
Photomicrographs 82
Synchrotron Light Source and FTIR Microspectroscopy 82
Chemical Imaging 82
Results and Discussion 83
Macroscopic and Photomicrograph Evaluation of Brown Midrib Millet 83
Mapping and Spot Spectra of Brown Midrib Millet Microstructures 83
Conclusions 84
Literature Cited 86
Figures 88
Figure 1. 88

Figure 2. 89
Figure 3. 90
Figure 4. 91
Figure 5. 92
Project 6: Evaluation of the ability of soft X-ray absorption near-edge spectroscopy (XANES) to evaluate zinc supplementation of cattle. 93
Project Summary 93
Project Details 93
Introduction 93
Objective 94
Materials and Methods 95
Zinc Samples 95
Ruminal, Duodenal, and Fecal Samples 95
Preparation of Zn 'Doped' Samples 95
Synchrotron Scanning 95
Results and Discussion 96
Conclusion 97
Literature Cited 98
Figures 99
Figure 1. 99
Figure 2. 100
Figure 3. 101
Research Publications and Seminars 102

Abstract

The objective was to evaluate synchrotron Fourier transform infrared microspectroscopy (SR-FTIR) and soft X-Ray absorption spectroscopy (XANES) as analytical tools for determining chemical information of plant tissues and relating this information to nutritional value. Results indicated that SR-FTIR can reveal the plant distribution of lignin, cellulose, protein, lipid, starch and total carbohydrate. Inherent differences in plant tissue (seed vs. forage stems and leaves) were found to influence the value of the technique. SR-FTIR can also be used to identify inherent differences in seed structure (i.e. protein:starch ratio of the endosperm) and protein secondary structure (alpha helix vs. beta sheet) that may influence rumen degradation rate. Preliminary work using XANES to identify zinc speciation state and to relate that information to digesta flow was not successful. Results indicate that SR-FTIR-based techniques have potential as analytical tools for determining nutritive value of plants.

Executive Summary

This final report provides information on the completed status of this project. Advance synchrotron radiation based analytical technique – synchrotron Fourier transform infrared microspectroscopy (SR-FTIR) is able to detect ultra-structural chemical information without destruction of the intrinsic plant structure. This technique has been used for medical science research, but not for plant feed research. Our objective was to develop this technique based on synchrotron light for animal feed research.

The first project was carried out at the Synchrotron Radiation Center, University of Wisconsin, Madison, WS, USA. In this project, we used synchrotron infrared microspectroscopy (SR-FTIR) to explore chemical differences in the matrix of micro-endosperm tissue between two types of barleys: Harrington (malting-type) vs. Valier (feed-type) in relation to rumen degradation characteristics. This was accomplished by comparing spot spectra of endosperm tissue between the two barleys. Rumen degradation characteristics of the two barleys were determined using the *in situ* nylon bag technique at University Research Farm, University of Saskatchewan. The spot spectral characteristic measurements were completed at the Synchrotron Radiation Center, Madison, Wisconsin. We then related *in situ* rumen nylon bag disappearance data to spectral data and found that the starch to protein matrix of the micro-endosperm tissue differed between the two barley varieties and that these differences were

correlated with significant differences between the two varieties in rumen degradation behavior. This work has been accepted as a peer-reviewed paper by the Canadian Journal of Animal Science and the results presented in the Annual Conference of the Canadian Society of Animal Science.

A second project was carried out to use this non-invasive technique to chemically map the intrinsic structures of plant tissues at ultra-spatial resolution to reveal the structural chemistry of the plant. This study clearly showed that using the synchrotron-based technique (SR-FTIR) we were able to map individual parts of the plant structure in pixel sized increments (10 μm). This allowed us to virtually "see" plant tissue in a chemical sense on a cellular level. The results indicate that the distribution of key chemical components of the plant tissue such as lignin, cellulose, protein, lipid and total carbohydrate could be imaged and mapped across the seed. Nutrient content was found to vary markedly with location across the seed. Such information can be used to identify differences in the plant intrinsic structure in relation to digestion characteristics in animals and used as an aid in plant breeding programs. This work has been accepted as a peer-reviewed paper by Journal of Agriculture and Food Chemistry.

The third project examined the use of synchrotron-based techniques for determining the secondary protein structure of feed sources in relation to protein availability in the animal. The secondary protein structures are primarily α- helix and β-sheet. Proteins with greater the proportion of β-sheet have poorer digestibility. In this project we attempted to determine if synchrotron-based FTIR microspectroscopy could be used to determine the secondary protein structure of several feed sources. A poorly digested protein source, feathers, was compared to common cereal grains with relatively easily digested protein. The results showed that synchrotron-based FTIR microspectroscopy can be used to reveal the secondary protein structure of feeds. The secondary structure of feather protein differed from other feed protein sources in terms of the line shape and position of amide I in mid-IR within cellular dimensions. By using multi-component peak modeling, we were able to resolve the amide I component peaks - α- helix and β-sheet. The results indicated that on a relative basis, the secondary structure of feather protein contains higher proportion of β-sheet and lower proportion of α-helix compared to the grain protein sources. This may be part of the reason that feather protein has a poor nutritional value in comparison with other feed protein sources. The results demonstrate the potential of synchrotron-based infrared microspectroscopy to reveal feed protein secondary structure. The

technique may find use as a selection tool in plant breeding and selection programs as well as for determining the effects of feed processing on protein availability in livestock. Further study is needed to quantify the relationship between protein secondary structure and digestive behavior of various feeds.

The fourth study used synchrotron Fourier transform infrared microspectroscopy (S-FTIR) as a novel approach to reveal ultra-structural chemical features of protein secondary structures of flaxseed tissues affected by variety and heat processing and quantify protein secondary structures using Gaussian and Lorentzian methods of multi-component peak modeling. By using multi-component peak modeling at protein amide I region of 1700-1620 cm^{-1}, the results showed that the golden flaxseed contained relatively higher percentage of α-helix (47.1 vs. 36.9%), lower percentage of β-sheet (37.2 vs. 46.3%) and higher ($P < 0.05$) ratio of α-helix to β-sheet than the brown flaxseed (1.3 vs. 0.8). The roasting reduced ($P < 0.05$) percentage of a-helix (from 47.1 to 36.1%), increased percentage of β-sheet (from 37.2 to 49.8%) and reduced α-helix to β-sheet ratio (1.3 to 0.7) of the golden flaxseed tissues. However the roasting did not affect percentage and ratio of α-helix and β-sheet in the brown flaxseed tissue. No significant differences were found in quantification of protein secondary structures between Gaussian and Lorentzian methods. These results demonstrate the potential of highly spatially resolved S-FTIR to localize relatively pure protein in the tissue and reveal protein secondary structures at a cellular level and indicated relative differences in protein secondary structures between flaxseed varieties and differences in sensitivities of protein secondary structure to the heat processing. Further study is needed to understand the relationship between protein secondary structure and protein digestion and utilization of flaxseed and to investigate whether the changes in the relative amounts of protein secondary structures are primarily responsible for differences in protein availability.

The fifth study involved an evaluation of the adaptability of SR-FTIR to characterization of forages using sections of leaf and stem material from brown midrib millet forage samples. Spectra obtained from both leaf and stem tissues using mapping and spot sampling methods with sampling focused on the vascular tissues. Lignin was identified using the spectra peak at 1510 cm^{-1}, which is characteristic of C-C stretching in the aromatic ring of phenolic compounds. However, this peak did not allow the different forms of lignin to be distinguished (polymers vs. monomers and different forms of monomers). Other peaks characteristic of the different forms of

pure lignin overlapped and were masked by other chemical species in these biological samples. The large voids in the non-vascular regions of the brown midrib millet stem and leaf tissues made obtaining quality spectra problematic and the lack of other millet varieties for scanning in this incidence prevented variety comparisons. In conclusion, lignin was detectable but not readily characterized (in terms of form or species) when at low concentrations in heterogeneous tissues, and the porosity (i.e. numerous holes) of forage tissues causes SR-FTIR microspectroscopy of forage tissue to be problematic.

The sixth and last project involved evaluation of common forms of Zn supplements (ZnO, $ZnSO_4 \cdot H_2O$, and Zn methoinine) used in cattle diets. Samples were evaluated in 'pure' form, or after mixing with dried and ground ruminal, duodenal, and fecal materials using the SGM soft X-ray beam line at CLS. Distinct spectra that could be used as 'fingerprints' were generated for the 'pure' feed grade samples showing some promise for use of X-ray absorption near-edge spectroscopy (XANES) in evaluation of trace mineral supplements for cattle. However, when lower concentrations of Zn supplements were evaluated the distinct spectral features were greatly diminished and masked by signal noise. Several different approaches were attempted in effort to improve spectral clarity were unsuccessful, and Zn speciation could not be identified against the largely carbohydrate background of ruminal, duodenal, or fecal material at concentrations as low as what would be expected *in vivo*. Based on the current results of this evaluation, we can not recommend use of XANES for characterization of Zn speciation from *in vivo* samples. However, recent improvements in the detector sensitivity at the SGM end station at the CLS hold promise and we are awaiting an opportunity to determine if the improvement will allow characterization of Zn speciation at the low concentrations presented by *in vivo* samples.

Research Progress

Introduction

The construction of the Canadian Light Source (Synchrotron) provides a new and potentially dramatic technology to improve high fibre plant materials for use as livestock feeds. Our strategy was to examine the structure of available and unavailable plant cell wall components particularly those related to ruminant animals as guidance for both animal nutritionists and plant breeders in selecting improved varieties. The synchrotron in Saskatoon was not expected to be available for use until some time in 2004 (The CLS has issued a first call for proposals using the mid-IR beam line closing October 2, 2006) and arrangements were made for start-up projects using synchrotrons at other locations including NSLS at Brook Haven, NY, and SRC at Madison, WI. Preliminary discussions were held with staff of the Canadian Light Source on campus (Rob Slinger, Tim May, and Colleen Christensen) on the suitability of the synchrotron for examining molecular structure of plant cell walls from a nutritional perspective. It was their recommendation that the infrared beam line be used for this purpose. We also consulted with Dr. Ted Raab of the Carnegie Institute and Stanford University on the use of this technology for identification of lignin in particular separation of lignin features from that of protein and pectin. He indicated that this technology is a very good tool for the objectives of our study.

Note that synchrotron infrared technology is a much more powerful diagnostic tool than older near infrared technology. Nevertheless, a limited amount of initial research carried out initially using low resolution infrared spectrum analysis by Dr. Yu under his NSERC Post-Doctoral Scholarship, had shown both quantitative and qualitative differences between low and high lignin oat hulls. Using Fourier transform vibrational infrared spectroscopy, he was able to show differences in specific absorbance bands associated with compounds that interfere with animal digestion and utilization of plant material (i.e. phenolic compounds and lignin). This initial work lent support to the use of the more powerful synchrotron infrared technology as a tool for identifying those structural components of plant cell walls that interfere with animal utilization. The information from this project will allow animal nutritionists and plant geneticists to more fully understand and take steps to improve the nutritional quality of high fibre plant material for ruminants.

Overall Project Objectives

1. To develop methodology that allows synchrotron technology to be used on plant tissues that generates information of use to animal nutritionists and plant breeders.
2. To use new technology (infrared beam lines of the Brook Haven and/or the Stanford and the University of Saskatchewan Synchrotrons) to determine the molecular structure of complex cell walls both prior to and after fermentation in the rumen and the effects of physical and chemical processing on these structures and their availability.
3. To collaborate with plant geneticists in selecting plant material that has a wide range in cell wall structure to determine the molecular nature of available and unavailable cell wall material.
4. To determine the degradation kinetics of specific compounds in complex cell walls that are identified using the synchrotron technology. In the initial phase of this work, forage and plant material that is already being used in research projects will be examined using this new technology. This application of the synchrotron will be a first for feed evaluation.

Completed Projects

Project 1: Use of Synchrotron Infrared Microspectroscopy (SR-FTIR) to Determine Chemical Differences in the Matrix of Micro-Endosperm Tissue of Two Barley (Harrington vs. Valier) Varieties in Relation to Rumen Degradation Characteristics

Details of this project were reported in our first interim report (June 2003). Those details are again reported below, following a summary of this project that was extracted from a peer-reviewed article published in the Canadian Journal of Animal Science (Yu et al., 2004).

Project Summary

Valier (feed-type) and Harrington (malting-type) barley differ in rumen degradation characteristics. Harrington, a typical malting variety, exhibits a high rate and extent of rumen degradation which can lead to metabolic problems such as acidosis and bloat in ruminants. Traditional "wet" chemical analysis cannot detect biological differences between barley varieties due to destruction of endosperm structure during processing. Synchrotron Fourier transform infrared microspectroscopy (SR-FTIR) is capable of exploring the chemical makeup of intact plant tissue with high signal to noise ratio at spatial resolutions as fine as 3-10 μm. The objective of this study was to use SR-FTIR microspectroscopy to explore and identify chemical differences in the ultra-structural matrix of the endosperm tissue of the two barley varieties as related to differences in rumen degradation characteristics. The results showed that the infrared absorbance intensity (Log 1/R) of the starch and protein varied considerably between the two varieties, but were not statistically significant. Harrington had a wider range of starch to protein IR absorbance intensity ratio (1.406 to 10.119 vs. 1.419 to 4.274), suggesting that it is more heterogeneous than Valier in endosperm chemical makeup. Valier had a lower ratio of starch to protein IR absorbance intensity than Harrington ($P<0.05$), which implies that the starch granules in Valier are more closely associated with the protein matrix. This closer association may prevent the starch granules from being rapidly degraded in the rumen. This work shows that the chemical makeup of intact plant tissues can be carried out by SR-FTIR microspectroscopy at ultra-spatial resolution (10×10 μm).

Project Details

Introduction

Harrington is a malting-type barley with a high rate and extent of rumen fermentation (Yu et al., 2003). It also releases sugar very fast during fermentation and is therefore suitable for beer making (AMBAINC, 2001). A significant consequence of rapid fermentation is that if ruminants consume this highly fermentable barley they are prone to digestive disorders which can result in reduced animal performance such as bloat and acidosis (Nocek and Tamminga 1991; Givens et al. 1993). Valier is a newly developed feed-type barley (Gibson et al. 1994; Bowman et al. 1996) with a lower rate and extent of rumen degradation (Yu et al., 2003) which is beneficial for utilization and animal health.

Traditional "wet" chemical analysis cannot detect the biological differences that exist between the two barleys. This is because the intrinsic structures and structural chemical characteristics of barley (Figure 1) are destroyed during the processing required for analysis. As such, we do not know how chemical make-up is related to digestive behavior in animals. Recently, an advanced synchrotron based analytical technique –synchrotron Fourier transform infrared microspectroscopy (SR-FTIR) has been developed. This technique has been used for medical science research. It is capable of exploring the molecular chemistry within microstructures with high signal to noise ratio at high spatial resolutions as fine as 3-10 μm (Miller et al. 1998; Holman et al., 2002). It can be used to determine ultra structural chemistry information without destruction of the intrinsic microstructures of the plant or seed.

The hypothesis that we wanted to test in this work was that the different rumen degradation characteristics between the two barleys were due to differences in the chemical matrix of the micro-endosperm tissue of the two barley varieties.

Objective

The objective of this study was to use the non-invasive and non-destructive SR-FTIR microspectroscopy to identify structural chemical differences in the matrix of micro-endosperm tissue of Harrington and Valier barley in order to obtain a better understanding of the known differences in rumen degradation behavior of these two barley varieties.

Materials and Methods

Harrington and Valier Barley

Valier (1999-MTLB-30) (a two-rowed, white kernelled, midseason spring barley) and Harrington barley (2000-BI-704) (a two-row, broad and diamond shaped kernel barley bred for malting characteristics with extremely rapid rate of fermentation) were grown in university research plots near Saskatoon (Canada) in 1999 and 2000, respectively. The barley samples were supplied by Brian Rossnagel, Crop Development Center (CDC), University of Saskatchewan (Saskatoon, SK, Canada).

In situ Rumen Incubations

Ruminal degradation characteristics for each barley variety were determined using the *in situ* method in two Hereford steers. Incubation of all treatments in the rumen was with 7 g DM in coded nylon bags (5×7 cm) with a pore size of approximately 50 μm. The rumen incubations were performed according to the 'gradual addition/all out' schedule. Samples were incubated in the rumen for 0, 2, 4, 8, 12, and 24 h. The total number of bags for each treatment was 12. After incubation, the bags were removed from rumen and rinsed under a cold stream of tap water. The bags were washed with cool water without detergent and subsequently dried at 55°C for 48 h. Dry samples were stored in a refrigerated room (4°C) until analyzed. The residues were pooled according to barley variety, incubation time and steer for chemical analysis.

Chemical Analysis

The dry matter (DM, AOAC official method 930.15) and crude protein (CP, AOAC official method 984.13) content of the barley grains were analyzed according to the procedure of AOAC (1990). The starch was analyzed using the Megazyme Total Starch Assay Kit.

The Synchrotron IR Slide Preparation

The barley samples were frozen at -20 °C on the object disks in a cryostatic microtome and then were cut into thin cross sections (ca. 5 μm thick) using disposable razor blade microtome knives in the Western College of Veterinary Medicine (The University of Saskatchewan, Canada). The unstained cross-sections were dry mounted onto Low-e IR microscope slides (Kevley Technologies, Chesterland, OH) for SR-FTIR in reflectance mode.

Photomicrograph of Cross-Section of Endosperm Tissue

Photomicrographs (10×40 magnification) of cross-sections of endosperm tissue of the two barleys were taken by Olympus microscope (Olympus BH-2) with a digital camera from regular glass slides.

Synchrotron Fourier Transform Infrared Microspectroscopy (SR-FTIR)

The SR-FTIR was performed using a Nic-PlanTM IR microscope (Nicolet Instruments, Madison, WI) with a programmable mapping stage. The bench was configured with a synchrotron source beam line with energy level 800 MeV at Port 031, Synchrotron Radiation Centre (SRC), University of Wisconsin, Madison, USA. The SR-FTIR spectra were collected in the mid-infrared range of 4000-800 cm^{-1}. The aperture setting was 10 μm × 10 μm. Stage control and data collection and processing used OMNIC (Spectra-Tech) software.

Experimental Design and Data Analysis

Two SR-FTIR slides were prepared for each barley endosperm tissue and each SR-FTIR slide had five to eight cross-sections examined (Table 1). Three spots of micro-endosperm tissue (size: ca. 10×10 μm) in each cross-section were randomly chosen. The SR-FTIR spectral data of each spot were collected, corrected the background spectrum, displayed in the absorbance mode and analyzed using OMNIC software (Spectra-Tech). A baseline correction was applied to generate the final spectra.

The SR-FTIR absorbance intensities of starch and protein, which are indicated at 1025 cm^{-1} and 1650 cm^{-1} (amide I) in grain endosperm reported by Wetzel et al. (1998), were analyzed by the spectral peak heights after a baseline correction. The ratio of starch to protein SR-FTIR absorbance intensity was calculated as: Ratio = SR-FTIR absorbance intensity of starch / SR-FTIR absorbance intensity of protein.

Statistical Analysis

Data were analyzed with the T-test procedure of SAS (SAS Inst. Inc., Cary, NC) at a 95% confidence level.

Results and Discussion

In situ Rumen Degradation Characteristics

The effects of barley variety on rumen degradation characteristics of DM, CP and starch are illustrated in Figures 2 - 4. These results show that Harrington barley has higher ($P<0.05$) degradation rate (Figure 2), effective degradability (Figure 3) and effective degradable content (Figure 4) of DM, CP and starch. All the *in situ* rumen results show that Harrington and Valier barley are different in terms of rumen fermentation characteristics. However, traditional "wet" chemical analysis can not detect such biological differences in biodegradation behaviors, as mentioned previously. Traditional analytical chemistry usually looks for a specific known component through homogenization of the tissue and separation of the components of interest from the complex matrix. As a result, the information about the spatial origin and distribution of the component of interest is lost and the object of the analysis is destroyed (Budevska, 2002). For example, using traditional chemical analysis, the two barleys have similar starch content. However, using in situ animal trial, the starch degradation rates are very different: the effective starch degradability is also different between the two barleys.

Photomicrograph of Barley Endosperm

The photomicrograph of cross-sections of the endosperm tissue of Harrington and Valier barley are presented in Figure 5 and 6. Harrington barley appeared to have larger starch granules that are less dense, relative to Valier Barley. However, it is very hard to identify exact differences between the two varieties through visual examination. No structural chemical information of barley micro-endosperm tissue is obtained from this type of analysis.

The SR-FTIR Spectral Analysis

The study of the intrinsic microstructure of plant tissues at ultra-spatial resolution (3-10 μm) within tact tissue is rare. To our knowledge, at the time of this study only one publication from another research laboratory had been found using SR-FTIR for mapping plant tissues *in situ* (Wetzel et al. 1998). The effect of barley varieties on SR-FTIR absorbance intensity of protein and starch and the ratio of starch to protein SR-FTIR absorbance intensity of micro-endosperm tissue of barley seed are present in Table 1. The results show that some spots (each spot: ca. 10 μm × 10 μm) of micro-endosperm tissue had higher SR-FTIR absorbance intensity for protein

whereas others had higher SR-FTIR absorbance intensity for starch. This indicates chemical differences within different areas in micro-endosperm tissue (Table 1). Plant tissues are not like human and animal tissues which are homogeneous (Lisa Miller, Personal Communication). These results confirm this observation.

The ranges of SR-FTIR absorbance intensity of protein, starch and starch to protein ratio are also different between the two barleys. Harrington barley has ranges of 1.41 to 10.12 for the ratio of starch to protein IR absorbance intensity. Valier barley has ratio ranges of 1.42 to 4.27. This result suggests that Harrington barley is more heterogeneous than Valier barley in structural chemical makeup.

The ratio of starch to protein IR absorbance intensity is different ($P<0.05$) between the two varieties. Harrington barley was higher than Valier barley (4.12 vs. 2.78). This indicates that the starch and protein matrix of micro-endosperm tissues are different between the two barleys. Valier barley was lower in the ratio of starch to protein SR-FTIR absorbance intensity, which implicates that Valier barley starch granules are associated with greater amounts of protein. This is likely the explanation as to why the in situ rumen degradation rate of Valier barley is slower than that of Harrington barley. These results agree with those reported by McAllister et al. (1993), that the protein matrix seemed to be the major factor responsible for differences in ruminal digestion of cereal grains. Use of this information generated by synchrotron analysis can be of great significance to plant breeders who which to specifically select barley varieties for ruminant feed purposes.

Conclusion

The results show that the chemical makeup of intact micro-structural plant tissues can be determined at ultra-spatial resolution (10×10 μm) using SR-FTIR, and that SR-FTIR can identify differences in barley varieties that affect feeding value but are not identifiable through conventional 'wet' chemistry analysis.

Literature Cited

AMBAINC. 2001. Malting Barley Breeding Guidelines: Ideal malt criteria. Retrieved in June 2001 from http://www.ambainc.org/ ni/ 2001%20GUIDELINES.pdf.

AOAC. 1990. Official Methods of Analysis (15th Ed.). Association of Official Analytical Chemists, Arlington, VA.

Bowman, J. G. P, Blake, T. K., Surber, L. M. M., Habernicht, D. K., Daniels, T. K., and Daniels. J. T. 1996. Genetic factors controlling digestibility of barley for ruminants. Proceedings, Western Section, American Society of Animal Science. Retrieved in June 2001 from http://hordeum.oscs.montana.edu/cowdocs/cow596.htm.

Budevska, B. O. 2002. Vibrational Spectroscopy. pp 3720-3732.

Holman, Hoi-Ying N., Bjornstad, K. A., McNamara, M. P., Martin, M. C., McKinney, W. R., and Blakely, E. A. 2002. Synchrotron infrared spectromicroscopy as a novel bioanalytical microprobe for individual living cells: cytotoxicity considerations. J. Biomedical Optics. 7:1–10.

Gibson, L. A., Bowman, J. G. P., Oberthur, L. E., and Blake, T. K. 1994. Determination of genetic markers associated with ruminant digestion of barley. Proceedings, Western Section, American Society of Animal Science. Vol 45.

Givens, D. I., Clark, P., Jacklin, D., Moss, A. R., and Savery, C. R.. 1993. Nutritional aspect of cereal, cereal grain by-products and cereal straw for ruminants. HGCA Research Review. 24:1-180. Home-grown Cereal Authority, Hamlyn House, Highgate Hill, London, England.

McAllister, T. A., Phillippe, R. C., Rode, L. M., and Cheng, K. J. 1993. Effect of the protein matrix on the digestion of cereal grains by ruminal microorganisms. J. Anim. Sci. 71:205-212.

Miller, L. M., Carlson, C. S., Carr, G. L., and Chance, M. R. 1998. A method for examining the chemical basis for bone disease: synchrotron infrared microspectroscopy. Cell. Mol. Bio. 44:117-127.

Nocek, J. E., and Tamminga, S. 1991. Site of digestion of starch in the gastrointestinal tract of dairy cows and its effect on milk yield and composition. J. Dairy Sci. 74: 3598-3629.

Wetzel, D. L., Eilert, A. J., Pietrzak, L. N., Miller, S. S., and Sweat, J. A. 1998. Ultraspatially resolved synchrotron infrared microspectroscopy of plant tissue in situ. Cell. Mol. Bio.

44:145-167.

Yu, P., Meier, J. A., Christensen, D. A., Rossnagel, B., and McKinnon, J. J. 2003. Using the NRC model and the DVE/OEB system to evaluate nutritive values of Harrington and Valier barley for ruminants. Anim. Feed Sci. Technol. 107:45-60.

Tables

Table 1. The SR-FTIR absorbance intensity (Log 1/R; Mean ± SE[z]) of starch and protein of endosperm tissue of Harrington (malting-type) and Valier (feed-type) barley.

Barley variety	SR-FTIR Slide	Section	Starch	Protein	Ratio[y] starch/protein
Harrington	A	1	1.190 (±0.165)	0.278 (±0.082)	6.094 (±3.175)
		2	0.755 (±0.187)	0.411 (±0.077)	2.081 (±0.702)
		3	0.963 (±0.061)	0.389 (±0.132)	5.238 (±3.058)
		4	0.750 (±0.120)	0.474 (±0.247)	2.379 (±0.773)
		5	1.082 (±0.135)	0.371 (±0.032)	2.901 (±0.177)
		6	1.491 (±0.256)	0.165 (±0.021)	10.119 (±2.900)
		7	0.815 (±0.263)	0.423 (±0.084)	2.481 (±1.027)
		8	1.228 (±0.089)	0.469 (±0.070)	3.040 (±0.726)
Harrington	B	1	1.080 (±0.256)	0.409 (±0.107)	3.281 (±1.016)
		2	0.777 (±0.058)	0.496 (±0.046)	1.572 (±0.029)
		3	0.754 (±0.113)	0.612 (±0.126)	1.406 (±0.490)
		4	0.980 (±0.028)	0.489 (±0.233)	3.780 (±2.101)
		5	1.139 (±0.206)	0.226 (±0.088)	7.311 (±2.139)
Valier	A	1	0.970 (±0.118)	0.509 (±0.056)	2.065 (±0.528)
		2	0.804 (±0.118)	0.561 (±0.026)	1.419 (±0.149)
		3	1.093 (±0.085)	0.429 (±0.112)	2.896 (±0.671)
		4	1.089 (±0.154)	0.558 (±0.200)	3.717 (±2.477)
		5	1.138 (±0.157)	0.287 (±0.043)	4.274 (±1.037)
		7	0.917 (±0.145)	0.340 (±0.046)	2.894 (±0.741)
		8	0.450 (±0.062)	0.354 (±0.160)	1.692 (±0.555)
Valier	B	1	1.102 (±0.075)	0.462 (±0.090)	2.767 (±0.660)
		2	1.246 (±0.089)	0.437 (±0.070)	3.117 (±0.836)
		3	1.038 (±0.119)	0.460 (±0.122)	2.818 (±0.832)
		4	0.810 (±0.199)	0.475 (±0.056)	1.655 (±0.286)
		5	1.120 (±0.154)	0.301 (±0.095)	4.219 (±0.860)

[z]SE = standard error.

[y]Ratio starch/protein absorbance intensity is calculated for each section using individual starch and protein absorbance values from the three areas scanned in each section.

Figures

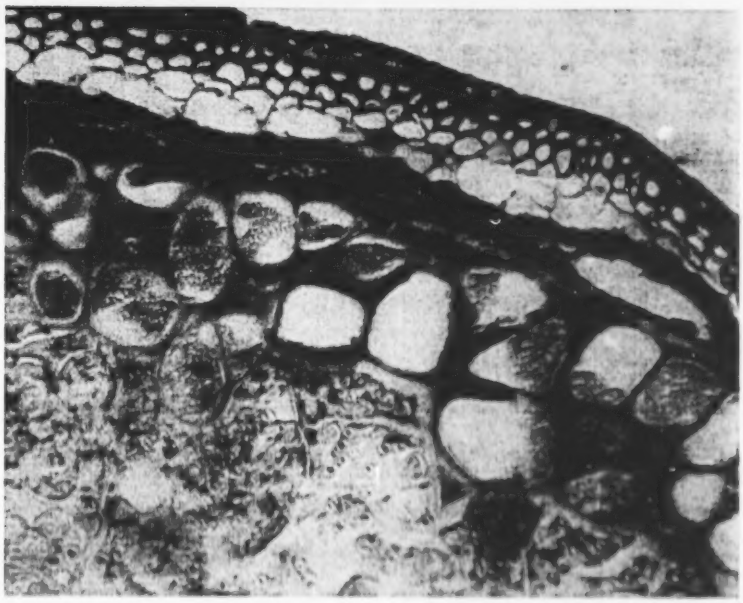

Figure 1. Photomicrograph of cross-section of barley (cv. Harrington) showing the intrinsic structure from the pericarp, seed coat, aleurone to endosperm (10×40 magnification, photo size 8.7 × 10.8 cm).

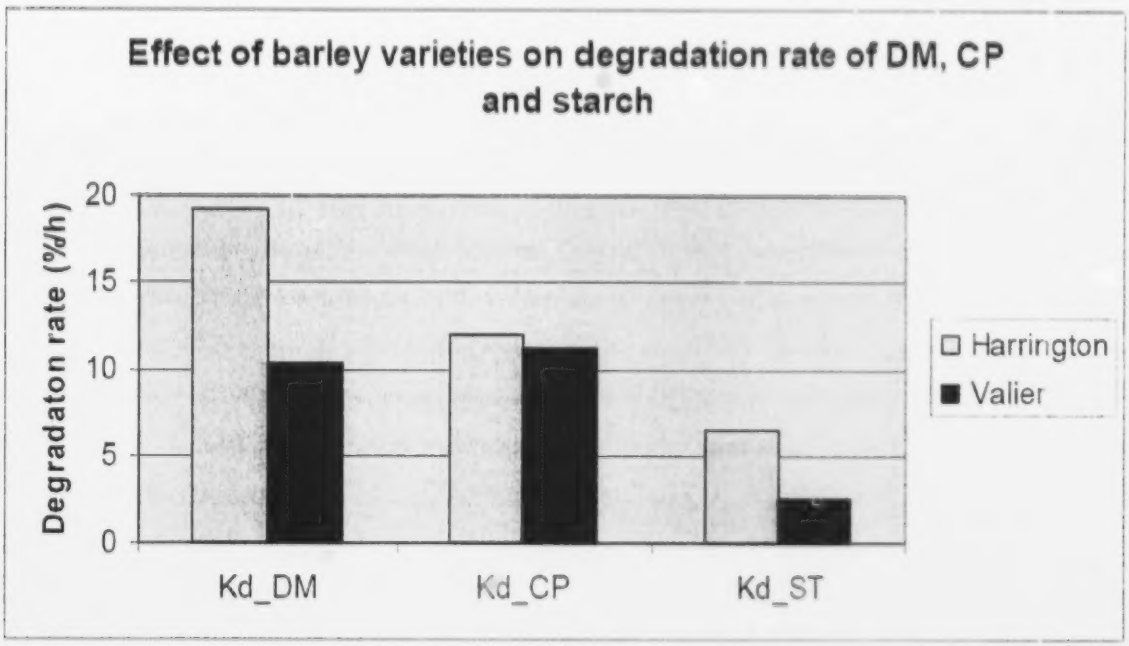

Figure 2. Comparison of the rate of degradation (Kd, %/h) of dry matter (DM), crude protein (CP) and starch (ST): Harrington vs. Valier barley.

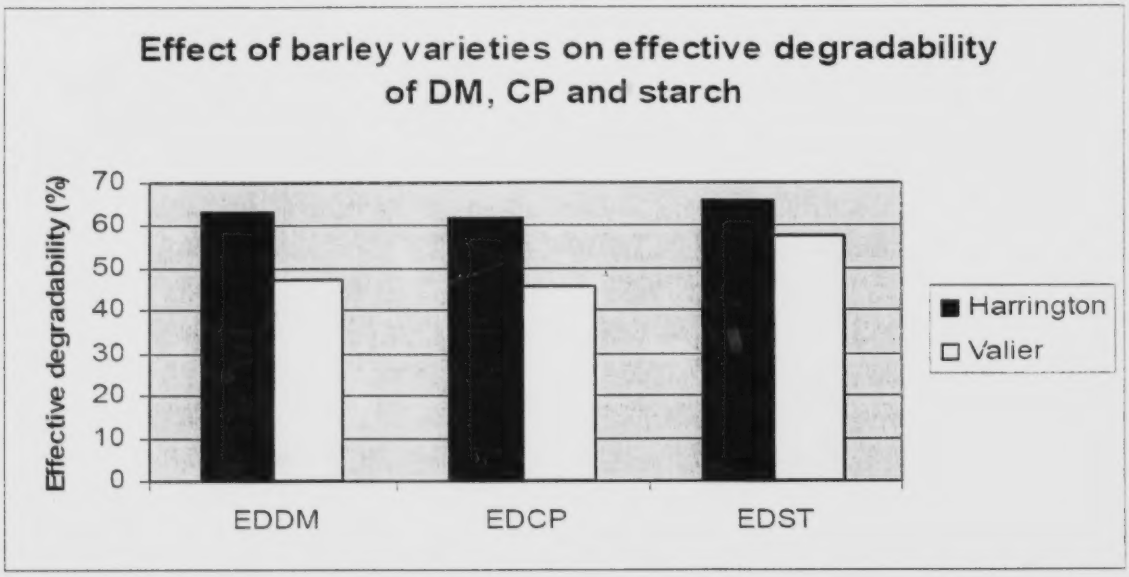

Figure 3. Comparison of the effective degradability of dry matter (EDDM, %), crude protein (EDCP, %) and starch (EDST, %): Harrington vs. Valier barley.

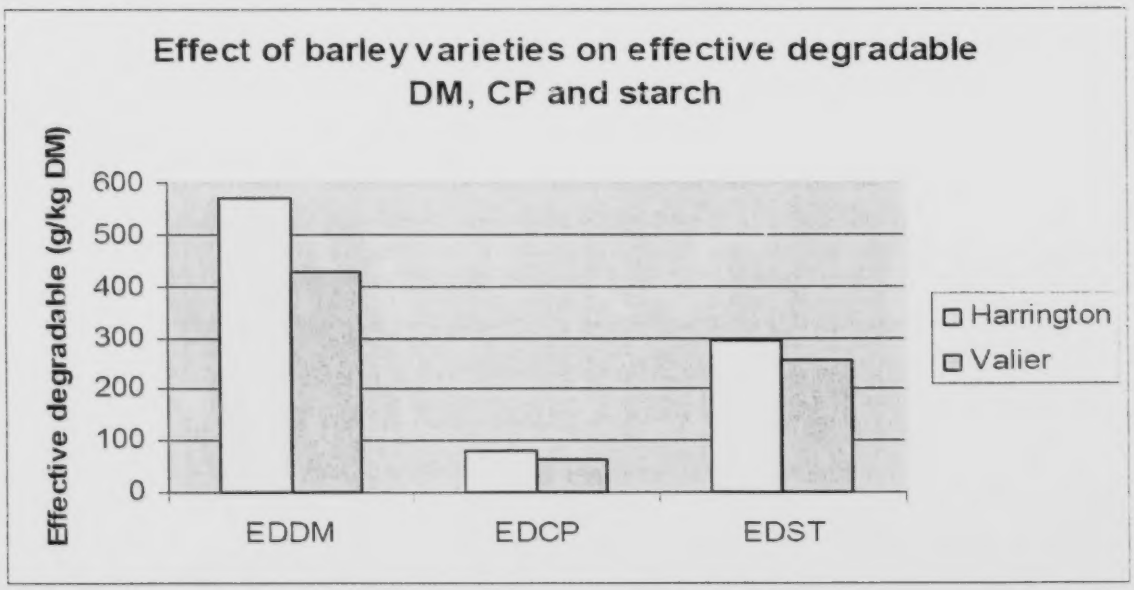

Figure 4. Comparison of the effective degradable content of dry matter (EDDM, g/kg DM), crude protein (EDCP, g/kg DM) and starch (EDST, g/kg DM): Harrington vs. Valier barley.

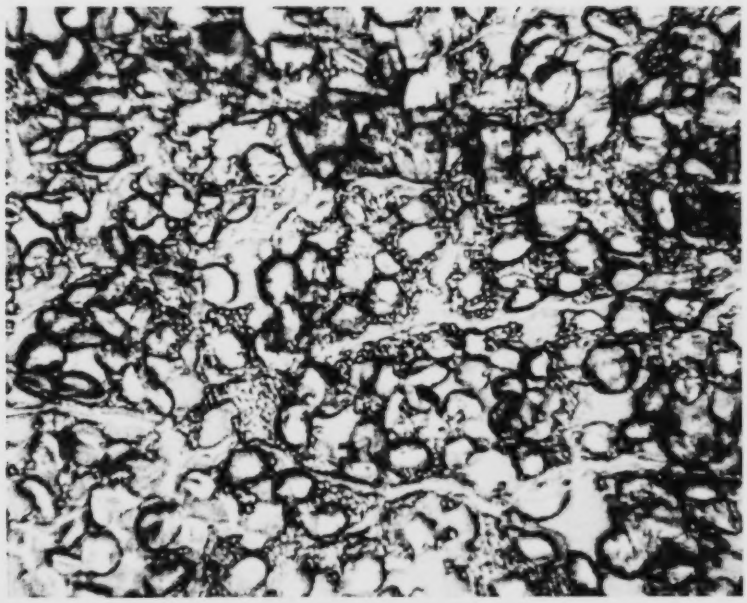

Figure 5. Photomicrograph of cross-section of the endosperm of malting type barley (cv. Harrington) by microscopy with digital camera (Olympus BH-2) (10×40 magnification, photo size 8.7 × 10.8 cm).

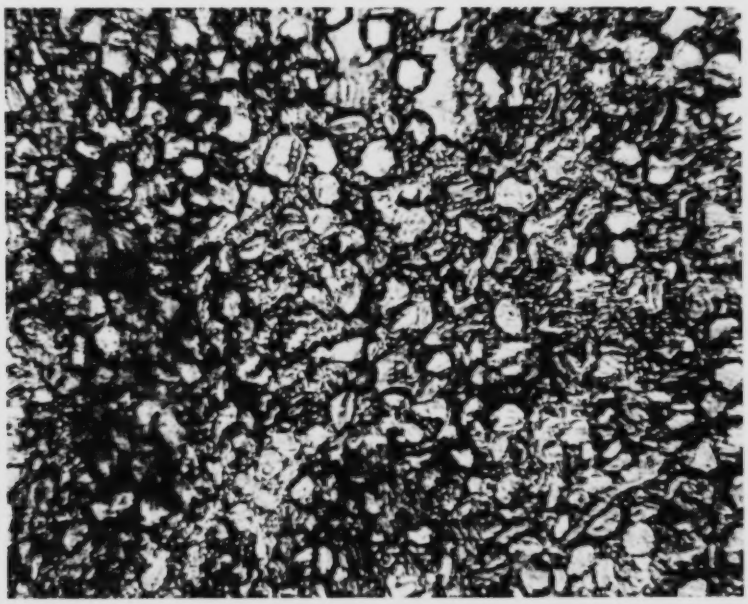

Figure 6. Photomicrograph of cross-section of the endosperm of feed-type barley (cv. Valier) by microscopy with digital camera (Olympus BH-2) (10×40 magnification, photo size 8.7 × 10.8 cm).

Project 2: Chemical Imaging of Micro-Structures of Plant Tissues within Cellular Dimension Using Synchrotron Infrared Microspectroscopy

Details of this project were reported in our second interim report (February 2004). Those details are again reported below, following a summary of this project which was extracted from a peer-reviewed article published in the Journal of Agriculture and Food and Food Chemistry (Yu et al., 2003b).

Project Summary

Synchrotron radiation based Fourier transform infrared microspectroscopy (SR-FTIR) is an advanced bioanalytical technique capable of exploring the chemistry within microstructures of plant and animal tissues with a high signal to noise ratio at high ultra-spatial resolutions (3-10 μm) without destruction of the intrinsic structures of a tissue. This technique is able to provide information relating to the quantity, composition, structure and distribution of chemical constituents and functional groups in a tissue. The objective of this study was to illustrate how SR-FTIR technique can be used to image inherent structures of plant tissues on a cellular level (pixel size: ~ 10×10 μm). The results showed that with the extremely bright synchrotron light, high-signal-to-noise-ratio spectrum were obtained from plant tissue areas as small as 10×10μm, which allowed us to "see" plant tissue in a chemical sense on a cellular level. The ultra-spatial resolved imaging of plant tissues by stepping in pixel sized increments was obtained. Chemical distributions of plant tissues such as lignin, cellulose, protein, lipid and total carbohydrate could be mapped. These images revealed the chemical information of plant intrinsic structure. In conclusion, SR-FTIR can provide chemical and functional characteristics of plant tissue at high ultra-spatial resolutions. The SR-FTIR microspectroscopic images can generate spatially localized chemical information and reveal chemistry information within cellular dimensions.

Project Details

Introduction

Traditional analytical chemistry usually looks for a specific known component through homogenization of the tissue and separation of the components of interest from the complex

matrix. As a result, the information about the spatial origin and distribution of the component of interest is lost and the object of the analysis is destroyed (Budevska, 2002).

Recently, an advanced bioanalytical technique - synchrotron radiation based Fourier transform infrared microspectroscopy (SR-FTIR) - has been emerging (Holman et al. 2002). This technique, taking advantages of synchrotron light brightness (which is usually 100-1000 times more than conventional globar source and has a small effective source size), is capable of exploring the molecular chemistry within microstructures with high signal to noise ratio at high spatial resolutions, as fine as 3-10 μm (Miller et al. 1998; Wetzel et al. 1998; Miller et al. 2000 and 2002; Marinkovic et al., 2002). This technique can encompass a wider spectral range so that more detailed structural information can be extracted. It can be used to detect information of ultrastructural chemistry by imaging or mapping without destruction of the intrinsic microstructures.

Microspectroscopic imaging by SR-FTIR can generate spatially localized chemical information without the need to homogenize the sample as is done with traditional analytical chemistry. It combines chemical and spatial information. The chemical information (qualitative and quantitative analytical results) can be linked to structural information. The technique can be used to increase the fundamental understanding of plant structures at the cellular level and bring a new level of understanding of analytical information (Budevska, 2002).

Objective

The objective of this study was to use this non-invasive bioanalytical technique - SR-FTIR technique to chemically image the intrinsic structures of plant tissues at ultra-spatial resolution to reveal the plant feed structural chemistry information. The ultimate objective is to use this information to relate plant intrinsic microstructure to rumen digestion characteristics in cattle and to provide information to plant breeders for use in selection programs targeted at improved feeds for cattle.

Materials and Methods

Plant Tissue

Harrington barley (2000-BI-704) (a two-row, broad and diamond shaped kernel barley bred for malting characteristics with extremely rapid rate of fermentation) was grown in a

University research plot near Saskatoon (Canada). The barley samples were supplied by B. Rossnagel, Crop Development Center (CDC), University of Saskatchewan (Saskatoon, SK, Canada).

SR-FTIR Microspectroscopic Window Preparation

The plant samples were frozen at -20 °C on the objective disks in a microtome (Tissue tech, NJ, USA) and were then cut into thin cross sections (ca. 6 μm thickness) using a microtome at Western College of Veterinary, University of Saskatchewan, Canada. The cross-sections of the plant tissues were rapidly transferred to BaF_2 windows (size: 13×1 mm disk; part number: 915-3015, Spectral Systems, NY, USA) for SR-FTIR microspectroscopic scanning in transmission mode. Several cross-sections were prepared on each BaF_2 window.

Photomicrograph of Plant Tissue Cross-Sections

Photomicrographs of cross-sections of the barley tissue (thickness: ca. 6-10 μm) were taken by a microscope with digital camera from regular glass slides.

Synchrotron Light Source and SR-FTIR

This experiment was performed at the National Synchrotron Light Source in Brookhaven National Laboratory (NSLS-BNL, New York, USA). The spectroscopic images were recorded using a Nicolet Magna 860 FTIR (Thermo Nicolet, USA) equipped with a Continuum IR microscope (Spectra Tech, USA), mapping stage controller, 32× objective and a mercury cadmium telluride (MCT-A) detector. The bench was configured with a synchrotron light beam line with an energy level 800 MeV (U10B, NSLS-BNL). The spectra were collected with an aperture setting of ca. 10×10 μm in the mid-infrared range of 4000-800 cm^{-1} and a resolution of 4 cm^{-1} with 64 scans co-added. A background spectroscopic image file was collected from an area free of sample. The mapping steps were equal to aperture size. Scanned visible images were obtained using a charge-coupled device (CCD) camera linked to the infrared images.

Data Analysis and Chemical Imaging

The spectral data of the plant tissues were collected, corrected for the background spectrum, displayed in the absorbance mode and analyzed using OMNIC software 6.0 (Spectra

Tech, USA). A baseline correction was applied to generate the final spectra. The SR-FTIR absorbance was expressed as Log (1/R). The data can be displayed as either as a series of spectroscopic images collected at individual wavelengths or as a collection of infrared spectra obtained at each pixel position in the image.

Chemical imaging of functional groups - protein indicated by amide I (1650 cm^{-1}), lipid indicated by carbonyl C=O ester linkage band (1738 cm^{-1}), total carbohydrates (1180 to 1000 cm^{-1}), lignin (1510 cm^{-1}), cellulosic materials (1246 cm^{-1}) (Wetzel et al., 1998) as well as chemical component ratio (such as protein:total carbohydrate; cellulose:total carbohydrate) in the intrinsic structures of the plant feeds were determined by the OMNIC software 6.0 (Spectra Tech, USA) (Himmelsbach et al., 1998; Wetzel et al., 1998; Miller, 2002).

Results and Discussion

Traditional Chemical Analysis vs. Advanced Analytical Technique (SR-FTIR)

At the time of this experiment, there had been little research conducted with ultra-spatially resolved chemical mapping or imaging of micro-structures of plant tissues using synchrotron based FTIR microspectroscopy with only one publication from another research laboratory (Wetzel et al., 1998) being found. Such information is important for a better understanding of plant tissue chemistry in relation to rumen digestion characteristics.

As mentioned previously, when using traditional "wet" chemical analysis, we are usually looking for a specific known component through homogenization of the plant tissue and separation of the components of interest from the complex matrix. Therefore chemical structures and molecular characteristics of the intrinsic structures of the plant are destroyed during such processing. This makes it impossible to relate digestive function in animals to plant structures. For example we found in our initial study reported above that using wet chemical analysis, Harrington barley had a starch content similar to Valier barley. However, an *in situ* rumen study showed that Harrington barley rumen degradation behavior that differs from Valier barley (Yu et al., 2003c). Predicted potential nutrient supply by NRC-2001 model and DVE/OEB model (Yu et al., 2003a) also differs between the two types of barley (Yu et al., 2003c). Why does traditional "wet" chemical analysis fail to detect such biological differences? This is because information on the spatial origin and distribution of the starch in the barley grains was lost during the processing for wet chemical analysis.

Ultra-Spatially Resolved Chemical Mapping of Plant Tissue

The chemical microstructure of barley seeds has been of interest in our laboratory (Yu et al., 2002 and 2004) in regard to utilization for ruminants. Of particular concern has been their characteristically rapid degradation (Yu et al., 2003c). Figure 1 illustrates the intrinsic structure of barley tissue (cv: Harrington; 6 μm-thickness cross-section) from the pericarp at the outside of the seed, to the seed coat, through to the aleurone layer and the endosperm. The pericarp forms the tough outer covering of the seed kernel and provides protection for the interior components. The seed coat is found between the pericarp and the aleurone layer. The aleurone cells play an important role during seedling development. The endosperm consists mainly of cells filled with starch granules.

Figure 2 represents color maps of functional groups of a cross-section of barley tissue through the pericarp, seed coat, aleurone and endosperm area and single pixel spectra measuring an area as small as 10×10 μm. It shows visible and chemical images in false-color representation of chemical component intensities and 3D images and spectra at various pixel locations. Using SR-FTIR, the distribution and relative concentration of the chemical components associated with the inherent plant structures were mapped.

Figure 2(a) shows the spatial lignin distribution and concentration of the area under peaks centered at 1510 cm^{-1}. This infrared image was taken from the region of the visible image outlined by the dotted area. The 1510 cm^{-1} band corresponds to the stretch associated with para-substituted benzene rings and can be associated with aromatic species present only in the pericarp of barley seeds.

Figure 2(b) shows the area under the 1650 cm^{-1} peak attributed to protein absorption (amide I). The amide I (1650 cm^{-1}) and amide II (1550 cm^{-1}) are characteristics of C=O and N-H bonds in the protein backbone and indicate areas of the sample where protein is present. Figure 2(b) shows that the pericarp region has no protein associated with it and protein concentration increases from the seed coat to the endosperm. The highest protein concentration is found in the subaleurone and endosperm layers.

The area under the peaks between 1180 and 1000 cm^{-1} is plotted in Figure 2(c). It represents total carbohydrate absorption. This includes starch absorption in the endosperm and the structural carbohydrates (cellulose and hemicellulose) (1246 cm^{-1}) in the pericarp and the

aleurone layers. The starch peak is centered at 1025 cm^{-1}. The 3D image in Figure 2(c) shows uneven distribution of total carbohydrate. Levels are high in the pericarp and aleurone and endosperm areas and very low in the seed coat.

The area under the peaks centered at 1246 cm^{-1} indicates cellulose (Wetzel et al., 1998) (Figure 2(d)). The concentrations were highest in the pericarp area and very low in the endosperm region (3D image).

Figure 2(e) shows the lipid distribution at 1738 cm^{-1}. The band at 1738 cm^{-1} is due to the carbonyl group (C=O) stretching vibration in the ester linkage in the pericarp and aleurone layer. The aleurone and endosperm areas contain little lipid.

The spectrum on the right in each figure corresponds to the pixel in the cross-hair and was selected to represent the value of the integrated peak. The represented spectra show a wide variety of spectral characteristics which manifest the chemical composition in different morphological parts of the seed.

Figure 3 presents spectra of the pericarp and aleurone layers, showing that similar morphological parts exhibit similar spectral characteristics and chemical composition. The pericarp region contains higher concentration of lignin (1510 cm^{-1}), cellulose (1246 cm^{-1}) and lipid (1738 cm^{-1}) materials and low concentration of protein (1650 cm^{-1} for amide I band and 1550 cm^{-1} for amide II band). Contrarily, the aleurone layer has practically no lignin and higher protein.

Figure 4 presents line mapping across the seed and again illustrates that similar morphological parts of the seed exhibit similar spectral characteristics. This indicates spatial chemical homogeneity in the seed and that those different morphological parts exhibit different spectral characteristics, which indicates spatial chemical heterogeneity in the seed.

The above work clearly shows that imaging chemical and functional group distribution across plant tissue at ultra-spatial resolution at a cellular level can be accomplished using the FTIR microspectroscopy powered by synchrotron light. Such information could be analyzed for clues of the plant intrinsic structures in relation to biodegradation characteristics in animals. For example, the previous studies in our laboratory (Yu et al., 2003c and 2004) showed that feed-type barley (cv. Valier) and malting-type barley (cv. Harrington) differ markedly in degradation behavior in ruminants. Harrington barley has a higher rate and extent of rumen degradation than Valier barley. A high rate of degradation may result in digestive disorders in ruminants when

feeding barley-based concentrate diets. Traditional "wet" chemical analysis methods cannot detect such biological differences. Using SR-FTIR, it was found that synchrotron infrared absorbance intensity of starch to protein ratio was different (4.12 vs. 2.78 for Harrington and Valier barley, respectively), indicating the chemical matrix of micro-endosperm tissue are different. Lower starch to protein ratio in the micro-endosperm tissue of Valier barley indicates that starch granules in Valier barley are more closely associated with protein, a fact that may prevent Valier barley from being rapidly degraded in the rumen.

Conclusion

This study clearly showed that using the synchrotron-based technique-SR-FTIR, we were able to map individual parts of the plant structure in pixel sized increments (10×10 μm). This allowed us to virtually "see" plant tissue in a chemical sense on a cellular level. The results showed that the distribution of key chemical components of the plant tissue such as lignin, cellulose, protein, lipid and total carbohydrate could be imaged and mapped across the seed. These images generated spatially localized chemical information and revealed chemical heterogeneity of the intrinsic plant structure. Such information can be analyzed for clues in the plant intrinsic structures that relate to digestion characteristics in animals and as an aid in plant breeding programs.

Literature Cited

Budevska, B. O. 2002. Vibrational Spectroscopy. pp 3720-3732.

Himmelsbach, D. S., Khalili, S., Akin, D. E. 1998. FT-IR microspectroscopic imaging of flax (linum usitatissimum L.) stems. Cell. Mol. Bio. 44:99-108.

Holman, H. Y. N., Bjornstad, K. A., McNamara, M. P., Martin, M. C., McKinney, W. R., and Blakely, E. A. 2002. Synchrotron infrared spectromicroscopy as a novel bioanalytical microprobe for individual living cells: cytotoxicity considerations. J. Biomedical Optics. 7:1–10.

Marinkovic, N. S., Huang, R., Bromberg, P., Sullivan, M., Toomey, J., Miller, L. M., Sperber, E., Moshe, S., Jones, K. W., Chouparova, E., Lappi, S., Franzen S., and Chance, M. R. 2002. Center for Synchrotron Biosciences' U2B beam line: an international resource for biological infrared spectroscopy. J. Synchrotron Rad. 9:189-197.

Miller, L. M. 2000. The impact of infrared synchrotron radiation on biology: past, present, and future. Synchrotron Radiation News. 13:31-37.

Miller, L. M. 2002. Infrared Microspectroscopy and Imaging. Retrieved in October 2002 from http://www.nsls.bnl.gov/newsroom/publications/otherpubs/imaging/workshopmillerhighres.pdf#search=%22infrared%20microspectroscopy%20and%20imaging%22

Miller, L. M., Carlson, C. S., Carr, G. L., and Chance, M. R. 1998. A method for examining the chemical basis for bone disease: synchrotron infrared microspectroscopy. Cell. Mol. Bio. 44:117-127.

Wetzel, D. L., Eilert, A. J., Pietrzak, L. N., Miller, S. S., and Sweat, J. A. 1998. Ultraspatially resolved synchrotron infrared microspectroscopy of plant tissue in situ. Cell. Mol. Bio. 44:145-167.

Yu, P., Christensen, D. A., and McKinnon, J. J. 2003a. Comparison of the National Research Council-2001 model with the Dutch system (DVE/OEB) in the prediction of nutrient supply to dairy cows from forages. J. Dairy Sci. 86:2178-2192.

Yu, P., Christensen, D. A., Christensen, C. R., Drew, M. D., Rossnagel, B. G., and McKinnon, J. J. 2004. Use of synchrotron Fourier transform infrared microspectroscopy to identify chemical differences in barley endosperm tissue in relation to rumen degradation characteristics. Can J. Anim. Sci. 84:523-527.

Yu, P. Q., McKinnon, J. J., Christensen, C. R., Christensen D. A., Marinkovic N. S., and Miller

L. M. 2003b. Chemical imaging of microstructures of plant tissues within cellular dimension using synchrotron infrared microspectroscopy. J. Agric. Food Chem. 51:6062-6067.

Yu, P., McKinnon, J. J., Christensen, C., Drew, M., and Christensen, D. A. 2002. Synchrotron Fourier Transform Infrared Microspectroscopy (S-FTIR) as a novel bioanalytical microprobe for ultrastructural matrix of barley endosperm tissue. Proc. the 5th CLS Users Meeting and Synchrotron Workshop - Applications of Synchrotron Radiation in the Biological/ Life Sciences. Canadian Light Sources, University of Saskatchewan, Saskatoon, Canada. November 15-16, 2002. pp. 39.

Yu, P., Meier, J. A., Christensen, D. A., Rossnagel, B., and McKinnon, J. J. 2003c. Using the NRC model and the DVE/OEB system to evaluate nutritive values of Harrington and Valier barley for ruminants. Anim. Feed Sci. Technol. 107:45-60.

Figures

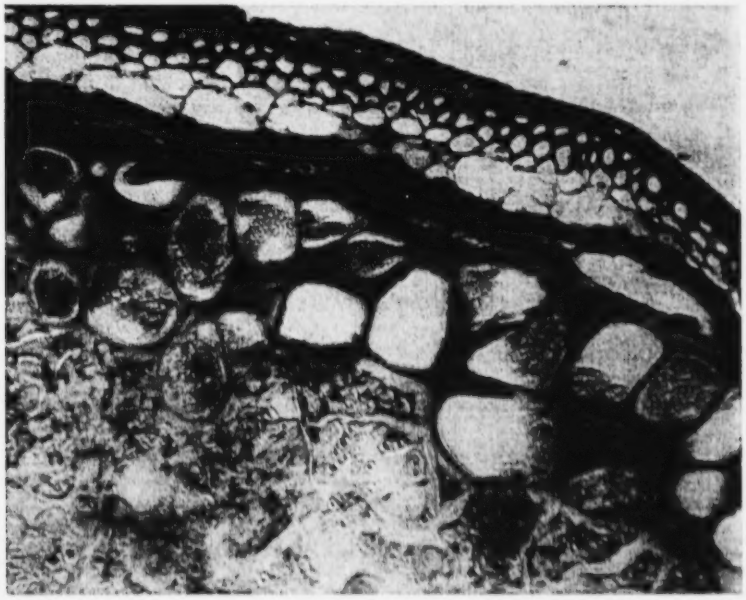

Figure 1. Photomicrograph of cross-section of barley (cv. Harrington) showing the intrinsic structure from the pericarp, seed coat, aleurone to endosperm (10×40 magnification, photo size 8.7 × 10.8 cm).

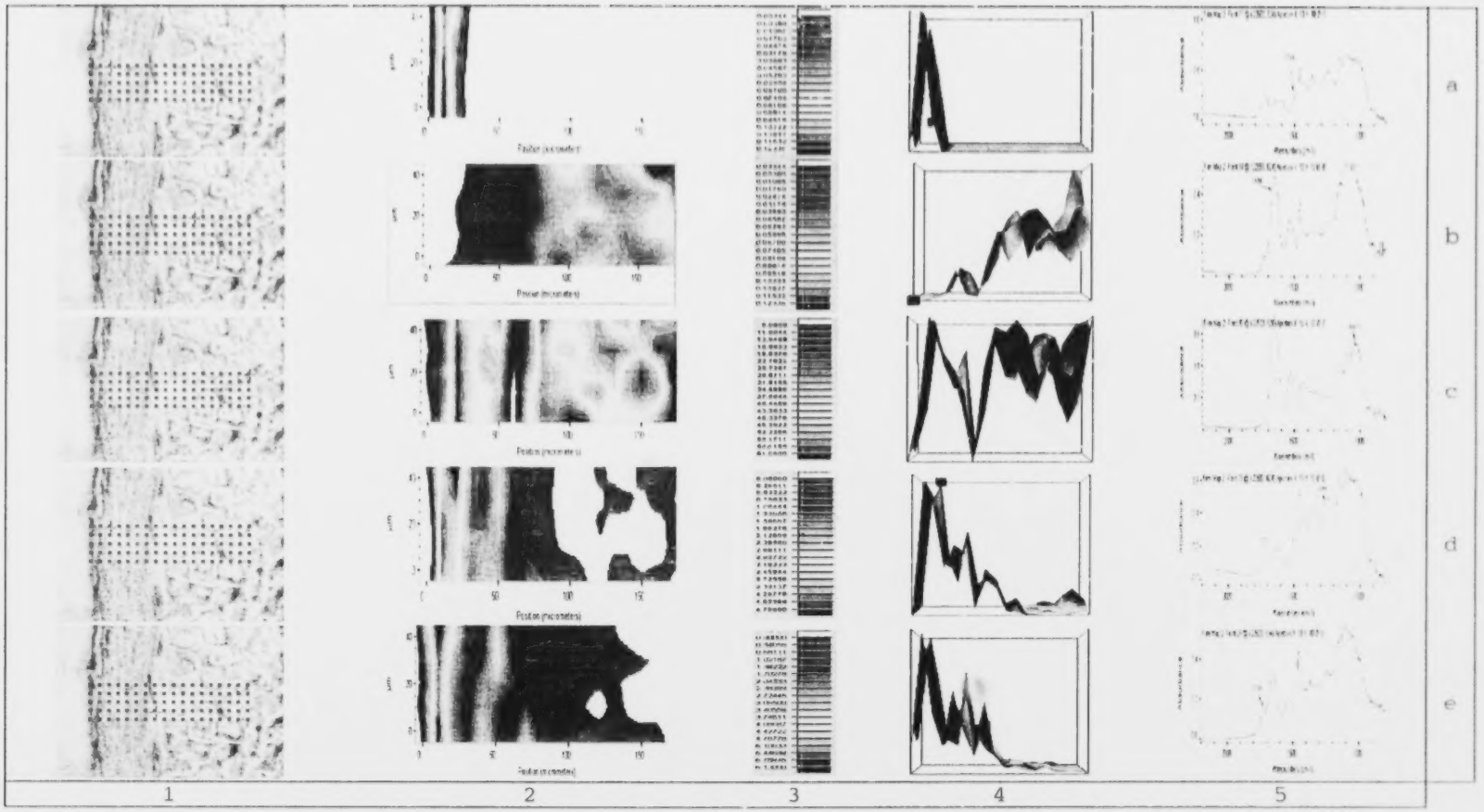

Figure 2. Functional group images of the barley tissue from the pericarp, seed coat, aleurone and endosperm (1. Visible image; 2 Chemical image; 3. Chemical intensity; 4. 3-D image; 5. Spectra corresponding to the pixel at the cross-hair in the visible image). (a) Area under peaks centered at 1510 cm^{-1} showing lignin concentration; (b) Area under 1650 cm^{-1} peak (amide I) showing protein distribution; (c) Area under the peaks between 1180 and 1000 cm^{-1} (carbohydrates); (d) Area under peaks at 1246 cm^{-1} indicating cellulosic material concentration; (e) Area under peaks at 1738 cm^{-1} (C=O ester linkage) showing lipid concentration.

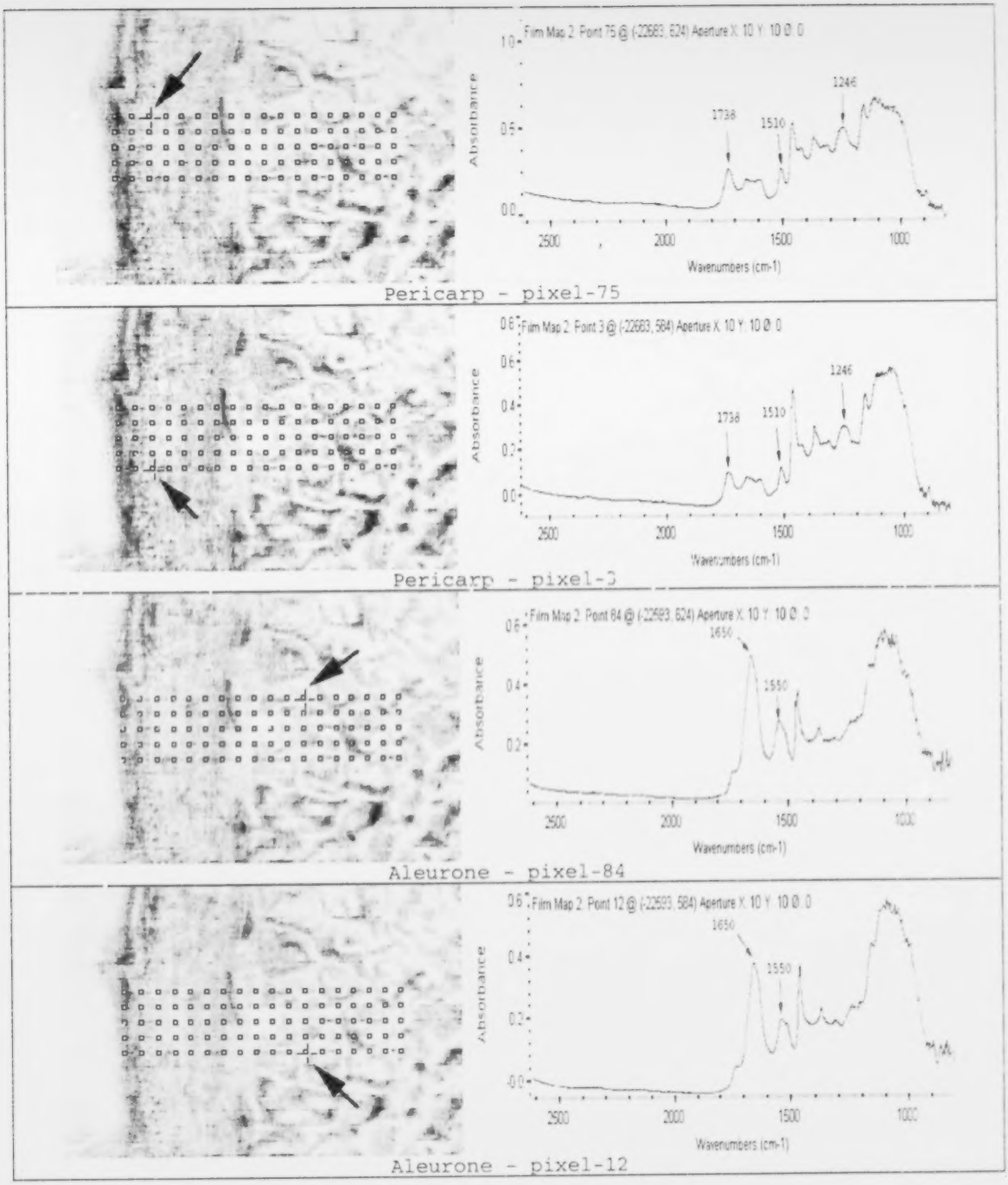

Figure 3. Spectra of pericarp and aleurone layer of barley seeds selected from corresponding area from the visible mages, showing that similar morphoiogical parts exhibit similar spectral characteristics and chemical composition.

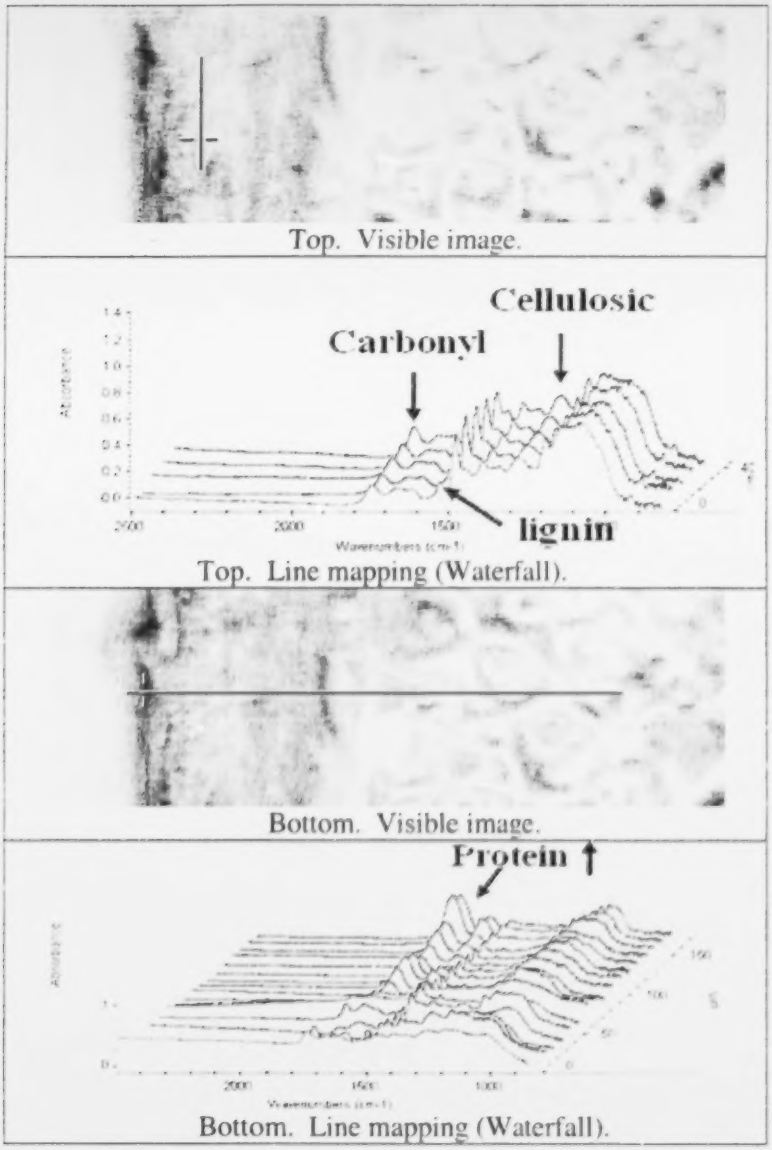

Figure 4. Line mapping illustrating that similar morphological parts of the seed have similar spectral characteristics indicating spatial chemical homogeneity (Top) and different morphological parts of the plant exhibit different spectral characteristics indicating spatial chemical heterogeneity of barley tissue (Bottom).

Project 3: Using Synchrotron-Based FTIR Microspectroscopy to Examine Protein Secondary Structure of Feather and Other Feed Protein Sources in Relation to Digestibility.

Details of this project were reported in our third interim report (February 2004). Those details are again reported below, following a summary of this project which was extracted from a peer-reviewed article published in the Journal of Agricultural and Food Chemistry (Yu et al. 2004a).

Project Summary

Studying the secondary structure of proteins leads to an understanding of the components that make up a whole protein. An understanding of the structure of the whole protein is often vital to understanding its digestive behavior in animals and nutritive quality. Usually protein secondary structures include α-helix and β-sheet. The percentage of these two structures in protein secondary structures may influence feed protein quality and digestive behavior. Feathers are widely available as a potential protein supplement. They are very high in protein (84%), but the digestibility of the protein is very low (5%). The objective of this study was to use synchrotron-based Fourier transform infrared (FTIR) microspectroscopy to reveal chemical features of feather protein secondary structure within amide I at ultra-spatial resolution (pixel size: 10×10 μm), in comparison with other protein sources from easily digestive feeds such as barley, oat and wheat tissue at endosperm regions (without destruction of their inherent structure). This experiment was performed at beamline U2B of the Albert Einstein Centre for Synchrotron Biosciences at the National Synchrotron Light Source (NSLS) in Brookhaven National Laboratory (BNL), US Dept of Energy (NSLS-BNL, NY). The results showed that ultra-spatially resolved chemical imaging of feed protein secondary structure in terms of β-sheet to α-helix peak height ratio in pixel sized increments was obtainable. Using synchrotron FTIR microspectroscopy can distinguish structures of protein amide I among the different feed protein sources. The results show that the secondary structure of feather protein differed from other feed protein sources in terms of the line-shape and position of amide I. The feather protein amide I peaked at ca. 1630 cm^{-1}. However, other feed protein sources showed a peak at ca. 1650 cm^{-1}. By using multi-component peak modeling, the relatively quantitative amount of α- helix and β

sheet in protein secondary structure was obtained, which showed that feather contains 88% β-sheet and 4% α- helix, barley contains 17% β-sheet and 71% α- helix, oat contains 2% β-sheet and 92% α- helix, and wheat contains 42% β-sheet and 50% α- helix. The difference in percentage of protein secondary structure may be part of reason that feed proteins differ in digestive behavior. Our results demonstrate the potential of highly spatially resolved infrared microspectroscopy to reveal feed protein secondary structure. Information from this study by the infrared probing of feed protein secondary structure may be valuable as a guide for feed breeders to improve and maintain protein quality for animal use.

Project Details

Introduction

The order of the amino acids in a chain is known as its primary structure. As the amino acid chain (polypeptide) is being synthesized, it is somewhat flexible. The polypeptide can bend and twist in several ways, but it stops short of being able to flop about freely. Most polypeptide chains fold up into a stable, three-dimensional molecule shortly after synthesis. Due to interactions between chemical groups on the amino acids, a few characteristic patterns occur frequently within folded proteins. These recurring shapes are called protein secondary structure, and they occur repeatedly because they are particularly stable. The most commonly occurring protein secondary structures include the α-helix and the β-sheet (Dyson and Wright 1990; Carey 1996).

Studying the secondary structure of proteins leads to an understanding of the components that make up a whole protein. An understanding of the structure of the whole protein is often vital to understanding its digestive behavior in animals and nutritive quality.

Feather is widely available as a potential protein supplement in animal feed industry. There are over 1 million tones of feathers produced each year in the U.S. alone and as the consumption of poultry meat increases so will the production of this valuable raw material. Feather does not suffer from the disadvantages of anti-nutritional factors, such as tannins, glucosinolates, lectins and trypsin inhibiting factors (Chandler 2003). Feather are very high in protein (84%), but the digestibility of the protein is very low (5%) (Chandler 2003). The high protein content of feather has made it of interest in nutritional studies.

The low digestibility of feather protein are related to several structural characteristics

such as high keratin content and the strong disulphide bonding of the amino acids and the relationship of β-sheet to solubility (Ward and Lundgren 1954; Fraser et al. 1972; Greg and Rogers 1986; Chandler 2003).

Traditional analytical chemistry usually looks for a specific known component such as protein through homogenization of the tissue and separation of the components of interest (protein) from the complex matrix. As a result, the information about the spatial origin and distribution of the component of interest (protein) is lost and the object of the analysis is destroyed (Budevska 2002). No structural-chemical information can be obtained from this analysis.

Recently synchrotron-based vibrational Fourier transform infrared (FTIR) microspectroscopy has been developed as a rapid, non-destructive, non-invasive and advanced analytical technique to reveal molecular micro-structural features within biological tissues and determine tissue localized chemical microstructure (Wetzel et al. 2003). This technique, taking advantages of synchrotron light brightness (which is usually 100-1000 times brighter than conventional globar source and has a small effective source size) is capable of exploring the molecular chemistry within microstructures of biological samples with high signal to noise ratios at ultra-spatial resolutions without destruction of the sample's structure (Wetzel et al. 1998; Miller 2000; Holman et al. 2000; Marinkovic et al. 2002; Miller 2002; Yu et al. 2003a and 2003b).

Using a standard globar sourced FTIR- microspectroscopy cannot reveal chemical feature of micro-biomaterials, which are < 35 to 100 μm (depend on the type of FTIR microspectrometer). Using synchrotron based FTIR microspectroscopy, allows plant structural chemical features to be revealed within cellular dimensions (< 30 μm) (Yu et al. 2004c). This technique is also able to chemically define the intrinsic structure and analyze individual parts with intact biological tissues. It is able to compare the tissue (species / varieties) according to spectroscopic characteristics / functional groups / spatial distribution / chemical intensity within cellular dimensions. It can also be related feed intrinsic structures to nutrient utilization, digestive behavior and bioavailability in animals (Yu et al. 2004b and 2004c). Therefore synchrotron FTIR microspectroscopic imaging can be used to generate spatially localized chemical information, which can be linked to structural information (Budevska 2002). Our published results (Yu et al. 2003b and 2004c) show that with synchrotron infrared

microspectroscopy, localization of protein in cereal grains was achievable from synchrotron FTIR microscopic mapping data and protein structural features could be detected from protein amide I bands (Wetzel et al. 2003).

Objective

The objectives of this study were to spatially resolve secondary structure of protein in different feed sources using synchrotron infrared microspectroscopy and to reveal chemical features of protein secondary structure in feather microstructure in comparison with other protein sources from relatively easily digestive feeds.

Materials and Methods

Feed Protein Sources - Feather, Wheat, Oat and Barley

Feather samples were obtained from the Poultry Centre of the Department of Animal and Poultry Science, University of Saskatchewan (Saskatoon, Canada). Wheat (cv. Superb-2001) was obtained from Seed Increase Unit, Agriculture and Agri-Food, Canada (Indian Head, SK, S0G 2K0) with samples arranged by Vern Racz (Director, Prairie Feed Source Center). Dolly barley was supplied by the Dairy Nutrition Laboratory (Dr. David Christensen), Department of Animal and Poultry Science, University of Saskatchewan. Oat (cv. Derby) was obtained from the Crop Development Centre, University of Saskatchewan.

Synchrotron IR Slide Preparation

The feather, wheat, oat and barley were cut into thin cross-sections (ca. 6 μm thick) using disposable razor blade microtome knives at the Western College of Veterinary Medicine, University of Saskatchewan. The unstained cross-sections were mounted onto Low-e IR microscope slides (Kevley Technologies, Chesterland, OH) for synchrotron FTIR microspectroscopy in reflectance mode. More detailed methodology on slide preparation was reported by Yu et al. (2003b, 2004b, and 2004c).

Photomicrograph of Feather Tissue Cross-Sections

Photomicrographs of cross-section of the feather tissues (thickness: 6 μm) were taken with a digital camera from the slides.

Synchrotron Light Source and FTIR Microspectroscopy

The experiment was carried out on U2B beamline at Albert Einstein Centre for Synchrotron Biosciences in the National Synchrotron Light Source (NSLS) at Brookhaven National Laboratory (BNL) in Upton, New York. The beamline was equipped with a FTIR spectrometer (Nicolet Magna 860) with KBr beamsplitter and liquid nitrogen cooled MCT detectors coupled with an IR microscope (Nic-PlanTM, Nicolet Instruments, Madison, WI) with Schwartzshild 32× objective and 10× condenser. Synchrotron radiation from the VUV storage ring at beamline U2B entered the interferometer via a port on the instrument designed for use with infrared emission. The IR spectra were collected in the mid-IR range 4000-800 cm^{-1} at a resolution of 4 cm^{-1} with 64 scans co-added. The aperture setting was 10 × 10 μm. Stage control, spectrum data collection and processing were performed using OMNIC 6.0 (Thermo-Nicolet, Madison, WI). Scanned visible images were obtained using a charge-coupled device (CCD) camera linked to the infrared images.

Chemical Imaging

The spectral data were collected, corrected the background spectrum, displayed in the absorbance mode and analyzed using OMNIC 6.0 (Spectra Tech, USA). The data were displayed as either as a series of spectroscopic images collected at individual wavelengths (1630 cm^{-1}), or as a collection of infrared spectra obtained at each pixel position in the image. Chemical imaging of β-sheet to α-helix height ratio in protein secondary structures indicated by the amide I bands (peak at ca. 1650 cm^{-1} for α-helix or 1630 cm^{-1} for β-sheet) (Wetzel et al. 2003; Miller 2002) in the intrinsic structures of the feed samples were determined by the OMNIC 6.0 software (Spectra Tech, USA) at the spectral region (1650-1550 cm^{-1}) of greatest interest. The chemical mapping of feather tissue and barley, oat and wheat endosperm at beamline U2B provided data from which to choose spectra for modeling amide I component peaks.

Quantify the Percentage of α-helix and β-sheet in Feed Protein Secondary Structures

With the protein amide I component bands being overlapped, a specific multi-peaks fitting or modeling procedure was required. To determine the relative amount of α-helix and β-

sheet protein secondary structure, two steps were applied. The first step was using the secondary derivative in OMNIC (Thermo Nicolet, USA) to identify protein amide I component peaks frequencies. The second step was using a multi-peaks fitting program with Lorentz function in Origin to quantify the multi-component peak areas in protein amide I bands. The relative amount of α-helix and β-sheet based on modeled peak area was calculated according the report generated by the software.

Result and Discussion

Feather Photomicrograph

The photomicrographs of cross-sections of the feather are presented in Figure 1. These photomicrographs only show the structural information, but do not show the structural-chemical information. It is evident from these figures that there is limited chemical information available from these cross-sections. They do not give information on localized structural-chemical information. Furthermore, with traditional "wet" analytical methods, it is not possible to determine chemical features of the inherent structures at ultra-spatial resolution (3-10 μm) (Wetzel et al. 1998; Budevska 2002). This is because traditional analytical chemistry for determination of feed structures relies heavily on the use of harsh chemicals and derivatization, therefore altering the native plant structures and possibility generating artifacts (Stewart et al. 1995). Using such methods, the chemist attempts to look for a specific component through homogenization of the tissue and separation of the component of interest from the complex matrix. As a result, the information about the spatial origin and distribution of the component of interest is lost (Budevska 2002).

Unique Secondary Structures of Feather Protein Indicated by Amide I Infrared Band, Compared with Other Feed Protein Sources

Typical, protein secondary structures include the α-helix and β-sheet (Dyson et al. 1990; Carey 1996). The protein IR spectrum has two primary features, the amide I (ca. 1600-1700 cm^{-1}) and amide II (ca. 1500-1560 cm^{-1}) bands, which arise from specific stretching and bending vibrations of the protein backbone. The amide I band arises predominantly from the C=O stretching vibration of the amide C=O group. The vibrational frequency of the amide I band is particularly sensitive to protein secondary structure (Miller 2000; Martin 2001; Marinkovic et al.

2002) and can be used to predict protein secondary structure. For α-helix, the amide I is typically in the range of 1648-1658 cm^{-1}. For β-sheet, the peak can be found within the range of 1620-1640 cm^{-1} (Martin 2001). The amide II (predominantly an N-H bending vibration coupled to C-N stretching) is also used to assess protein conformation. However, as it arises from complex vibrations involving multiple functional groups they are less useful for protein structure prediction than the amide I band (Jackson and Mantsch 2000).

Figure 2(a-d) illustrates unique line-shape and position of protein amide I in mid-IR from the different protein sources (feather protein vs. barley, oat, and wheat protein) at ultraspatial resolution. The results show that the intrinsic structures (pixel size 10 × 10 μm) of amide I from feather, barley, wheat and oat proteins were different. The feather protein amide I peaks at ca. 1630 cm^{-1}, but barley, wheat and oat protein sources show a peak at ca. 1650 cm^{-1}. These results indicated that feather contains a higher percentage of β-sheet but a lower percentage of α-helix in the protein secondary structures. However, barley, wheat and oat contain lower percentage of β-sheet but higher percentage of α-helix. This may explain the difference in protein value between the feed proteins with the poorer protein value of feather. In order to improve feather protein value, one possibility is to alter the ratio of β-sheet to α-helix in feather protein secondary structures by a processing or treatment to improve access of digestive enzymes to protein structures.

Ultra-Spatially Resolved Chemical Mapping of Protein Amide I β-Sheet to α-Helix Ratio

Biological component ratio images showing structural chemical features can be obtained by the height or area under one functional group band divided by the height or area under another functional group band at each pixel. Figure 3 represents color maps of protein amide I β-sheet to α-helix ratio in feather tissue and barley, oat, and wheat endosperm tissue and single pixel spectra measuring an area as small as 10×10 μm of the sample, which is within cellular dimension. It shows visible and chemical images in false-color representation of the chemical functional group-amide I intensities, and spectra at various pixel locations. Using synchrotron FTIR microspectroscopy, the distribution and relative concentration of the chemical components associated with the inherent ultra-structure were mapped. Figure 3 shows the area under the ca. 1630 cm^{-1} peak height to ca. 1650 cm^{-1} peak height ratio mapping attributed to β-sheet and α-helix absorption ratio (amide I).

The component ratio mapping has two advantages. The first one is that by using those ratios any spectral intensity variations due to tissue thickness changes are eliminated. The second one is that the ratio maps are able to indicate relative tissue component contents, which could be used to determine food or feed quality, characteristics and nutritive values and for use in plant breeding program. It can be used to compare different feed varieties according to the inherent structural spectral characteristics, chemical functional group intensity and distribution (e.g. seed coat features and pericarp features between different seed varieties). It can be used to chemically define the feed intrinsic structure and analyze individual feed structure with intact tissue (Yu et al. 2004c).

Our results demonstrate the potential of highly spatially resolved infrared microspectroscopy to reveal cereal grains and other feed protein secondary structure.

Modeling of Protein Amide I Peaks to Quantify the Percentage of Protein Secondary Structures (α-Helix, β-Sheet)

With the feed protein amide I component peaks overlapping each other, the secondary derivative was used to identify amide I component peaks frequencies and then multi-component peaks fitted with the Lorentz function was used to quantify the multi-component peak areas in the protein amide I region. Figure 4 shows that feather contained ca. 88% β-sheet and 4% α-helix, barley contained ca. 17% β-sheet and 71% α- helix, oat contained ca. 2% β-sheet and 92% α-helix, and wheat contained ca 42% β-sheet and 50% α-helix. The difference in percentage of protein secondary structure may be part of the reason feed proteins differ in digestive behavior. Wetzel et al. (2003) compared hard wheat cultivars (included red, white, winter and spring wheat grown at different locations) and soft wheat cultivars and found that hard wheat contained, roughly, 40 to 60% α- helix and 25 to 30% β-sheet and soft wheat contained around 40% α- helix and 40% β-sheet (obtained from their Figure). These results show hard wheat had greater relative amount of α- helix than that in soft wheat. Our results showed that the wheat (cv. Superb-2001) contained ca 42% β-sheet and 50% α- helix. The peak area ratios of α- helix to β-sheet for the hard wheat cultivars were 1.57 to 2.10, compared to the ratios from 0.96 to 1.07 for the soft wheat cultivars. Our results showed that the peak area ratios of α- helix to β-sheet for the wheat (cv. Superb-2001) was 1.18. However, no published results have been found for oat or barley. It is needed to mention that our results should be considered as typical and not average

for the individual seed as many factors will affect the quality of feeds, such as location, climate and growth conditions. Information from this study on the infrared probing of feed protein secondary structure may be valuable as a guide for feed breeders to improve and maintain protein quality for animal use. Our results demonstrate the potential of high spatial resolution by infrared microspectroscopy in revealing the protein secondary structure of cereal grains and other feeds.

Conclusions

In conclusion, with synchrotron based FTIR microspectroscopy, the ultrastructrual-chemical makeup characteristics can be revealed at a high ultra-spatial resolution. Synchrotron-based FTIR microspectroscopy revealed that the secondary structure of feather protein differed from other feed protein sources in terms of the line shape and position of amide I in mid IR within cellular dimension. By using multi-component peaks modeling, the relatively quantitative of protein amide I components peaks- α- helix and β-sheet could be resolved. The results indicated that the secondary structure of feather protein contains higher percentage of β-sheet and lower percentage of α-helix on the relative basis, compared to the grain protein sources. This may be part of the reason that causes feather poor protein value in comparison with other feed protein sources. Our results demonstrate the potential of high spatial resolution infrared microspectroscopy to reveal feed protein secondary structure. Further study is needed to quantify the relationship between protein secondary structure and digestive behavior of various varieties of grain feed protein sources such as barley, oats, and wheat.

Literature Cited

Budevska, B. O. 2002. Vibrational Spectroscopy. pp 3720-3732.

Carey, F. A. 1996. Organic Chemistry. 3rd Edition. McGraw-Hill Companies, Inc.

Chandler, N. J. 2003. Dairy Cattle – Feather meal: It´s nutritional value and use in dairy and beef rations. Retrieved in Nov 2003 from http://www.engormix.com/e_articles_dairy_cattle.asp?ID=79.

Dyson, H. J., and Wright, P. E. 1990. Peptide conformation and protein folding. Current Opinion in Structural Biology. 3:60-65.

Fraser, R. D. B., MaCrae, T. P., and Rogers, G. E. 1972. Keratins. Charles C Thomas, III. USA.

Greg, K., and Rogers. G. E. 1986. Feather keratin: Composition, structure and biogenesis. Biology of Integuments. Volume 2. Springer, Verlag.

Holman, H. Y. N., Bjornstad, K. A., McNamara, M. P., Martin, M. C., McKinney, W. R., and Blakely, E. A. 2002. Synchrotron infrared spectromicroscopy as a novel bioanalytical microprobe for individual living cells: cytotoxicity considerations. J. Biomedical Optics. 2002. 7, 1-10.

Jackson, M., and Mantsch, H.H. 2000. Infrared spectroscopy *ex vivo* tissue analysis. Biomedical Spectroscopy.

Marinkovic, N. S., Huang, R., Bromberg, P., Sullivan, M., Toomey, J., Miller, L.M., Sperber, E., Moshe, S., Jones, K.W., Chouparova, E., Lappi, S., Franzen S., and Chance, M.R. 2002. Center for Synchrotron Biosciences' U2B beamline: an international resource for biological infrared spectroscopy. J. Synchrotron Rad. 9:189-197.

Martin, M. C. 2001. Fourier-Tranform Infrared Spectroscopy. Retrieved in October 2002 from http://infrared.als.lbl.gov/

Miller, L. M. 2000. The impact of infrared synchrotron radiation on biology: past, present, and future. Synchrotron Radiation News. 13:31-37.

Miller, L. M. 2002. Infrared Microspectroscopy and Imaging. Retrieved in October 2002 from http://www.nsls.bnl.gov/newsroom/publications/otherpubs/imaging/workshopmillerhighres.pdf#search=%22infrared%20microspectroscopy%20and%20imaging%22

Stewart, D., McDougall, G. J., and Baty, A. 1995. Fourier transform infrared microspectroscopy of anatomically different cells of flax (Linum usitatissimum) stems

during development. J. Agric. Food Chem. 43:1853-1858.

Ward, W. H., and Lundgren, H. P. 1954. Formation, composition and properties of keratins. Advances in Protein Chem. 9:244-297.

Wetzel, D. L., Eilert, A. J., Pietrzak, L. N., Miller, S. S., and Sweat, J. A. 1998. Ultraspatially resolved synchrotron infrared microspectroscopy of plant tissue in situ. Cell. Mol. Bio. 44:145-167.

Wetzel, D. L., Srivarin, P., and Finney, J. R. 2003. Revealing protein infrared spectral detail in a heterogeneous matrix dominated by starch. Vibrational Spectroscopy. 31:109-114.

Yu, P. McKinnon, J. J., Christensen, C. R., and Christensen, D. A. 2003a. Mapping plant composition with synchrotron infrared microspectroscopy and relation to animal nutrient utilization. Proceeding of the Canadian Society of Animal Science - Conference. University of Saskatchewan, Saskatoon, SK, Canada, June 10-13. pp 1-20.

Yu, P. Q., McKinnon, J. J., Christensen, C. R., and Christensen, D. A. 2004a. Using synchrotron-based FTIR microspectroscopy to reveal chemical features of feather protein secondary structure: Comparison with other feed protein sources. J. Agric. Food Chem. 52:7353-7361.

Yu, P., Christensen, D. A., Christensen, C. R., Drew, M. D., Rossnagel, B. G., and McKinnon, J. J. 2004b. Use of synchrotron Fourier transform infrared microspectroscopy to identify chemical differences in the ultrastructural matrix of endosperm tissue between Harrington (malting-type) and Valier (feed-type) barley in relation to rumen degradation characteristics. Can. J. Anim. Sci. 2004b. 84:523-527.

Yu, P., McKinnon, J. J., Christensen, C. R., and Christensen, D. A. 2004c. Using synchrotron transmission FTIR microspectroscopy as a rapid, direct and non-destructive analytical technique to reveal molecular microstructural-chemical features within tissue in grain barley. J. Agric. Food Chem. 52:1484 – 1494.

Yu, P., McKinnon, J. J., Christensen, C.R., Christensen, D. A., Marinkovic, N. S., and Miller, L. M. 2003b. Chemical imaging of micro-structures of plant tissues within cellular dimension using synchrotron infrared microspectroscopy. J. Agric. Food Chem. 51:6062-6067.

Figures

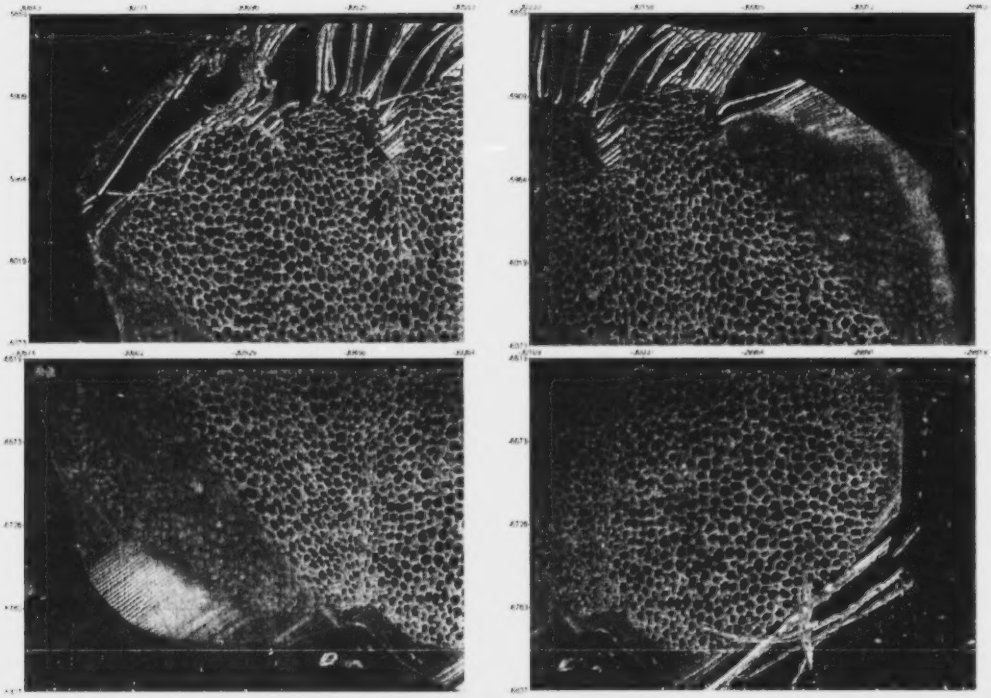

Figure 1. Photomicrograph of cross-section of the feather tissue (6 µm thick section).

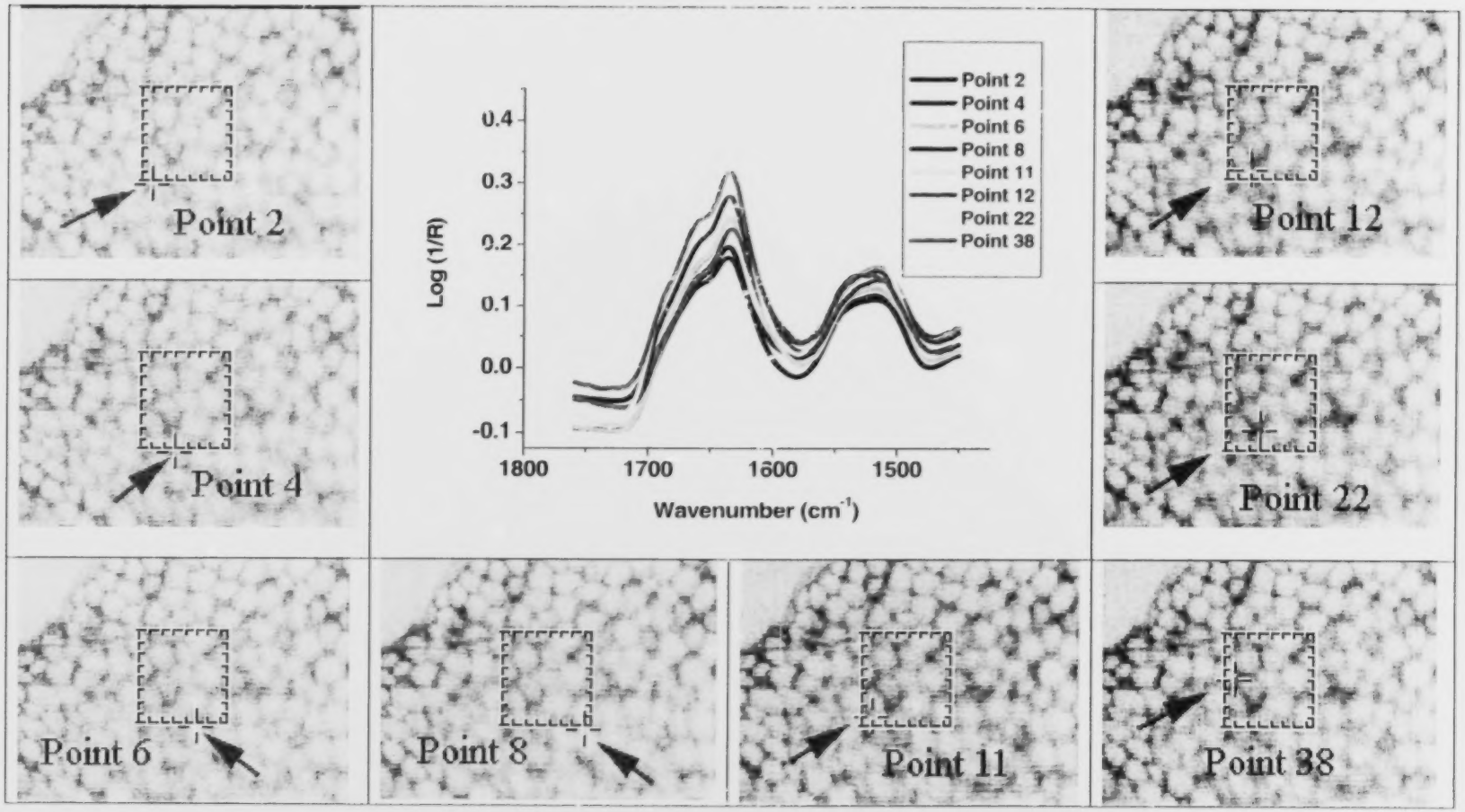

Figure 2(a). The line shape and position of feed protein amide I (a) from feather protein; (b) from barley protein; (c) from oat protein and (d) from wheat protein, respectively, indicating different protein secondary structures among protein sources (α-helix at ca. 1650 cm^{-1} and β-sheet at ca. 1630 cm^{-1}) (Note: the second the peaks are protein amide II; the peak height from different points were different due to separation of each peak allow easier visual evaluation).

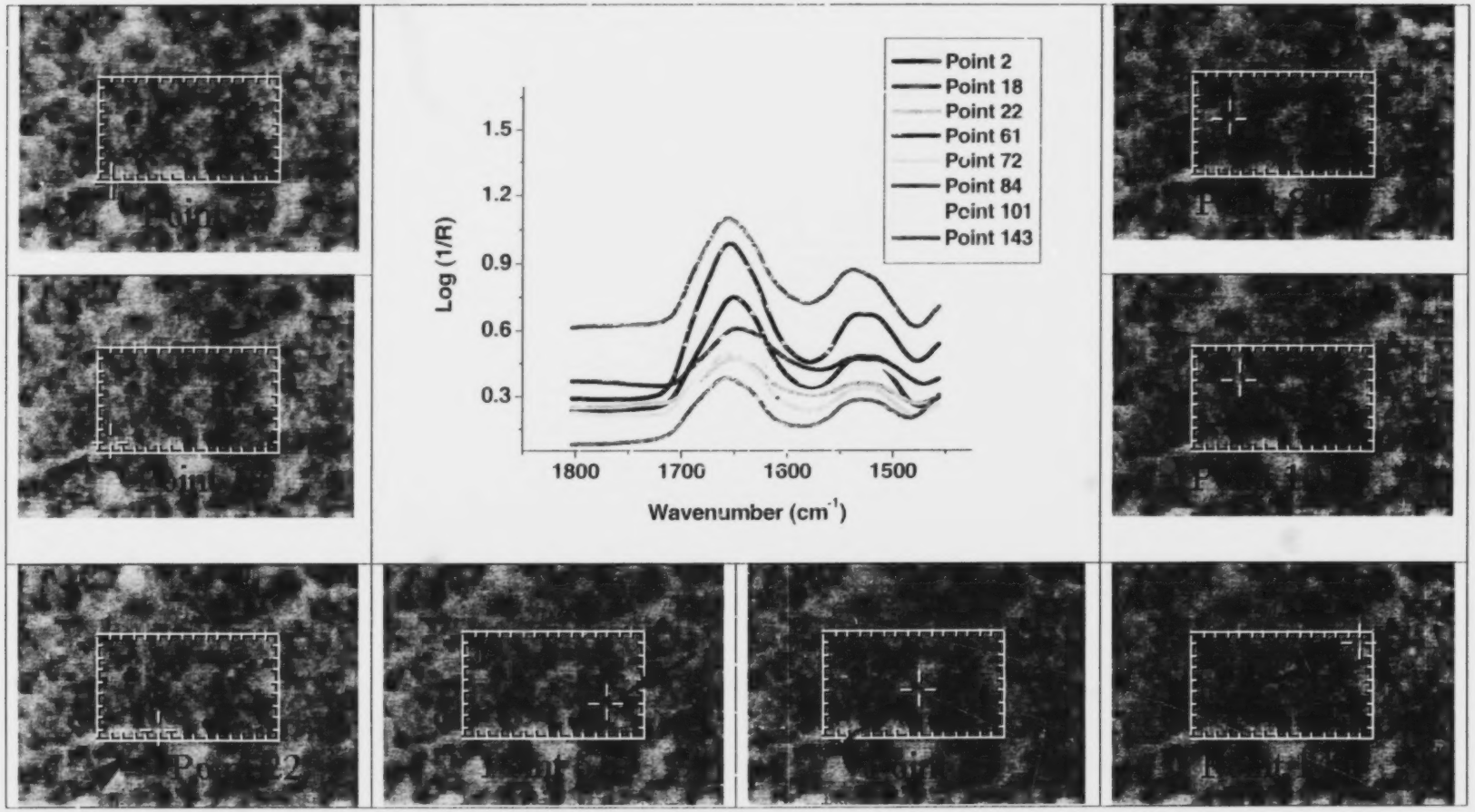

Figure 2(b). The line shape and position of feed protein amide i (a) from feather protein; (b) from barley protein; (c) from oat protein and (d) from wheat protein, respectively, indicating different protein secondary structures among protein sources (α-helix at ca. 1650 cm^{-1} and β-sheet at ca. 1630 cm^{-1}) (Note: the second the peaks are protein amide II; the peak height from different points were different due to separation of each peak allow easier visual evaluation).

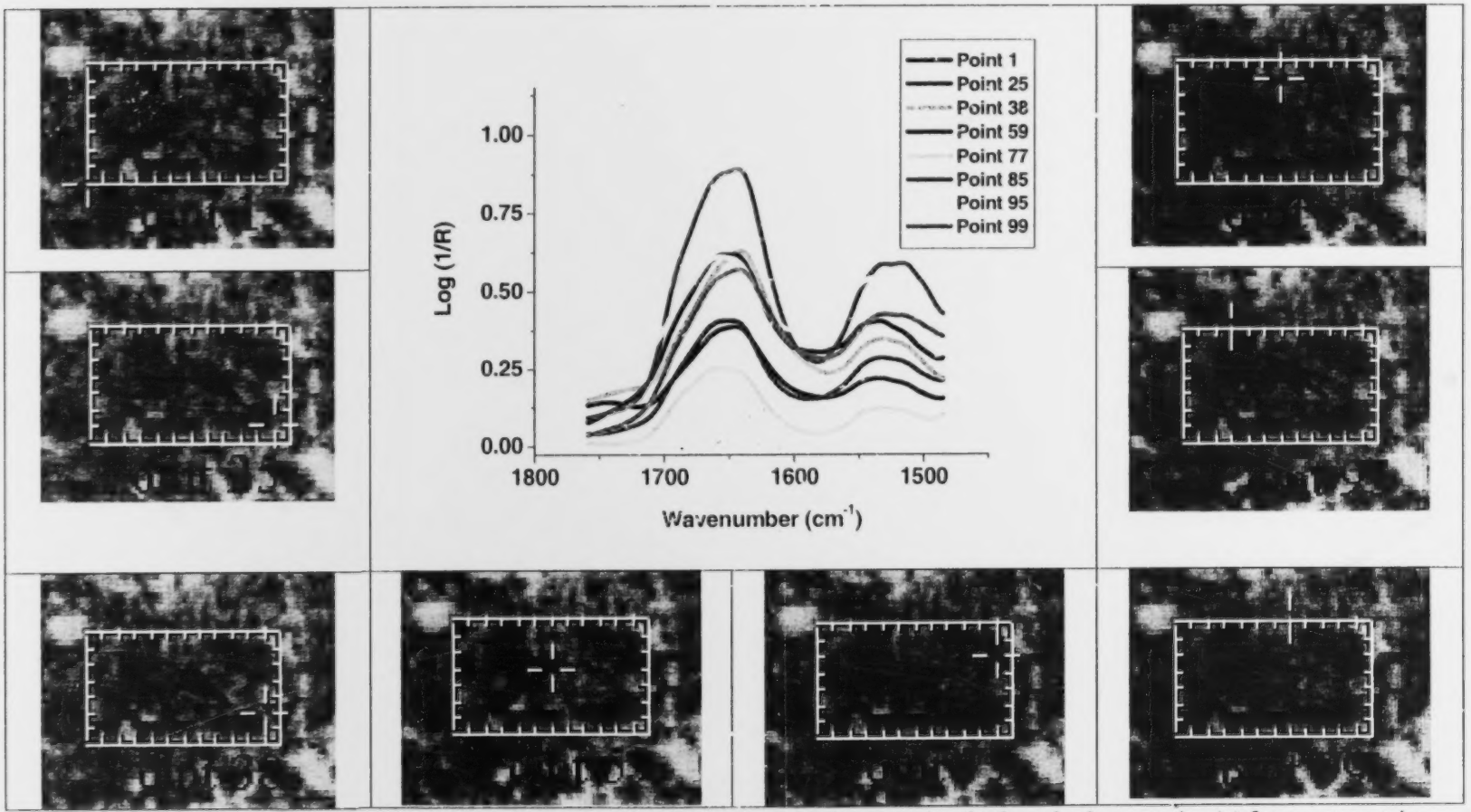

Figure 2(c). The line shape and position of feed protein amide I (a) from feather protein; (b) from barley protein; (c) from oat protein and (d) from wheat protein, respectively, indicating different protein secondary structures among protein sources (α-helix at ca. 1650 cm^{-1} and β-sheet at ca. 1630 cm^{-1}) (Note: the second the peaks are protein amide II; the peak height from different points were different due to separation of each peak allow easier visual evaluation).

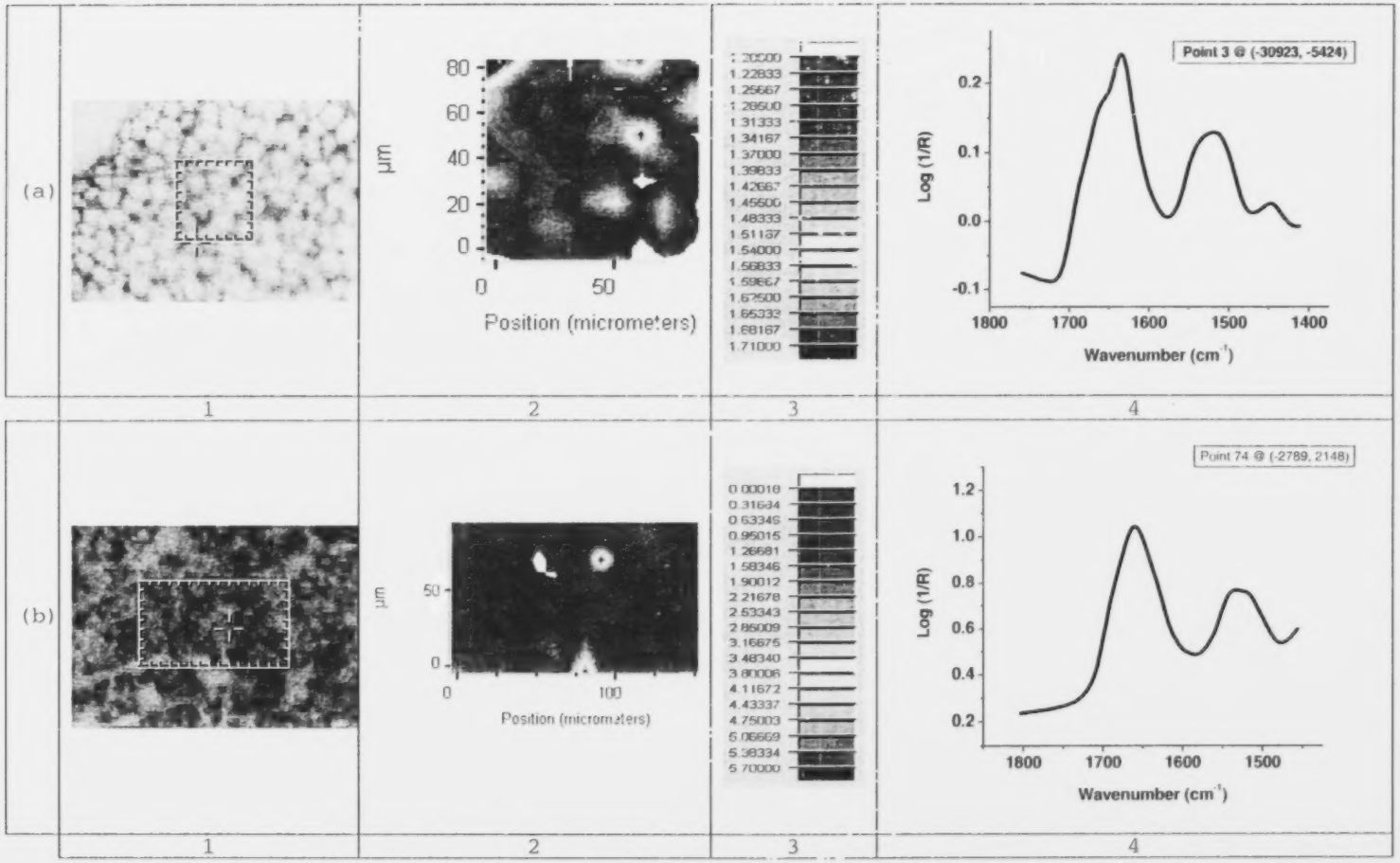

Figure 3. Functional group ratio images of the feather tissue (a), barley endosperm (b), oat endosperm (c) and wheat endosperm (d) (1. Visible image; 2 Chemical image; 3. Chemical intensity; 4. Spectra corresponding to the pixel at the cross-hair in the visible image 1b): area under 1630 cm^{-1} peak height divided 1650 cm^{-1} peak height showing protein amide I β-sheet to α-helix ratio distribution. (Note: some holes and blue "hot Spots" were due to mapping artifacts).

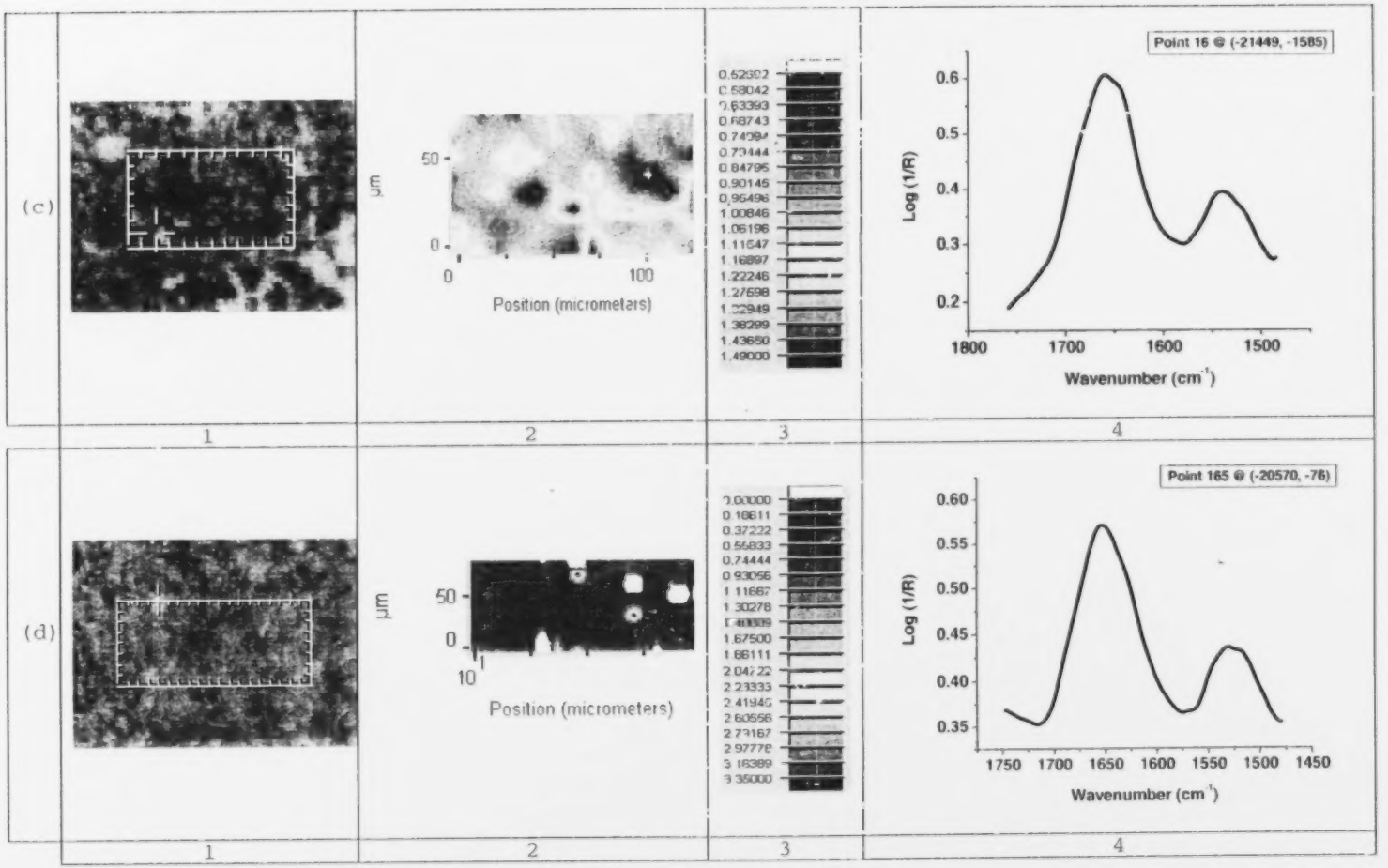

Figure 3. (Continued).

Project 4: Use of Synchrotron-Based FTIR Microspectroscopy to Determine the Effect of Heat Treatment on Protein Secondary Structures of Brown and Golden Flaxseeds at a Cellular Level in Relation to Nutritive Value of Protein.

Details of this project were reported in our fourth interim report (June 2005). Those details are again reported below, following a summary of this project that was extracted from a peer-reviewed article that was published in the Canadian Journal of Animal Science (Yu et al., 2005b).

Project Summary

The objectives of the study were to use synchrotron Fourier transform infrared microspectroscopy (S-FTIR) as a novel approach to: (1) reveal ultra-structural chemical features of protein secondary structures of flaxseed tissues affected by variety (golden and brown) and heat processing (raw and roasted), and (2) quantify protein secondary structures using Gaussian and Lorentzian methods of multi-component peak modeling. By using multi-component peak modeling at protein amide I region of 1700-1620 cm^{-1}, the results showed that the golden flaxseed contained relatively higher percentage of α-helix (47.1 vs. 36.9%), lower percentage of β-sheet (37.2 vs. 46.3%) and higher ($P < 0.05$) ratio of α-helix to β-sheet than the brown flaxseed (1.3 vs. 0.8). The roasting reduced ($P < 0.05$) percentage of a-helix (from 47.1 to 36.1%), increased percentage of β-sheet (from 37.2 to 49.8%) and reduced α-helix to β-sheet ratio (1.3 to 0.7) of the golden flaxseed tissues. However, the roasting did not affect percentage and ratio of α-helix and β-sheet in the brown flaxseed tissue. No significant differences were found in quantification of protein secondary structures between Gaussian and Lorentzian methods. These results demonstrate the potential of highly spatially resolved S-FTIR to localize relatively pure protein in the tissue and reveal protein secondary structures at a cellular level. The results indicated relative differences in protein secondary structures between flaxseed varieties and differences in sensitivities of protein secondary structure to the heat processing. Further study is needed to understand the relationship between protein secondary structure and protein digestion and utilization of flaxseed and to investigate whether the changes in the relative amounts of protein secondary structures are primarily responsible for differences in protein availability.

Project Details

Introduction

Studying the secondary structure of proteins leads to an understanding of the components that make up a whole protein (Dyson and Wright 1990; Carey 1996). An understanding of the structure of the whole protein is often vital to understanding its digestive behavior, nutritive quality, utilization and availability in animals. Protein secondary structures include α-helix and β-sheet (Carey 1996). The percentage of these two structures may influence protein quality, nutrient utilization, availability and digestive behavior (Yu et al. 2005b). High percentage of β-sheet structure may reduce access by gastrointestinal digestive enzymes, which results in low protein value and low protein availability. Research has shown that different protein sources have different percentages and ratios of α-helix and β-sheet in protein secondary structure (Yu et al. 2005b). These protein structures are associated with protein value. Feather contains a high protein content (84%), but the protein digestibility is very low (5%) in comparison with other protein sources such as barley, oat and wheat. The low digestibility of feather protein is closely related to structural characteristics such as the relationship of β-sheet to solubility, keratin content and the disulphide bonding of the amino acids (Ward and Lundgren 1954; Fraser et al. 1972; Greg and Rogers 1986; Chandler 2003). Our work (Yu et al., 2005b) shows that feather contained high β-sheet (88%) and low α-helix (4%), but the other protein sources with high protein nutritive value, such as barley at 17% β-sheet and 71% α- helix, contain much less β-sheet and high α-helix (Yu et al. 2005b). This study demonstrated that the differences in the proportion of protein secondary structures and α- helix to β-sheet ratio partially explained digestive behaviors, nutrient utilization and animal availability difference of various proteins.

Heat processing has been used to improve utilization and availability of the nutrients (Yu et al. 2002) and inactivate anti-nutritional factors (van der Poel et al. 1990), such as reducing the solubility of the protein, fermentation and metabolism in the rumen, increasing the amounts of protein entering the small intestine for absorption and digestion (Yu et al. 2002), and reducing conjugated linoleic acid (CLA) hydrogenation in the rumen and increasing the amount of CLA available in the small intestine (Soita et al. 2003). The mechanism of altering the protein digestive behavior (Goelema 1999) with heat processing involves denaturation (which is a disorganization of the overall molecular shape of a protein), unfolding or uncoiling of a coiled or

pleated structure, or the separation of the protein into its subunits, which may then unfold or uncoil (Holum 1982). Any temperature change in the environment of the protein which can influence the non-covalent interactions involved in the structure may lead to an alteration of the protein structure including protein secondary structures (Goelema 1999). Recent research (Seguchi et al. 2004) showed that heat processing affected protein secondary structures and changed the α-helix to β-sheet ratio. These changes affected nutritive quality. Published results show that the effects of heat processing on protein nutritive value, utilization and availability and performance in animals are variable (Yu et al. 2004d). Part of reason is that heating conditions may not be optimal, the feed being either underheated or overheated (Yu et al. 2004d). One proposed approach to check effects of heat processing on protein value and nutrient availability is to look at magnitude of changes of protein secondary structures in the intrinsic protein structures in terms of α-helix to β-sheet ratio within the intact tissue. Most studies have focused on total chemical composition affected by heat processing using traditional "wet" chemical analysis without consideration of any inherent structural effects.

We know that the protein value, quality, utilization and availability and digestive behavior are closely related to not only total chemical composition, but also inherent structures and matrix (Yu et al. 2003a; Yu, 2004; Yu et al. 2004a, c). Traditional "wet" chemical analysis fails to reveal feed structure and structural matrix information and fails to link tissue structural information to chemical information (Budevska 2002). Synchrotron-based Fourier transform infrared microspectroscopy (S-FTIR) has been developed as a rapid, direct, non-invasive, non-destructive and bioanalytical technique (Wetzel et al. 1998; Holman et al. 2002; Miller 2002; Marinkovic et al. 2002). It takes advantages of synchrotron light brightness (100-1000 million times brighter than sunlight) and small effective source size, is capable of exploring the molecular chemistry within microstructures of biological tissues without destruction inherent structures within cellular dimension (Wetzel et al. 1998; Wetzel 2001; Marinkovic et al. 2002; Miller 2000, 2002). With the synchrotron technology (S-FTIR), localization of protein in grain seeds was achievable. The protein structural features could be revealed at a cellular level (Wetzel et al. 2003; Yu et al. 2005b).

To date there has been very little application of this novel technique to the study of inherent feed structures in relation to nutrient utilization and availability in animals (Yu, 2004). No study has been carried out to study the ultra-structural chemical and nutritive features of

protein secondary structures in flaxseed tissues within intact tissue at a cellular level. These features are closely associated with protein quality, utilization and availability in human and animal diets.

Objective

The objectives of this study were to use the synchrotron technology (S-FTIR) as a novel approach to: 1) reveal chemical and nutritive features of the flaxseed tissue in terms of protein secondary structures affected by varieties and heating processing within intact tissue at a cellular level, and 2) quantify protein secondary structures using multi-component peak modeling Gaussian and Lorentzian methods, in relation to protein value and quality. Information from the study by the infrared probing of feed protein secondary structures will be valuable as a guide to maintain protein quality.

Materials and Methods

Flaxseeds and Heating Processing

Raw (ID# 194-F1) and roasted golden (ID# 196-F2, 163 °C) flaxseeds and raw (ID# 193-F3) and roasted brown (ID# F4, 145 °C) flaxseeds were obtained from CanMar Grain Products LTD and Professor David A. Christensen's Research Laboratory (Department of Animal and Poultry Science, University of Saskatchewan).

Synchrotron IR Slide Preparation

Randomly selected flaxseed samples were cut into thin cross-sections (ca. 6 μm thick) using disposable razor blade microtome knives at the Western College of Veterinary Medicine, University of Saskatchewan. The unstained cross-sections were mounted onto Low-e IR microscope slides (Kevley Technologies, Chesterland, OH) for synchrotron FTIR microspectroscopy in reflectance mode. More detailed methodology on slide preparation was reported by Yu et al. (2003b, 2004b, and 2005a).

Photomicrograph of Cross-Sections of Feather Tissues

Photomicrographs of cross-section of the flaxseed tissues (thickness: 6 μm) were taken with a digital camera.

Synchrotron Light Source and FTIR Microspectroscopy

This experiment was performed at the National Synchrotron Light Source in Brookhaven National Laboratory (NSLS-BNL, Department of Energy, New York, USA) on November 11-16, 2004. The U10B beamline was equipped with a FTIR spectrometer (Nicolet Magna 860) with KBr beamsplitter and liquid nitrogen cooled MCT detectors coupled with a Continuμm IR microscope (Spectra Tech, USA) with Schwartzshild 32× objective and 10× condenser. Synchrotron radiation from the VUV storage ring at beamline U10B (with an energy level 800 MeV) entered the interferometer via a port of the instrument designed to use for infrared emission. The IR spectra were collected in the mid-IR range 4000-800 cm^{-1} at a resolution of 4 cm^{-1} with 64 scans co-added The aperture setting was 10 × 10 μm. Stage control, spectrum data collection and processing were performed using OMNIC 6.0 (Spectra Tech, USA). Scanned visible images were obtained using a charge-coupled device (CCD) camera linked to the infrared images.

Data Analysis and Chemical Images

The spectral data of the flaxseed tissues were collected, corrected with the background spectrum, displayed in the absorbance mode and analyzed using OMNIC 6.0 (Spectra Tech, USA). The data were displayed as either as a series of spectroscopic images collected at individual wavelengths or as a collection of infrared spectra obtained at each pixel position in the image. The synchrotron FTIR absorbance was expressed as Log (1/R). Chemical functional groups were identified according to published reports (Kemp 1991; Himmelsbach et al. 1998; Wetzel et al. 1998; Jackson and Mantsch 2000; Wetzel 2001; Marinkovic et al. 2002; Miller 2002). Chemical imaging of protein (amide I) and protein to starch ratio in the intrinsic structures of the flaxseeds tissues were determined using the OMNIC 6.0 software at the spectral region (1650-1550 cm^{-1}, 1025 cm^{-1}) of greatest interest. The protein to starch peak ratios were obtained by the height under amide I functional group band (1650 cm^{-1}) divided by the height under starch functional group band (1025 cm^{-1}) at each scan area (scan size 10 μm ×10 μm).

The chemical mapping of protein and protein to starch ratio at the U10B beamline provided spectra data selected with relatively "pure" protein for modeling protein amide I component peaks. The selection procedure of the "pure" protein in the flaxseed tissues followed

the methodology published by Wetzel et al. (2003). The brief procedure is as follows:

Within each image of the raw and roasted golden and brown flaxseed tissues, ten area samples in the endosperm region with the relatively pure "protein" content were selected for quantification of protein secondary structures (α-helix to β-sheet ratio) at ultra-resolution (Wetzel et al. 2003). This is because the endosperm matrix is heterogeneous. In order to eliminate carbohydrate scattering effect on the protein spectrum, the relatively "pure" protein areas were selected for protein secondary structure analysis. The size of each probed area was 10 μm × 10 μm, which was within plant cellular dimensions (5 to 30 μm).

Quantifying the Proportion of α-Helix and β-Sheet in Feed Protein Secondary Structures

With the protein amide I component bands being overlapped (Figure 1), a specific multi-peak fitting or modeling procedure was required. To determine the relative amount of α-helix and β-sheet in the protein secondary structures, two steps were applied. The first step used Fourier self-deconvolution (FSD) in OMNIC to obtain the FSD spectrum in protein amide I region to identify protein amide I component peak frequencies (Figure 1). The second step was used Origin data analysis software multi-peak fitting with Gaussian and Lorentzian functions (Figure 2) to quantify the multi-component peak areas in protein amide I bands (Figure 3). The differences between Gaussian and Loretzian functions for multi-component peak fitting and sample curves are shown in Figure 2. The detailed descriptions were reported in Origin in terms of peak shape, centre, offset, width and area. The relative amount of α-helix and β-sheet based on modeled peak areas was calculated according to the report generated by the software (Figure 3).

Statistical Analysis

Statistical analyses were performed using Proc Mixed of SAS (SAS Inst. Inc., Cary NC) with the model:

$$Y = \text{mean} + \text{treatments} + \text{fitting methods} + \text{treatments} \times \text{fitting method} + \text{error}$$

Where: treatment = flax variety and processing combination (F1, F2, F3, F4), and
fitting method = Gaussian or Lorentzian functions.

Significance was declared at $P < 0.05$.

Results and Discussion

Photomicrograph of Flaxseed Tissues

The photomicrographs of cross-sections of the flaxseeds of the raw (F1) and roasted (F2) golden flaxseed and raw (F3) and roasted (F4) brown flaxseed tissues (6 μm thickness) are presented in Figure 4. These photomicrographs only show some of the structural information, but do not show any structural-chemical and nutritive information. It is evident from these figures that there is limited chemical information available from these cross-sections. They do not give any information on localized structural-chemical and nutritive (utilization and availability) information.

Ultra-Spatially Resolved Chemical Mapping of Protein and Protein to Starch Ratio in Flaxseeds

Each biological component has a unique molecular chemical-structural feature and its own unique IR spectrum. The unique characteristic of protein structure is the peptide bond. The peptide bond contains C=O, C-N, and N-H. The amide I bond is primarily C=O stretching vibration (80%) plus C-N stretching vibration. Amide I absorbs at ca. 1650 cm^{-1}. Amide II which absorbs at 1550 cm^{-1} consists primarily of N-H bending vibrations (60%) coupled with C-N stretching vibrations (40%). Carbohydrates are comprised sugars with OH and CO bonds. Depending on bond linkage and type of sugar, the IR position for carbohydrate is between 1180 and 950 cm^{-1}. For example, in grain endosperm, starch absorbs at ca. 1025 cm^{-1} (Himmelsbach et al. 1998; Wetzel et al. 1998, 2003; Wetzel 2001; Miller 2000, 2002; Marinkovic et al. 2002; Yu et al. 2003b; 2004b). Figure 5 represents color maps of functional groups of the endosperm tissue of the flaxseeds and single pixel spectra measuring areas as small as 10×10 μm. These maps show the distribution and relative concentration of the components associated with the flaxseed inherent micro-structure, imaged in false-color representation of chemical intensities. Blue stands for high, red stands for low intensity, and white stands for no functional groups. The spectrum in the figure corresponds to the pixel in the cross-hair and was selected to represent the value of the integrated peak. Figure 5(b) shows the areas under the 1650 cm^{-1} peak attributed to protein amide I absorption (Miller 2000; Wetzel 2001). The amide I (1650 cm^{-1}) is characteristic

of C=O and N-H bonds in the protein backbone and are indicators of the area of the sample where protein is present (Miller 2002; Wetzel 2001; Marinkovic et al. 2002). Figure 5(b) clearly shows that protein is unequally distributed in the endosperm areas of the flaxseed tissues, indicating heterogeneity of the flaxseed endosperm.

Biological component ratio images showing structural chemical features can be obtained by the height or area under one functional group band divided by the height or area under another functional group band at each pixel location. The biological component ratio image has two advantages. The first is that using those ratios, any spectral intensity variations due to tissue thickness changes are eliminated. The second is that the ratio maps are able to indicate relative biological component contents, which could be used to determine food or feed quality characteristics and nutritive values (nutrient utilization and availability). Figure 5(c) represents peak ratio maps, representing biological component ratio distribution and intensity in the inherent structure. The height under the 1650 cm^{-1} band divided by the height under the peaks around 1025 cm^{-1} at each pixel represents protein to total starch in the tissue. Again Figure 5(c) shows that the protein to starch ratio is unequally distributed in the endosperm areas of flaxseed tissue, indicating endosperm heterogeneity.

Our chemical mapping results demonstrate the potential of highly spatially resolved infrared microspectroscopy to reveal the flaxseed tissues within cellular dimensions. The protein distribution and intensity, even within cellular dimensions in the flaxseed tissues, is unequal, which justifies a need to select areas with relatively "pure" protein for the study of protein secondary structures with minimum disturbance by other biological components such as carbohydrates. Wetzel et al. (2003) and Yu et al. (2005b) also reported heterogeneous matrix dominated by starch in wheat endosperm.

Characteristics of Protein Secondary Structures of Flaxseed Tissue Indicated by Amide I

Typical, protein secondary structures include the α-helix and β-sheet (Dyson and Wright 1990; Carey 1996). The protein IR spectrum has two primary features, as indicated before, the amide I (ca. 1600-1700 cm^{-1}) and amide II (ca. 1500-1560 cm^{-1}) bands, which arise from specific stretching and bending vibrations of the protein backbone. The amide I band arises predominantly from the C=O stretching vibration of the amide C=O group. The vibrational frequency of the amide I band is particularly sensitive to protein secondary structure (Kemp

1991; Miller 2000, 2002; Martin 2002; Wetzel et al. 2003) and can be used to predict protein secondary structure. For α-helix, the amide I is typically in the range of 1648-1658 cm^{-1}. For β-sheet, the peak can be found within the range of 1620-1640 cm^{-1} (Martin 2002). The amide II (predominantly an N-H bending vibration coupled to C-N stretching) is also used to assess protein conformation. However, as it arises from complex vibrations involving multiple functional groups they are less useful for protein structure prediction than the amide I band (Jackson and Mantsch 2000). Figure 1 (a, b) show typical protein amide I and amide II spectrum of the flaxseed tissues. The spectrum of amide I original band shows peak center at ca. 1650, with two shoulders at ca. 1688 and ca. 1630 cm^{-1} [Figure 1(c)]. This was confirmed from FSD spectrum of amide I in the flaxseed tissues [Figure 1(d)] with three peaks at ca. 1650, 1688 and 1630 cm^{-1}.

Modeling of Protein Amide I Peaks to Quantify Percentage of Protein Secondary Structures (α-Helix, β-Sheet and the Ratio of α-Helix to β-Sheet)

Due to the fact that protein amide I component peaks overlay with each other (Figure 1), Fourier self-deconvolution was used to obtain FSD spectrum to identify amide I component peak frequencies (Figure 3) which were ca. 1688, 1650 and 1630 cm^{-1} and then multi-component peaks fitting with Gaussian and Lorentzian functions (Figure 2) was used to quantify the multi-component peak area in protein amide I region. Statistical analysis showed an effect ($P < 0.05$) of flaxseed treatments (F1, F2, F3, and F4) on all measured parameters, but there were no fitting methods (Gauss vs. Lorentzian) or fitting methods and treatment interaction effects ($P > 0.05$). Table 1 shows the R^2 and χ^2 from multi-component peak modeling of FSD spectrum of amide I in the flaxseed tissues. Table 2 shows percentage of α-helix and β-sheet in protein secondary structures of the flaxseed tissues in the different treatments (F1, F2, F3, and F4). Compared to the raw brown flaxseeds, the golden contained higher ($P < 0.05$) percentage of α-helix (47.1 vs. 36.9%) and lower percentage of β-sheet (37.2 vs. 46.3%), indicating higher protein quality and higher availability in the golden flaxseeds due to the lower level of β-sheet. Wetzel et al. (2003) also found variety differences in wheat. Comparing the raw and roasted golden flaxseeds, roasting reduced ($P < 0.05$) percentage of α-helix (from 47.1 to 36.1%) and increased percentage of β-sheet (from 37.2 to 49.8%). Comparing the raw and roasted brown flaxseeds, roasting did not change ($P > 0.05$) the percentage of α-helix and β-sheet. Table 3 shows ratios of α-helix and

β-sheet in protein secondary structures of the flaxseed tissues in the different treatments. Comparing the raw flaxseeds, the golden contained higher ($P < 0.05$) ratio of α-helix to β-sheet (1.3 vs. 0.8). Comparing the raw and roasted in the golden flaxseeds, the roasting reduced ($P < 0.05$) ratio of α-helix to β-sheet (1.3 to 0.7). Comparing the raw and roasted brown flaxseeds, the roasting did not change ($P > 0.05$) ratio of α-helix to β-sheet. No published results have been found for characteristics of protein secondary structures of flaxseeds. The results indicated that: 1) the golden and brown flaxseeds have different protein secondary structures in terms of percentage and ratio of α-helix to β-sheet, indicating variety difference in structural chemical make-up and features, which affects protein value, quality and utilization and availability, and 2) the effects of the heat processing has a different impact on different varieties of the flaxseed tissues, indicating that sensitivities of protein secondary structure of flaxseeds to heating are different. In terms of nutrition value, the difference in percentage of protein secondary structures is part of reason to cause different protein digestive behaviors and availability. It needs to be mentioned that our results should be considered as typical (not average) for the individual flaxseeds due to the many factors that affect the quality of flaxseeds, such as locations, climate and growth conditions. Information from this study by the infrared probing protein secondary structures may be valuable as a guide for flaxseed breeders and feed/food processing industry to improve and maintain protein nutritive value and quality for animal and human use. Our results demonstrate the potential of highly spatially resolved synchrotron-based infrared microspectroscopy to localize chemical microstructure and reveal protein secondary structure of flaxseeds at a cellular level, which provide an indication of protein quality.

Conclusions

In conclusion, with synchrotron based FTIR microspectroscopy, the ultrastructrual-chemical makeup and nutritive characteristics could be revealed at a high ultra-spatial resolution. Synchrotron-based FTIR microspectroscopy revealed that the secondary structure of protein differed between the golden and brown flaxseeds in terms of percentage and ratio of α- helix and β-sheet in mid IR within cellular dimension. By using multi-component peak modeling, the results show that the golden contained higher percentage of α-helix (47.1 vs. 36.9%), lower percentage of β-sheet (37.2 vs. 46.3%) and higher ($P < 0.05$) ratio of α-helix to β-sheet (1.3 vs. 0.8). The sensitivities of protein secondary structure of different flaxseeds to heat processing

were different. Roasting reduced ($P < 0.05$) percentage of α-helix (from 47.1 to 36.1%), increased percentage of β-sheet (from 37.2 to 49.8%) and reduced α-helix to β-sheet ratio (1.3 to 0.7) in the golden flaxseeds. However, roasting did not affect percentage and ratio of α-helix and β-sheet in the brown flaxseeds. These results indicate that protein values, utilization and availability between the two varieties of flaxseeds differed and whether the roasting affected nutritive value depended on the variety of flaxseeds. There was no difference between Gaussian and Lorentzian multi-component peak fitting methods in quantification of protein secondary structures. These results demonstrate the potential of highly spatially resolved infrared microspectroscopy to reveal feed protein secondary structures and protein nutritive values. Further study is needed to quantify the relationship between protein secondary structures and nutrient availability and digestive behavior of various varieties of flaxseed protein sources.

Literature Cited

Budevska, B. O. 2002. Vibrational Spectroscopy. pp 3720-3732.

Carey, F. A. 1996. Organic Chemistry. 3rd Edition. McGraw-Hill Companies, Inc.

Chandler, N. J. 2003. Dairy Cattle – Feather meal: It´s nutritional value and use in dairy and beef rations. Retrieved in Nov 2003 from http://www.engormix.com/e_articles_dairy_cattle.asp?ID=79.

Dyson, H. J., and Wright, P. E. 1990. Peptide conformation and protein folding. Current Opinion in Structural Biology. 3:60-65.

Fraser, R. D. B., MaCrae, T. P., and Rogers, G. E. 1972. Keratins. Charles C Thomas, III. USA.

Goelema, J. O., Smits, A., Vaessen, L. M., and Wemmers, A. 1999. Effects of pressure toasting, expander treatment and pelleting on in vitro and in situ parameters of protein and starch in a mixture of broken peas, lupins and faba beans. Anim. Feed Sci. Technol. 78:109-126.

Greg, K., and Rogers, G. E. 1986. Feather keratin: Composition, structure and biogenesis. Biology of Integuments. Volume 2. Springer, Verlag.

Himmelsbach, D. S., Khalili, S., Akin, D. E. 1998. FT-IR microspectroscopic imaging of flax (linum usitatissimum L.) stems. Cell. Mol. Bio. 44:99-108.

Holman, H. Y. N., Bjornstad, K. A., McNamara, M. P., Martin, M. C., McKinney, W. R., and Blakely, E. A. 2002. Synchrotron infrared spectromicroscopy as a novel bioanalytical microprobe for individual living cells: cytotoxicity considerations. J. Biomedical Optics. 2002, 7, 1–10.

Holum, J. R. 1982. Fundamentals of General, Organic, and Biological Chemistry. 2nd ed. J. Wiley and Sons, Inc. New York, NY, USA

Jackson, M., and Mantsch, H.H. 2000. Infrared spectroscopy ex vivo tissue analysis. Biomedical Spectroscopy.

Kemp, W. 1991. Organic Spectroscopy. 3rd ed. W.H. Freeman and Company, New York, USA.

Marinkovic, N. S., Huang, R., Bromberg, P., Sullivan, M., Toomey, J., Miller, L.M., Sperber, E., Moshe, S., Jones, K.W., Chouparova, E., Lappi, S., Franzen S., and Chance, M.R. 2002. Center for Synchrotron Biosciences' U2B beamline: an international resource for

biological infrared spectroscopy. J. Synchrotron Rad. 9:189-197.

Martin, M.C. 2002. Fourier-Tranform Infrared Spectroscopy. Retrieved in October 2002 from: http://infrared.als.lbl.gov/

Miller, L. M. 2000. The impact of infrared synchrotron radiation on biology: past, present, and future. Synchrotron Radiation News. 13:31-37.

Miller, L. M. 2002. Infrared Microspectroscopy and Imaging. Retrieved in October 2002 from: http://www.nsls.bnl.gov/newsroom/publications/otherpubs/imaging/workshopmillerhighres.pdf#search=%22infrared%20microspectroscopy%20and%20imaging%22

Seguchi, M., Takemoto, M., Mizutani, U., Ozawa, M., Nakamura, C., and Matsumura, Y. 2004. Effects of secondary structures of heated egg white protein on the binding between prime starch and tailings fractions in fresh wheat flour. Cereal Chem. 81:633-636.

Soita, H. W., Meier, J. A., Fehr, M., Yu, P., Christensen, D. A., McKinnon, J. J., Mustafa, A. F. 2003. Effects of flaxseed supplementation on milk production, milk fatty acid composition and nutrient utilization by lactating dairy cows. Archiv. Anim. Nutr. 57:107-116.

Van der Poel, A. F. B., Blonk, J., van Zuilichem, D. J., and van Gort, M. G. 1990. Thermal inactivation of lectins and trypsin inhibitor activity during steam processing of dry beans (Phaseolus vulgaris) and effects on protein quality. J. Sci. Food Agric. 53:215-228.

Ward, W. H., and Lundgren, H. P. 1954. Formation, composition and properties of keratins. Advances in Protein Chem. 9:244-297.

Wetzel, D. L. 2001. When molecular causes of wheat quality are known, molecular methods will supercede traditional methods. Pages 1-20 in Proc. Int'l Wheat Quality Conf. II, Manhattan, Kansas, USA, May.

Wetzel, D. L., Eilert, A. J., Pietrzak, L. N., Miller, S. S., and Sweat, J. A. 1998. Ultraspatially resolved synchrotron infrared microspectroscopy of plant tissue in situ. Cell. Mol. Bio. 44:145-167.

Wetzel, D. L., Srivarin, P., and Finney, J. R. 2003. Revealing protein infrared spectral detail in a heterogeneous matrix dominated by starch. Vibrational Spectroscopy. 31:109-114.

Yu, P. 2004. Application of advanced synchrotron-based Fourier transform infrared microspectroscopy (SR-FTIR) to animal nutrition and feed science: a novel approach. Brit. J. Nutr. 92:869-885.

Yu, P., Christensen, C. R. Christensen, D. A. and J. J. McKinnon. 2005a. Ultrastructural-chemical makeup of yellow- (Brassica Rapa) and brown-seeded (Brassica Napus) canola within cellular dimensions, explored with synchrotron reflection FTIR microspectroscopy. Can. J. Plant. Sci. 85: 533-541.

Yu, P., Christensen, D. A., Christensen, C. R., Drew, M. D., Rossnagel, B. G., and McKinnon, J. J. 2004a. Use of synchrotron Fourier transform infrared microspectroscopy to identify chemical differences in barley endosperm tissue in relation to rumen degradation characteristics. Can. J. Anim Sci. 84:523-527.

Yu, P., Goelema, J. O., Leury, B. J., Tamminga, S., and Egan, A. R. 2002. An analysis of the nutritive value of heat processed legume seeds for animal production using the DVE/OEB model: a review. Anim. Feed Sci. Technol. 99:141-176.

Yu, P., McKinnon, J. J., Christensen, C. R. and Christensen, D. A. 2004b. Imaging molecular chemistry of Pioneer corn. J. Agric. Food Chem. 52:7345-7352.

Yu, P., McKinnon, J. J., Christensen, C. R., and Christensen, D. A. 2004c. Using synchrotron transmission FTIR microspectroscopy as a rapid, direct and non-destructive analytical technique to reveal molecular microstructural-chemical features within tissue in grain barley. J. Agric. Food Chem. 52:1484–1494.

Yu, P., McKinnon, J. J., Christensen, C. R., Christensen, D. A. 2003b. Mapping plant composition with synchrotron infrared microspectroscopy and relation to animal nutrient utilization. Page 1-20 in Proc. the Canadian Society of Animal Science Annual Conference. Saskatoon, SK, Canada, June 10-13.

Yu, P., McKinnon, J. J., Christensen, C. R., Christensen, D. A., Marinkovic, N. S. and Miller, L. M. 2003a. Chemical imaging of micro-structures of plant tissues within cellular dimension using synchrotron infrared microspectroscopy. J. Agric. Food Chem. 51: 6062-6067.

Yu, P., McKinnon, J. J., Soita, H. W., Christensen, C.R., and Christensen, D. A. 2005b. Use of synchrotron-based FTIR microspectroscopy to determine protein secondary structures of raw and heat-treated brown and golden flaxseeds: A novel approach. Can. J. Anim. Sci. 85:437-448.

Yu, P., Tamminga, S., Egan, A. R., and Christensen, D. A. 2004d. Probing equivocal effects of heat processing of legume seeds on performance of ruminants – a review. Asian-Austral.

J. Anim. Sci. 17:869-876.

Tables

Table 1. R^2 and χ^2 of multi-component peak modeling of FSD spectrum of amide I (1700-1620 cm^{-1}) in flax seed tissues: comparison of raw and roasted golden and brown flax seeds[x, y].

Feeds	n	Modeling R^2 (±SD)	Modeling χ^2 (±SD)
Raw Golden Flax Seed (F1)	20	0.85 (±0.04) a	0.11 (±0.06) b
Roasted Golden Flax Seed (F2)	20	0.79 (±0.08) bc	0.26 (±0.19) a
Raw Brown Flax Seed (F3)	20	0.80 (±0.06) b	0.25 (±0.14) a
Roasted Brown Flax Seed (F4)	20	0.75 (±0.11) c	0.18 (±0.10) ab
SEM[z]		0.017	0.03

[x] The data analyzed by Proc Mixed with model: Y = mean + feed + fitting method + feed × fitting method + error, (where, feed = F1, F2, F3, F4; fitting method = Gaussian, Lorentzian) showing no significant differences of fitting method and interaction.

[y] Means with the same letter in the same column are not significantly different (P>0.05).

[z] SEM = standard error of mean.

Table 2. Relative percentage of α-helix and β-sheet and the ratios of α-helix to β-sheet in protein secondary structures of flax seed tissues: comparison of raw and roasted golden and brown flax seeds[x, y]

Feeds	Sample number	% α-helix ±SD	% of β-sheet ±SD	Ratio of α-helix to β-sheet (±SD)	Ratio of β-sheet to α-helix (±SD)
Raw Golden Flax Seed (F1)	20	47.1 (±3.2) a	37.2 (±3.4) c	1.3 (±0.2) a	0.8 (±0.1) b
Roasted Golden Flax Seed (F2)	20	36.1 (±2.9) b	49.8 (±4.0) a	0.7 (±0.1) b	1.4 (±0.2) a
Raw Brown Flax Seed (F3)	20	36.9 (±4.7) b	46.3 (±4.0) b	0.8 (±0.2) b	1.3 (±0.3) a
Roasted Brown Flax Seed (F4)	20	34.4 (±9.7) b	47.9 (±7.9) ab	0.8 (±0.4) b	1.6 (±0.7) a
SEM[z]		1.32	1.17	0.05	0.09

[x] The data analyzed by Proc Mixed with model: Y = mean + feed + fitting method + feed × fitting method + error, (where, feed = F1, F2, F3, F4; fitting method = Gaussian, Lorentzian) showing no significant differences of fitting method and interaction.

[y] Means with the same letter in the same column are not significantly different (P>0.05).

[z] SEM = standard error of mean.

Figures

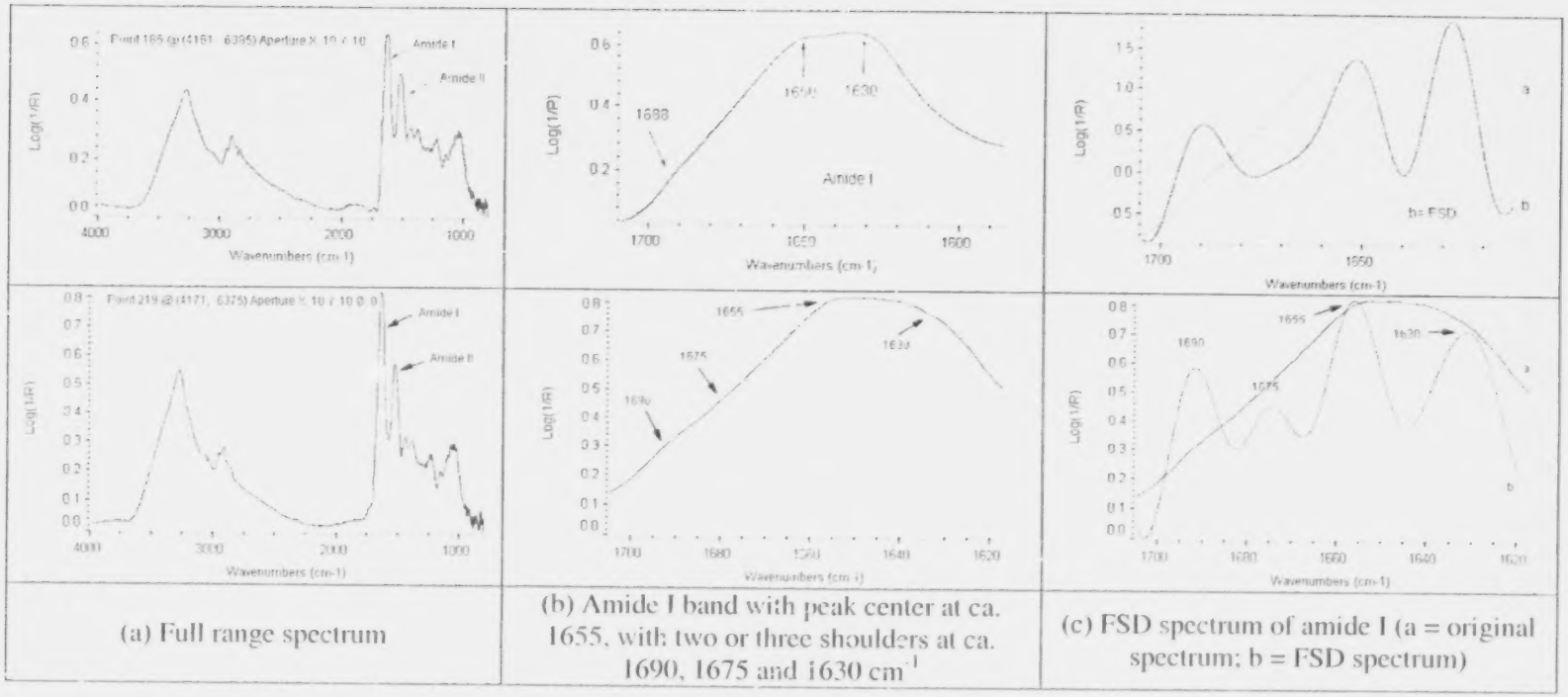

(a) Full range spectrum

(b) Amide I band with peak center at ca. 1655, with two or three shoulders at ca. 1690, 1675 and 1630 cm^{-1}

(c) FSD spectrum of amide I (a = original spectrum; b = FSD spectrum)

Figure 1. Typical synchrotron FTIR spectrum and Fourier self-deconvolution (FSD) spectrum at the amide I region of 1704-1620 cm^{-1} of flaxseed tissue.

Items	Multi-component peak fitting/modeling methods	
	1. Gaussian Function	2. Lorentzian Function
1. Equation and Description	$y = y_0 + \frac{A}{w\sqrt{\pi/2}} e^{-2\frac{(x-x_c)^2}{w^2}}$ Where, y_0, x_c, w and A represent offset, center, width and area, respectively.	$y = y_0 + \frac{2A}{\pi} \frac{w}{4(x-x_c)^2 + w^2}$ Where, y_0, xc, w and A represent offset, center, width and area, respectively.
2. Sample Curve	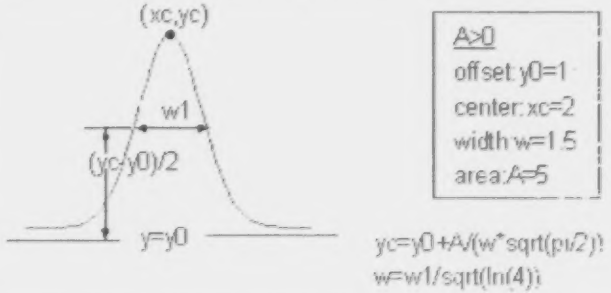	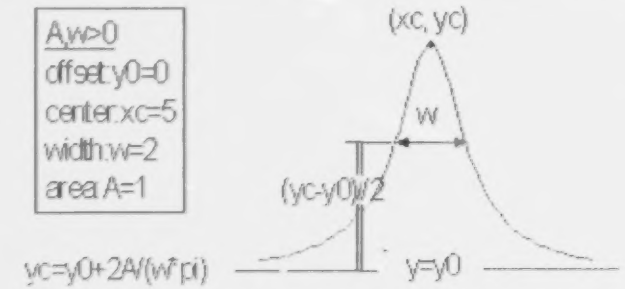

Figure 2. Gaussian and Lorentzian functions for multi-peaks fitting in protein amide I regions.

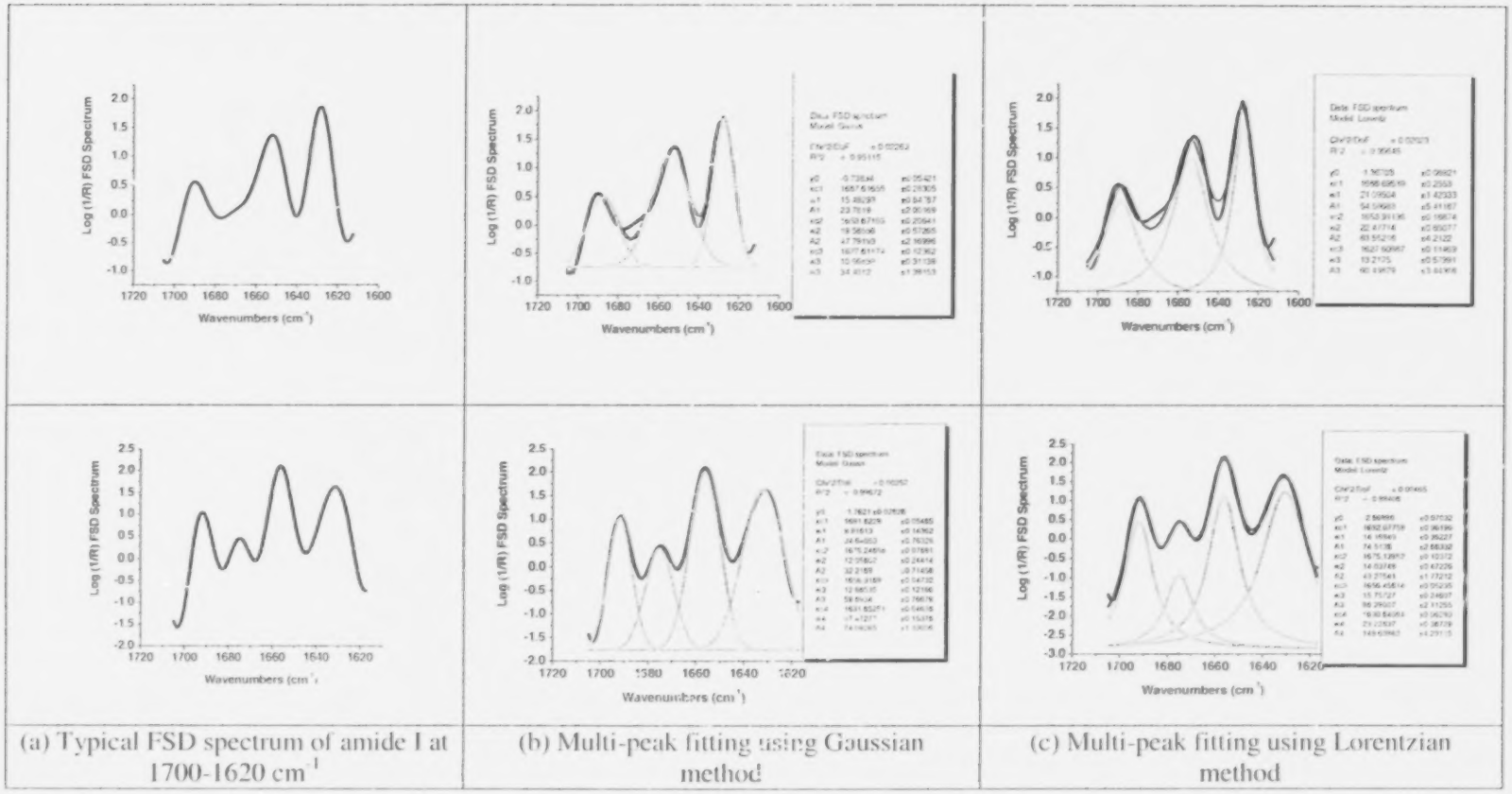

(a) Typical FSD spectrum of amide I at 1700-1620 cm^{-1}

(b) Multi-peak fitting using Gaussian method

(c) Multi-peak fitting using Lorentzian method

Figure 3. Multi-component peaks modeling of typical FSD spectrum of amide I at the region of 1700-1620 cm^{-1} in flaxseed tissue.

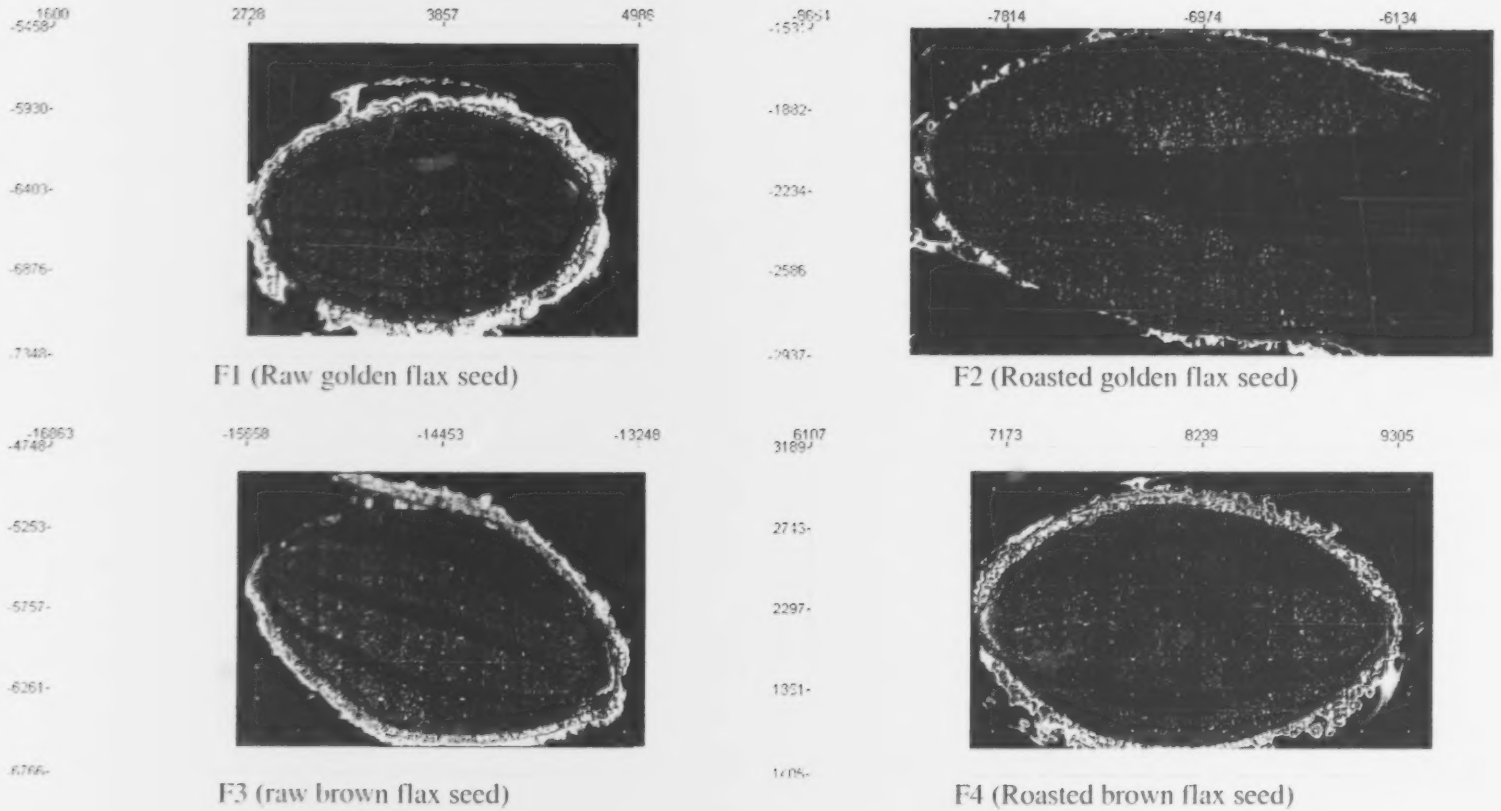

F1 (Raw golden flax seed)

F2 (Roasted golden flax seed)

F3 (raw brown flax seed)

F4 (Roasted brown flax seed)

Figure 4. Photomicrograph of cross-section of the raw (F1) and roasted (F2) golden flaxseed and raw (F3) and roasted (F4) brown flax seed tissues [Note: photomicrograph scale units are μm]

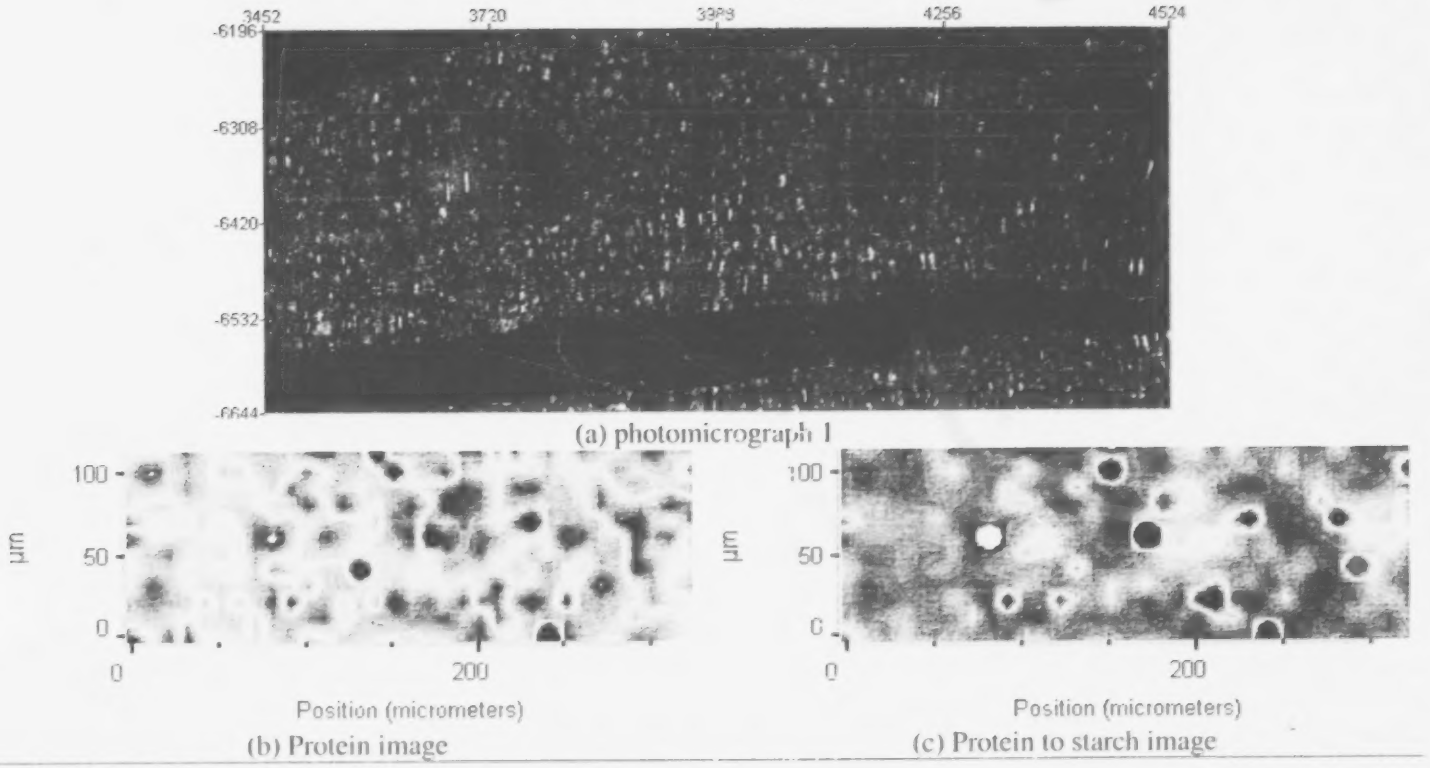

Figure 5. Ultra-structural chemical (functional group) images of the flax seed tissue (F1) (a) Photomicrographs show chemical image area indicated by the rectangle box; (b) protein image in the tissue: area under 1650 cm^{-1} peak area showing protein amide I intensity and distribution; (c) protein to starch ratio image: area under 1650 cm^{-1} peak height divided 1025 cm^{-1} peak height showing protein (amide I) to starch ratio intensity and distribution.

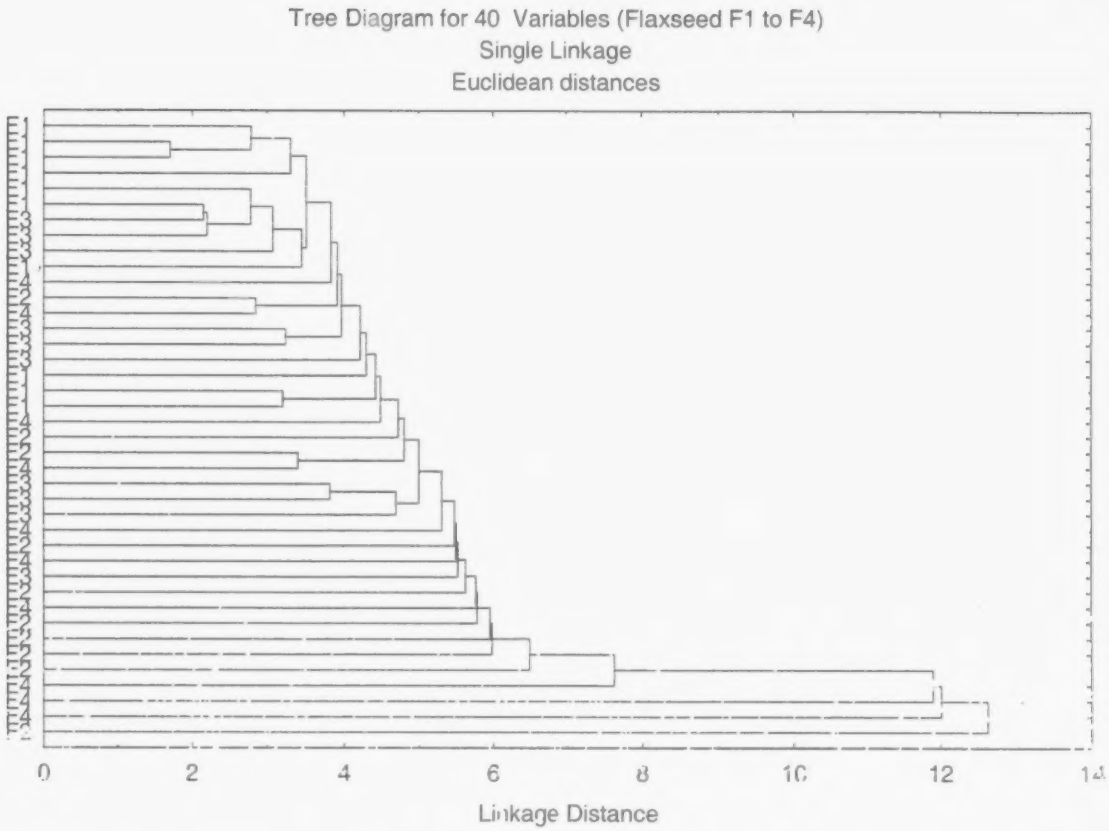

Figure 6. CLA cluster of synchrotron-based protein amide I FSD spectrum (1700-1620 cm^{-1}) obtained from the raw and roasted brown and golden flaxseed tissues (F1, F2, F3, F4) at the cellular level (pixel size 10 μm×10 μm): F1=Raw Golden Flax Seed, F2=Roasted Golden Flax Seed; F3=Raw Brown Flax Seed; F4=Roasted Brown Flax Seed (total sample number for each variety = 20) [CLA analysis: (1) FSD spectral region: amide I; (2) Distance method: Euclidean; (3) Cluster method: Ward's algorithm].

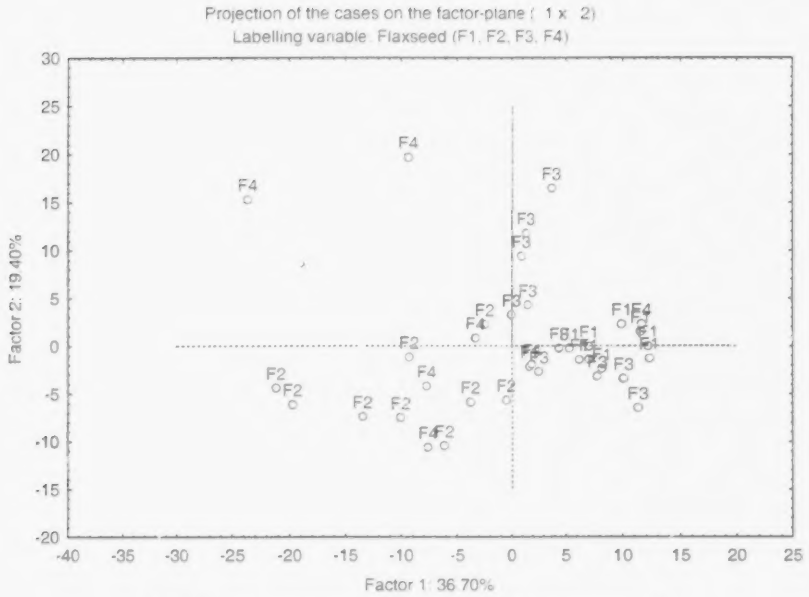

(a) PCA Component 1 vs. PCA Component 2

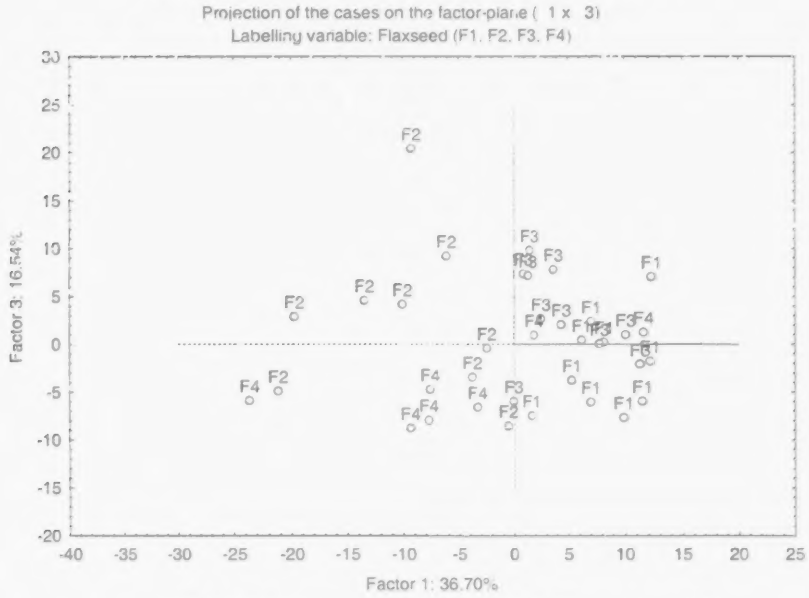

(b) PCA Component 1 vs. PCA Component 3

Figure 7. PCA analysis of synchrotron-based protein FSD amide I spectrum (1700-1620 cm^{-1}) obtained from flaxseed tissues at the cellular level (pixel size 10 μm×10 μm) [F1=Raw Golden Flax Seed, F2=Roasted Golden Flax Seed; F3=Raw Brown Flax Seed; F4=Roasted Brown Flax Seed (total sample number for each variety = 20)]: a) Scatter plot of the 1st principal component versus the 2nd principal component; b) Scatter plot of the 1st principal component versus the 3rd principal component.

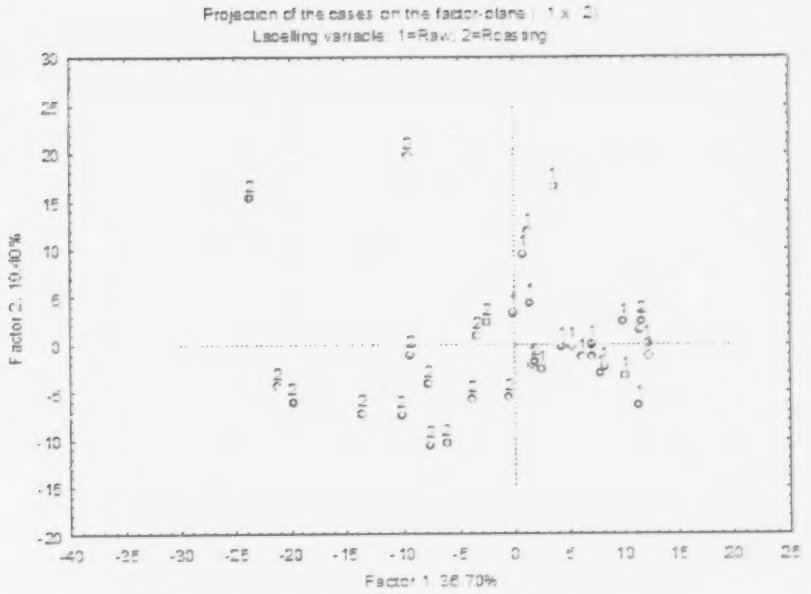

(a) PCA Component 1 vs. PCA Component 2.

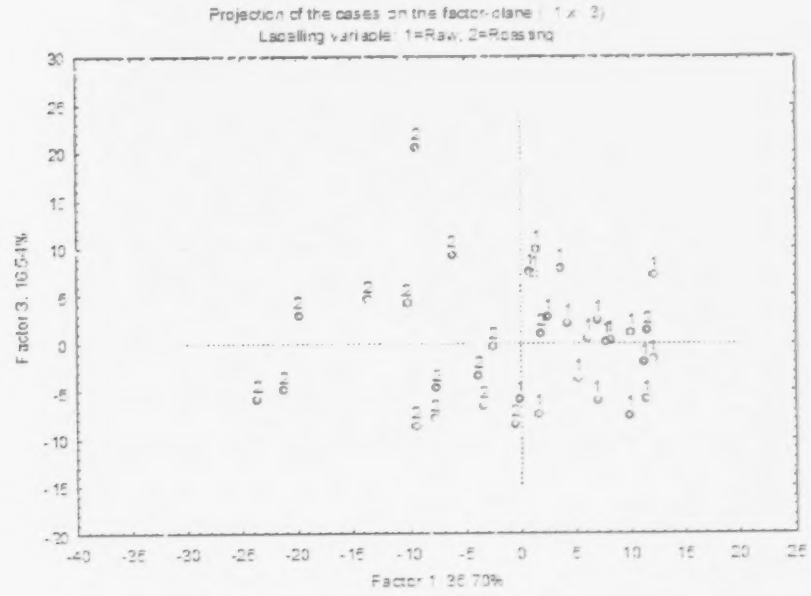

(b) PCA Component 1 vs. PCA Component 3.

Figure 8. PCA analysis of synchrotron-based protein FSD amide I spectrum (1700-1620 cm^{-1}) obtained from raw and roasted flaxseed tissues at a cellular level [1=Raw Flax Seed, 2=Roasted Flax Seed]: a) Scatter plot of the 1st principal component vs. the 2nd principal component; b) Scatter plot of the 1st principal component vs. the 3rd principal component (The 1st principal component explains 36.7% of the variance while the 2nd principal component explains 19.4% of the variance; the 3rd principal component explains 16.5% of the variance).

Project 5: Evaluation of the ability of SR-FTIR in reflectance mode to characterize lignin in brown midrib millet forage leaf and stem material.

Details of this project have not been reported previously as they resulted from a session of sample scanning at the Brookhaven National Laboratory (BNL) National Synchrotron Light Source (NSLS) UIIB end station from Wednesday, April 19, 2006 to Wednesday, April 26, 2006.

Project Summary

Sections of leaf and stem material from brown midrib millet forage samples were scanned using SR-FTIR in reflectance mode to evaluate the adaptability of SR-FTIR to characterization of forages. Spectra were obtained from both leaf and stem tissues using mapping and spot sampling methods. Sampling was focused on the more tightly packed vascular tissues (typically lignified) to avoid the inter- and intra-cellular voids present in the forage tissue. Lignin was identified using the spectra peak at 1510 cm^{-1}, which is characteristic of C-C stretching in the aromatic ring of phenolic compounds. However, this peak did not allow the different forms of lignin to be distinguished (polymers vs. monomers and different forms of monomers. Other peaks characteristic of the different forms of pure lignin overlapped and were masked by other chemical species in these biological samples. The large voids in the non-vascular regions of the brown midrib millet stem and leaf tissues made obtaining quality spectra for analysis very problematic and the lack of other millet varieties for scanning in this incidence prevented comparisons of variety differences in term of total lignin, or ratios of lignin to other chemical species. In conclusion, lignin is detectable but not readily characterized (in terms of form or species) when at low concentrations in heterogeneous tissues, and the porosity of forage tissues causes SR-FTIR microspectroscopy of forage tissue to be problematic.

Project Details

Introduction

Brown midrib mutants exhibit reddish-brown coloration of lignified tissues including leaf midrib and stalk pith (Barrière et al. 2004). Mutants have been identified for corn, sorghum, and millet crops (Cherney et al. 1991). Plants bearing brown midrib mutations demonstrate alter

lignin synthesis resulting in lower levels and less developed lignin (Van Soest 1994). The lower lignin content of brown midrib millet mutants has been associated with increased DM, CP, and NDF *in situ* ruminal degradability (Mustafa et al. 2004; Hassanat et al. 2006).

Synchrotron radiation based Fourier transform infrared microspectroscopy (SR-FTIR) with its intense and small effective source size allows evaluation of molecular chemistry with spatial resolution of 3-10 μm (Miller et al. 1998; Wetzel et al. 1998; Miller et al. 2000 and 2002; Marinkovic et al., 2002). An major advantage of SR-FTIR evaluation is the ability to retain on the spatial origin and distribution of components of interest that is lost during more traditional 'wet' chemistry analysis (Budevska 2002). The ability of SR-FTIR to perform direct *in situ* evaluations (Dokken et al. 2005) also avoids the need for complex chemical analyses.

Conventional infrared spectroscopy was first applied to plant cell wall analysis in 1978 (Morikawa and Senda 1978) and diagnostic spectra of carbonyl stretching for lignin have been found in the 1750-1600 cm^{-1} range, with more intense ring stretching at 1510 cm^{-1} and less intense C-H bond stretching at 1460 cm^{-1} for syringyl than guaiacyl lignins. Characteristic spectral features for lignin and ferulic acid can be observed in the 1700-1500 cm^{-1} range, although overlaps with protein, uronic acid, carboxyl, and carboxylate are problematic (Kačuráková et al. 1999). Akin et al. (1993) found that with conventional globar microspectroscopy, a reduced absorbance at 1510 cm^{-1} (aromatic C-C ring vibration), the pith of stems from bmr (brown midrib) pearl millet plants was less lignified than wild-type plants.

Objective

The objective of this study was to evaluate the suitability of SR-FTIR microspectroscopy to characterization of lignin features in brown midrib millet leaf and stem materials.

Materials and Methods

Brown Midrib Millet

Samples of leaf and stem material from brown midrib millet (CFPBMR) grown in southwestern Québec were obtained from Arif Mustafa, McGill University, Ste. Anne de Bellevue, Quebec.

Synchrotron IR Slide Preparation

The brown midrib millet samples were embedded in paraffin and cut into thin (ca. 6 µm thick) cross-sections with a microtome (Tissue tech, NJ, USA) at the Western College of Veterinary Medicine, University of Saskatchewan. The unstained cross-sections were mounted onto Low-e IR microscope slides (Kevley Technologies, Chesterland, OH, USA) for S-FTIR microspectroscopy in reflectance mode.

Photomicrographs

Photomicrographs of cross-sections (thickness ca. 6 µm) of the brown midrib millet leaf and stem were taken with a digital camera from the slides.

Synchrotron Light Source and FTIR Microspectroscopy

The experiment was carried out on U2B beamline at the National Synchrotron Light Source (NSLS) at Brookhaven National Laboratory (BNL) in Upton, New York. The beamline was equipped with a FTIR spectrometer (Nicolet Magna 860) with KBr beamsplitter and liquid nitrogen cooled MCT detectors coupled with an IR microscope (Nic-Plan™, Nicolet Instruments, Madison, WI) with Schwartzshild 32× objective and 10× condenser. Synchrotron radiation from the VUV storage ring at beamline U2B entered the interferometer via a port on the instrument designed for use with infrared emission. The IR spectra were collected in the mid-IR range 4000-800 cm^{-1} at a resolution of 4 cm^{-1} with a 14 µm diameter round upper aperture. Microscope stage and samples were continuously purged using dry N_2 to minimize IR absorption from water vapor and CO2 in ambient air. Spectra were based on 128 co-added scans for background and 64 co-added scans for samples. Both spot samples and automated mapping samples were collected. Automated mapping steps of 12 µm were slightly smaller than the 14 µm diameter round upper aperture used. Stage control, spectrum data collection and processing were performed using OMNIC 7.2 (Thermo-Nicolet, Madison, WI). Scanned visible images were obtained using a charge-coupled device (CCD) camera linked to the infrared images.

Chemical Imaging

The spectral data were collected and evaluated using OMNIC 7.3 (Spectra Tech, USA). Interest was focused on the 1510 cm^{-1} peak characteristic of aromatic C-C ring vibration and

considered diagnostic for lignin (Akin et al. 1993). The data were displayed as either as a series of spectroscopic images collected at individual wavelengths (1510 cm^{-1}), or as a collection of infrared spectra obtained at each pixel position in the image.

Results and Discussion

Macroscopic and Photomicrograph Evaluation of Brown Midrib Millet

Digital images of the paraffin embedded brown midrib millet (Figure 1) allow macroscopic evaluation of the brown midrib millet stem and leaf material. Lignified areas of the plant, particularly vascular tissue, are visibly pigmented with the reddish brown color characteristic of brown midrib mutants. These images can be contrasted with phloroglucinol stained (phloroglucinol stains lignin and cinnamyl aldehydes red) images of normal and brown midrib corn samples prepared by Halpin et al. (1998). With these images by Halpin et al. (1998), the increased staining intensity of the brown midrib mutant was considered indicative of increased cinnamyl aldehyde. However, phloroglucinol stain dissipates over time.

Photomicrograph of brown midrib millet leaf and stem material (Figure 3) allows some of the structural features of the forage leaf and stem to be evaluated but does not provide any information on the chemical composition of the tissues. The vascular tissues of both the leaf and stem material appear as clusters of tightly packed cells and it is within these clusters that lignified tissues were expected to be imaged. Outside of the vascular tissues, the millet leaf and stem material was quite porous with large voids.

Mapping and Spot Spectra of Brown Midrib Millet Microstructures

A map of vascular tissue from the stem of brown midrib millet (Figure 4) and samples of spot spectra collected from the leaf and stem tissues (Figure 5) demonstrate some of the challenges of using SR-FTIR microspectroscopy on forage tissues to identify and characterize lignin. The mapped image (Figure 4) does show some variations in signal intensity at 1510 cm^{-1}, as expected from existing understanding of lignification of vascular tissue in plants (Halpin et al. 1998). However the spectra for the selected pixel location the shows relatively small size of the 1510 cm^{-1} peak used to diagnose lignin, and regions of low lignin intensity in the mapped image are due to voids in the scanned tissue. The impact of these voids is particularly apparent when considering the spot sample spectra from the pith tissues of the brown midrib millet stem

material (Figure 5, bottom). These spectra show very low signal and very high noise, not just at the peak associated with lignin, but also at the peaks associated with protein (amide 1 and amide 2) and carbohydrate. There are two explanations for this observation: 1) the reflectance mode used for the SR-FTIR microspectroscopy scanning does not yield as 'clean' a spectra as does the transmission mode scanning (not considered an option with the size of the millet sections (Figure 1) vs. the 13 mm BaF_2 disks used for SR-FTIR transmission microspectroscopy; and 2) the porosity of forage tissue. The sample preparation (embedding in paraffin for sectioning and then removal of the paraffin) strips all cell contents leaving on cell wall material. Travis et al. (1997) used confocal laser microspectroscopy to measure cell wall thickness in maize internode tissues and found the thickness of cell walls to vary from 1.13 to 2.14 µm depending on tissue type. Combined with the cell dimensions of the tightly packed vascular tissue imaged in Figure 4 (minimum cell width and height ≈ mapping step size of 12 µm) and the upper aperture diameter of 14 µm (approaching the diffraction limit for the longer wavelengths as apparent for the ca. 800 cm^{-1} spectra from the bottom of Figure 5) the chemical features within a cell wall can not be resolved with regard to location and the scan for chemical features any location selected for a spot spectra will consist of largely void where cell content material had been present.

A last complication in the characterization of lignin in plant tissue is that the peak at 1510 cm^{-1} that is considered diagnostic for lignin does not provide information on the type of lignin present (monomer vs. polymer or variety of monomer), and can even be confused with the aromatic ring features present in some amino acids. The spectral features of lignin species that differ with the various forms of lignin overlap with many of the other chemical signatures present in plant tissues making it very difficult to distinguish these features, especially with the relatively low lignin content of forage tissues (the brown midrib millet in this study contained 8 to 17 g ADL per kg DM (Mustafa et al. 2004; Hassanat et al. 2006) as opposed to wood tissues or purified lignins.

Conclusions

From this initial investigation into use of SR-FTIR in reflectance mode to evaluate and characterize lignin in brown midrib millet forage leaf and stem materials, it is apparent that this methodology can detect lignin in these samples. However, the porosity of the samples makes it difficult to achieve strong signal to noise ratio unless sampling (via mapping or spot sampling) is

confined to areas of small tightly packed cells (vascular tissue). Further, the spectral characteristics that would distinguish different forms of lignin, as opposed to merely identifying the aromatic C-C ring vibration of phenolic groups at 1510 cm^{-1}, are not readily resolvable when lignin is present at low concentrations in plant tissues preventing lignin form (monomer vs. polymer, and variety of monomer) from being identified. With samples from only one variety of millet, it was not possible to determine if differences in the total amount of lignin present or the ratio of lignin to other chemical species of interest differed between varieties.

Literature Cited

Akin, D. E., Himmelsbach, D. S., Carl, R. T., Hanna, W. W., and Barton, II, F. E. 1993. Mid-infrared microspectroscopy to assess lignin in plant tissues related to digestibility. Agron. J. 85:171–175.

Barrière, Y., Ralph, J., Mèchin, V., Guillaumie, S., Grabber, J. H., Argillier, O., Chabbert, B., and Lapierre. 2004. Genetic and molecular basis of grass cell wall biosynthesis and degradability. II. Lessons from brown mid-rib mutants. C. R. Biologies. 327:847-860.

Budevska, B. O. 2002. Vibrational Spectroscopy. pp 3720-3732.

Cherney, J. H., Cherney, D. J. R., Akin, D. E., and Axtell, J. D. 1991. Potential of brown-midrib, low-lignin mutants for improving forage quality. Adv. Agron. 46:157-198.

Dokken, K. M., Davis, L. C., and Marinkovic, N. S. 2005. Use of infrared microspectroscopy in plant growth and development. Appl. Spectroscopy Rev. 40:301–326.

Halpin, C., Holt, K., Chojecki, J., Oliver, D., Chabbert, B., Monties, B., Edwards, K., Barakate, A., and Foxon, G. A. 1998. Brown midrib maize (bm1) – a mutation affecting the cinnamyl alcohol dehydrogenase gene. The Plant Journal. 14:545-553.

Hassanat, F., Mustafa, A. F., and Seguin, P. 2006. Chemical composition and ensiling characteristics of normal and brown midrib pearl millet harvested at two stages of development in southwestern Québec. Can. J. Anim. Sci. 86:71-80.

Kačuráková, M., Wellner, N., Ebringová, A., Hromádková, Z., Wilson, R. H., and Belton, P. S. 1999. Characterisation of xylan-type polysaccharides and associated cell wall components by FT-IR and FT-Raman spectroscopies. Food Hydrocolloids. 13:35–41.

Martin, M.C. 2002. Fourier-Tranform Infrared Spectroscopy. Retrieved in October 2002 from: http://infrared.als.lbl.gov/

Miller, L. M. 2000. The impact of infrared synchrotron radiation on biology: past, present, and future. Synchrotron Radiation News. 13:31-37.

Miller, L. M. 2002. Infrared Microspectroscopy and Imaging. Retrieved in October 2002 from: http://www.nsls.bnl.gov/newsroom/publications/otherpubs/imaging/workshopmillerhighres.pdf#search=%22infrared%20microspectroscopy%20and%20imaging%22

Morikawa, H., and Senda, M. 1978. Infrared analysis of oat coleoptile cell walls and oriented structure of matrix polysaccharides in the walls. Plant Cell Physiol. 19:327–336.

Mustafa, A. F., Hassanat, F., and Seguin, P. 2004. Chemical composition and *in situ* nutrient

degradability of normal and brown midrib forage pearl millet grown in southwestern Québec. Can. J. Anim. Sci. 84:737-740.

Travis, A. J., Murison, S. D., Perry, P., and Chesson, A. 1997. Measurement of cell wall volume using confocal microscopy and its application to studies of forage degradation. Annals of Botany. 80:1-11.

Van Soest, P. J. 1994. Nutritional ecology of the ruminant. 2nd ed. Cornell University Press, Ithaca, NY. Page 92.

Wetzel, D. L., Eilert, A. J., Pietrzak, L. N., Miller, S. S., and Sweat, J. A. 1998. Ultraspatially resolved synchrotron infrared microspectroscopy of plant tissue in situ. Cell. Mol. Bio. 44:145-167.

Figures

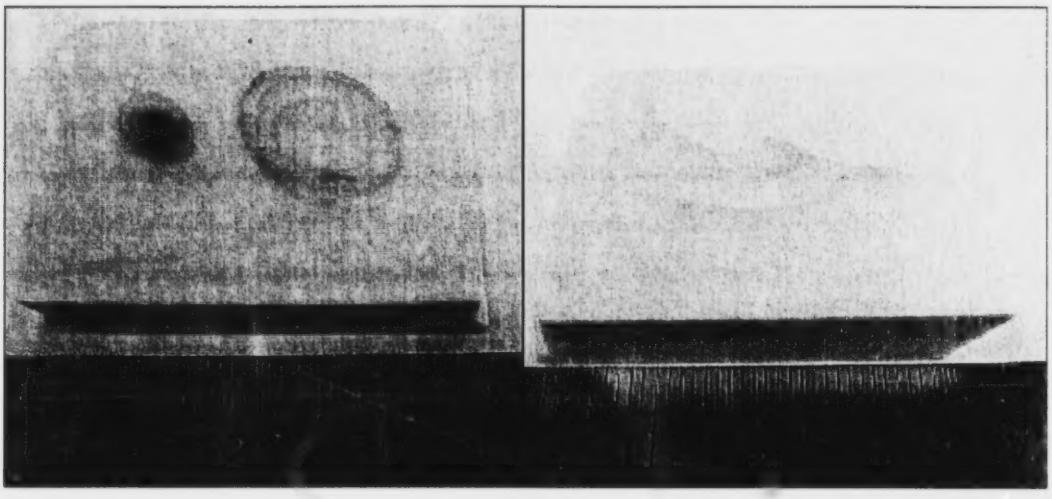

Figure 1. Paraffin embedded brown midrib millet stem (left image) and leaf (right image) samples. Note the brown coloration of the lignified vascular tissues due to the brown midrib mutation. Scale is in cm.

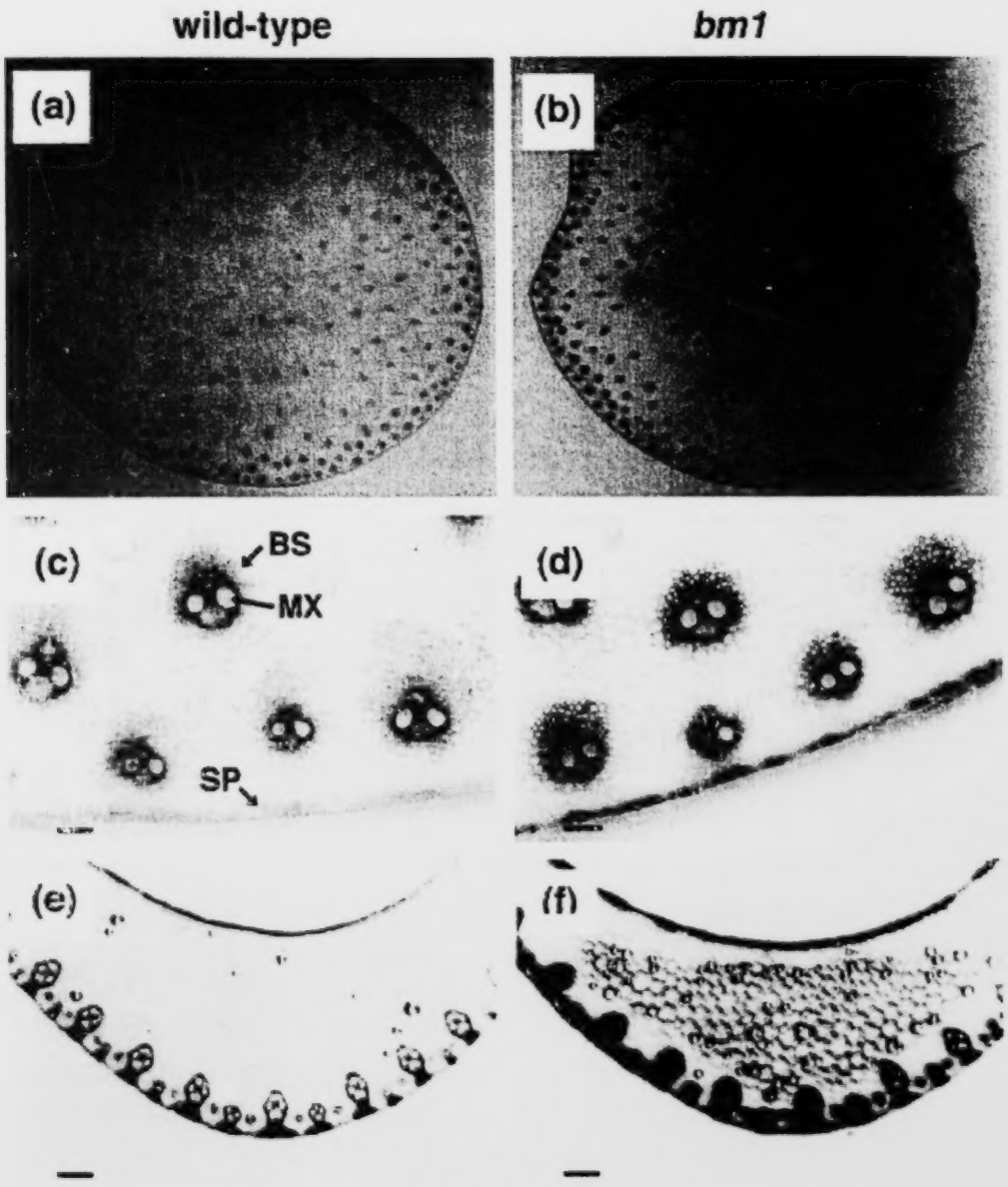

Figure 2. Phloroglucinol staining of tissue sections from bm1 and wildtype maize. Sections of stem (a–d) and midrib (e,f) were taken from wildtype (a,c,e) and bm1 mutant (b,d,f) plants and stained with acid phloroglucinol. Magnification bars represent 100 μm. SP = subepidermal sclerified parenchyma; BS = bundle sheath; MX = metaxylem vessels. From Halpin et al. (1998).

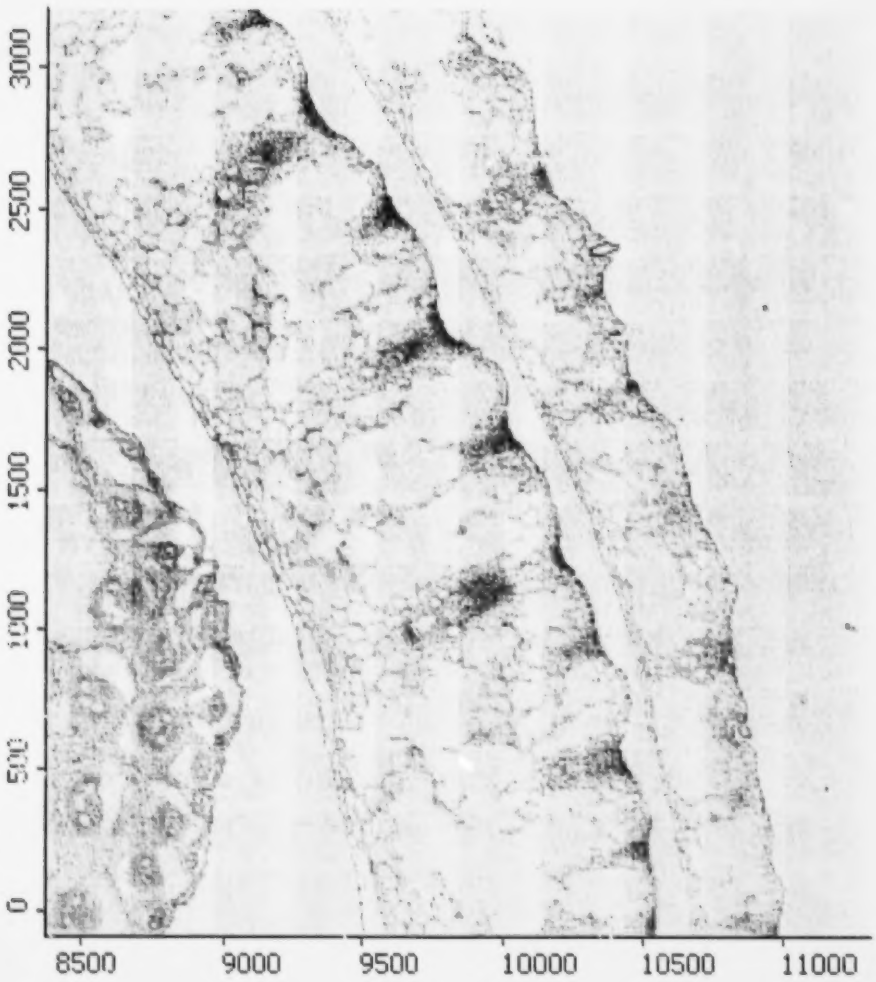

Figure 3. Photomicrograph of brown midrib millet stem and leaf material. Organizational differences between stem (left section) and leaf (center and right section) are apparent. Note the porosity of the forage tissues and the lack of chemical information obtainable from visible light images. Scale is in µm.

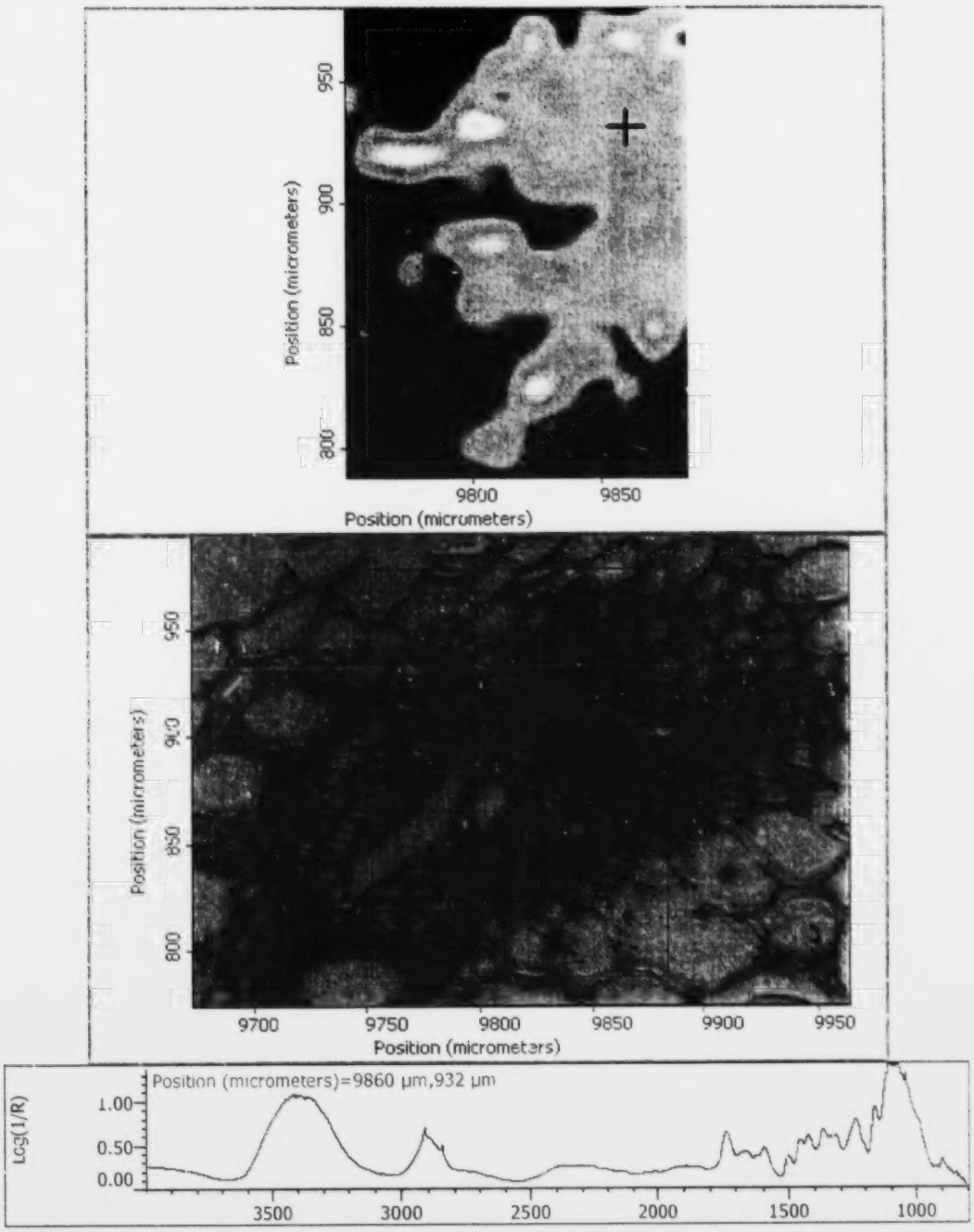

Figure 4. Mapped image from a vascular bundle within the stem of brown midrib millet. False color image (top) represents signal intensity at 1510 cm^{-1} (blue =0, red =1) which is indicative of aromatic C-C ring vibration and diagnostic of lignin. Photomicrograph (center) shows the visual image of the mapped vascular bundle. Absorption spectra (bottom left) for the selected scan location (indicated by the red cross in the top left and right images) shows the 1510 cm^{-1} peak.

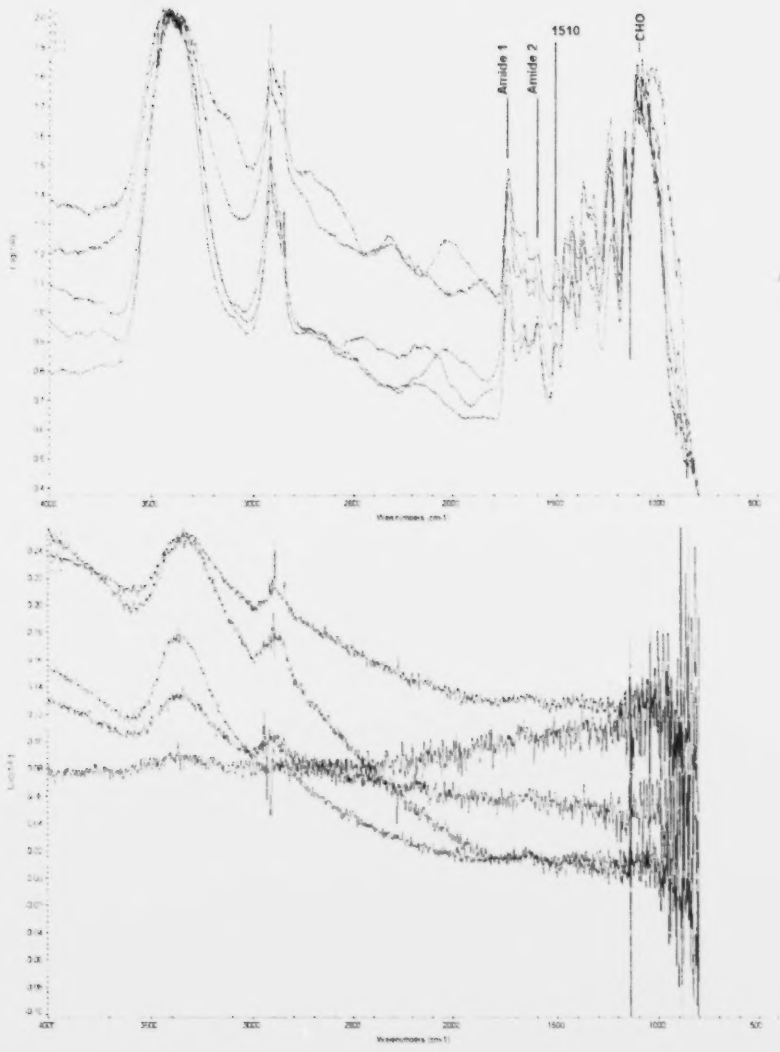

Figure 5. Spot sample spectra from brown midrib millet leaf vascular (top) and millet stem non-vascular pith tissues (bottom). The top image has the amide 1, amide 2, carbohydrate (CHO), and lignin diagnostic (1510) peaks identified. The bottom image shows very low signal and very high noise in sampled spectra and is unusable for spectral analysis.

Project 6: Evaluation of the ability of soft X-ray absorption near-edge spectroscopy (XANES) to evaluate zinc supplementation of cattle.

Details of this project have not been reported previously as they resulted from a session of sample scanning at the Canadian Synchrotron Light Source (CLS) spherical grating monochromator (SGM) end station from Friday, July 7, 2006 to Saturday, July 8, 2006.

Project Summary

Samples of common forms of Zn supplements (ZnO, $ZnSO_4 \cdot H_2O$, and Zn methoinine) were evaluated in 'pure' form, or after mixing with dried and ground ruminal, duodenal, and fecal material collected from dairy cattle fed a diet containing ca. 65 mg/kg (at concentrations ranging from 0 mg/kg to 50000 mg/kg) using the SGM soft X-ray beamline at CLS. Distinct spectra that could be used as 'fingerprints' were generated for the 'pure' feed grade samples of ZnO, $ZnSO_4 \cdot H_2O$, and Zn methoinine showing some promise for use of X-ray absorption near-edge spectroscopy (XANES) in evaluation of trace mineral supplements for cattle. However, when lower concentrations of Zn supplements were prepared by diluting the feed grade supplements with ZnO, $ZnSO_4 \cdot H_2O$, or Zn methoinine, the distinct spectral features were greatly diminished and masked by signal noise. Several different approaches attempted in effort to improve spectral clarity were unsuccessful, and Zn speciation could not be identified against the largely carbohydrate background of ruminal, duodenal, or fecal material at concentrations as low as what would be expected *in vivo*. Based on the current results of this evaluation, we can not recommend use of XANES for characterization of Zn speciation from *in vivo* samples. However, there have been recent improvements in the detector sensitivity at the SGM end station at the CLS and we are awaiting an opportunity to determine if the improvement will allow characterization of Zn speciation at the low concentrations presented by *in vivo* samples.

Project Details

Introduction

Zinc is an essential trace mineral required by beef cattle at 30 mg per kg of DM (NRC 2000). Both inadequate and excessive consumption of zinc results in problems with animal health and production due to nutrient deficiencies or toxicities (NRC 2000). Zinc

supplementation is effective at preventing disease with deficient animals, but not normal animals (Lopez et al. 1999). However, elevated supplementation of zinc (up to 120 ppm) has been promoted and utilized as a therapeutic agent to prevent lameness. This is a concern as excess zinc interacts with other nutrients (Figure 1) (Puls 1988; NRC 2000) and has been shown to reduce *in vitro* digestion and growth of digestive microflora (Martinez and Church 1970; Martinez 1973). Ott et al. (1966) observed a 73% decrease in energy yielding volatile fatty acids with high zinc supplementation.

Despite the relatively extensive study of trace mineral nutrition, numerous issues remain to be addressed. Importantly, nutritional recommendations do not take into account differences in availability or the interactions that can occur when different forms of a given trace mineral are fed, and in many cases the details of mineral interactions are not well defined. As an example, zinc oxide and zinc sulfate are common forms of inorganic zinc used to supplement cattle diets. Both forms are considered to be equally available despite the fact that zinc oxide is insoluble in water. Additionally, organic chelates of zinc, including zinc methionine or zinc proteinate, may be used to provide supplementary zinc and are thought to be beneficial, not because of a greater rate of absorption, but because of different metabolism and less potential for interaction with other microminerals within the digestive tract. However, changes in the form of trace minerals as they pass through the digestive tract and are exposed to microbial fermentation and digestive enzymes and changes in pH ranging from strongly acidic to weakly alkaline, have not been well studied. To our knowledge, there is only one article published using synchrotron radiation to evaluate selenium (Christensen et al. 2004).

Historically, identifying mineral availability in the digestive tract has been problematic, requiring radioactive materials and/or multiple chemical methods and yielding little information on mineral speciation. Synchrotron XANES radiation provides a method of evaluating speciation and oxidation state in "as is" samples, avoiding errors in traditional wet chemistry techniques and use of radioactive materials in animals.

Objective

The objective of this study was to use synchrotron radiation to generate distinct XANES spectra for different zinc species from purified samples (feed grade) and determine if the zinc concentration in biological samples with varying levels of added zinc is within the detection

threshold of the synchrotron instrumentation.

Materials and Methods

Zinc Samples

Shawn Fairbairn of New Life Feeds (Saskatoon, Saskatchewan) courteously provided us with the following:

Company	Trade Name	Chemical Name	Amount	Zinc concentration
Pestell Minerals & Ingredients	Zinc sulphate monohydrate Mini Granule & Powder	Zinc sulphate monohydrate	1 kg	35.5%
Zinc Nacional, S. A.	Maximo 720	Zinc oxide	1 kg	72.0%
ZinPro Corp.	ZinPro 100	Zinc methionine	1 kg	10.0%

Ruminal, Duodenal, and Fecal Samples

Samples of ruminal, duodenal, and fecal material were collected from ruminally and duodenally cannulated lactating Holstein cows on trial at the University of Saskatchewan Dairy Unit (Saskatoon, SK). Cows were fed a barley grain, barley silage, and hay based diet supplemented to contain ca. 65 ppm Zn. Samples were freeze dried to remove most of the moisture and then dried at 55 °C in a forced air drying oven prior to grinding to pass through a 1 mm screen. Samples were later reground to pass through a 0.25 mm screen.

Preparation of Zn 'Doped' Samples

Dried and ground ruminal, duodenal, and fecal materials were initially mixed with each of the Zn supplement forms to result in final mixtures containing ca. 100 to 900 mg/kg added zinc (in 200 mg/kg increments). Later, dried and ground ruminal, duodenal, and fecal materials were mixed with each of the Zn supplement forms to generate mixtures with ca. 1 to 5% added Zn (10,000 or 50,000 mg/kg).

Synchrotron Scanning

Synchrotron scanning used the SGM soft X-ray beamline at the CLS (Saskatoon, SK) on July 7 and 8, 2006. Scans were focused on the first harmonic with gap set points of 27.5 to 27.6

mm and no gap offset. The entrance slit was 0.25 mm and the exit slit ranged from 20 to 500 μm. With an exit slit of 20 μm, the sample scan area was ca. 0.2 mm horizontal by 0.5 mm vertical; at 500 μm, the sample scan area is ca. 5 mm horizontal by 0.5 mm vertical. Scans focused on the energy range of 1025 to 1080 eV with step sizes of 0.1 to 0.5 eV. Samples were mounted on the sample holder with conductive carbon tape. Both total electron yield and fluorescence were evaluated.

Results and Discussion

The standardized spectra for each of the 'pure' forms of the common source of supplemental Zn for livestock feeds are presented in Figure 2. That the relative intensity of the standardized spectra differ with each of the forms is not unexpected as each supplement contains a different level of supplemental Zn. It is important to not that the spectral features differ for each of the Zn supplement forms. One of the advantages of XANES analysis is that these differences can provide information on the oxidation state (Zn has only one oxidation state) and chemical species of elements. A further advantage is that this information on chemical species and oxidation state does not require detailed spectral analysis. Rather, the spectra of known 'pure' samples can be used as 'fingerprints' to identify the oxidation state and chemical species of elements in unknown samples. With these spectra (Figure 2), we were able to achieve our first objective of generating distinct XANES images for the various forms of Zn which could potentially be used to identify Zn speciation in unknown samples.

Standardized spectra from duodenal digesta samples 'doped' with 5% Zn as ZnO are presented in Figure 3. From these spectra, some of the distinctive features of ZnO are apparent. However, also apparent is the poor signal to noise ratio with these samples. This situation worsened with the fecal material 'doped' with 1 or 5% Zn as Zn methionine where fewer spectral features were observable and much poorer signal to noise ratio (Figure 3). When analysis of samples with 100 to 900 mg/kg Zn was attempted, no discernable Zn spectral features could be observed. Several different approaches were attempted to achieve improved spectrum from these low level samples including finer grinding and sample layering to reduce 'charging', use of indium metal to increase signal strength, increasing exit slit width to increase sample scan area, leaving the soft X-ray beamline focused on an area for an extended period of time before scanning to 'burn off' interfering material, and sample fluorescence.

Sample charging results from the accumulation of displaced electrons on insulative materials, such as the carbohydrates present in ruminal, duodenal, and fecal material, prior to discharges that manifest as increased spectral noise. Fine grinding and thinner sample layering were able to reduce the amount of charging occurring and therefore the amount of noise in the spectra, but not sufficiently to allow spectral features to be identified. Use of indium metal improve electrical conductivity and was able to improve overall signal strength resulting in an increase in spectral baseline height, but was unable to improve signal to noise ratio and identification of spectral features. Increasing sample scan area by increasing exit slit width likewise did not improve spectral resolution. Charring of the sample with the soft X-ray beamline prior to scanning to reduce sample charging did not noticeably improve spectral resolution beyond that observed with finer sample grinding and thinner layering. Use of fluorescence detection also proved unsuccessful at improving spectral resolution due to the low fluorescence of Zn.

Since the completion of this series of scanning, the SGM beamline at the CLS has improved the sensitivity of its detectors through conditioning. There was an opportunity to re-evaluate some samples on September 9, 2006 to determine if the improved detector sensitivity would allow for good spectral resolution with low levels of Zn, or if other trace minerals of interest could be resolved. Unfortunately, equipment problems at the CLS at that time prevented sample scanning and we are still waiting for a future opportunity.

Conclusion

Based on the results of this initial investigation, soft X-ray XANES is capable of differentiating between different chemical species of Zn supplements when Zn is present a relatively high concentrations. However high signal to noise ratio prevents adequate spectral resolution when attempting to evaluate Zn speciation with low concentrations of Zn (<5%). Given that the maximum tolerable level of Zn in cattle diets is 500 mg/kg (NRC 2000), it appears that soft X-ray XANES is currently unsuitable for evaluation of Zn trace mineral speciation in cattle digesta and will remain so unless improvements are made in detector sensitivity and spectral resolution.

Literature Cited

Puls, R. 1988. Mineral Levels in Animal Health: Diagnostic Data. Sherpa Int. Claerbrook, BC.

NRC. 2000. Nutrient Requirements of Beef Cattle: Seventh Revised Edition: Update 2000. National Academy Press. Washington, DC.

Lopez, J. R., Montana, J. R. G., Diez, A. J. A., and Montana, F. P. 1999. Failure of oral zinc supplementation to control ovine foot rot. Small Rum. Res. 31: 273-276.

Martinez, A. 1973. The effects of mineral elements on *in vitro* rumen cellulose digestion. Ph. D. Thesis. Oregon State University, Corvalis, OR.

Martinez, A. and Church, D. C. 1970. The effects of various mineral elements on *in vitro* rumen cellulose digestion. J. Anim. Sci. 31:982-990.

Ott, E. A. , Smith, W. H., Harrington, R. B., Stob, M., Parker, H. E.m and Beeson, W. M. 1966. Zinc toxicity in ruminants. 3. Physiological changes in tissues and alterations in rumen metabolism in lambs. J. Anim. Sci. 25:424-431.

Christensen, C. R., Cutler, J. N., and Christensen, D. A. 2004. Using X-ray absorption near edge structure (XANES) spectroscopy to determine selenium oxidation states in animal mineral supplements and feeds. Can. J Anim. Sci. 84:171–175.

Figures

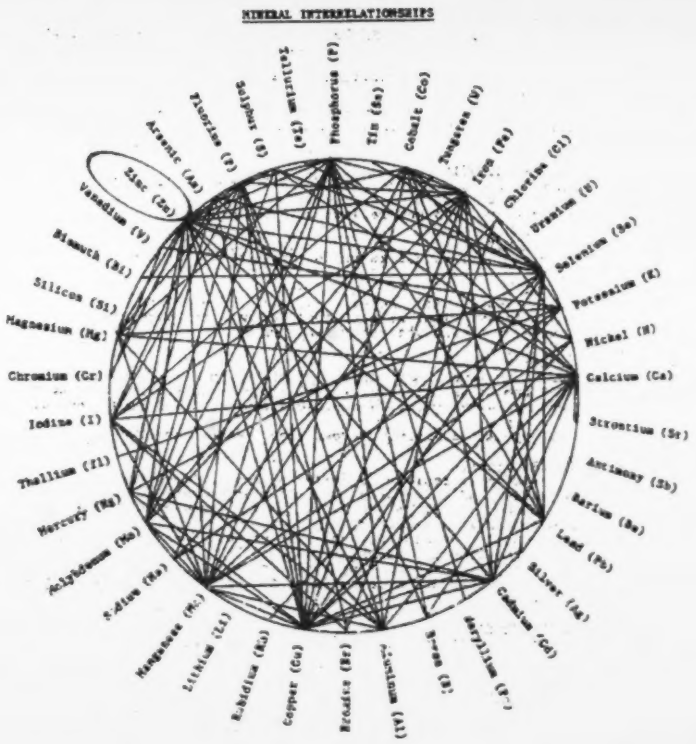

Figure 1. Mineral interrelationships. (Puls 1988)

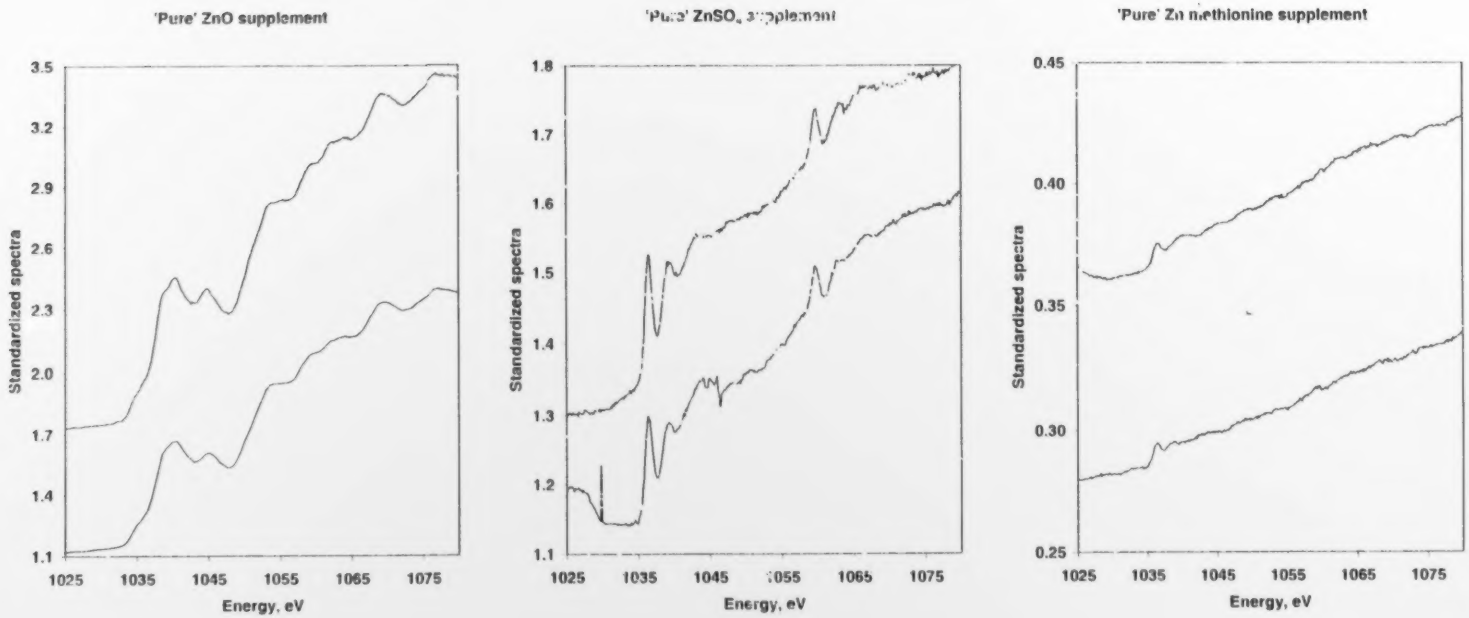

Figure 2. Standardized spectra for the various 'pure' forms of Zn commonly used as feed supplements. The ZnO (left) contains ca. 72% Zn, the $ZnSO_4$ (center) contains ca. 35.5% Zn, and the Zn methionine (right) contains ca. 10% Zn. Note the very different spectral 'fingerprints' for each of the supplement forms.

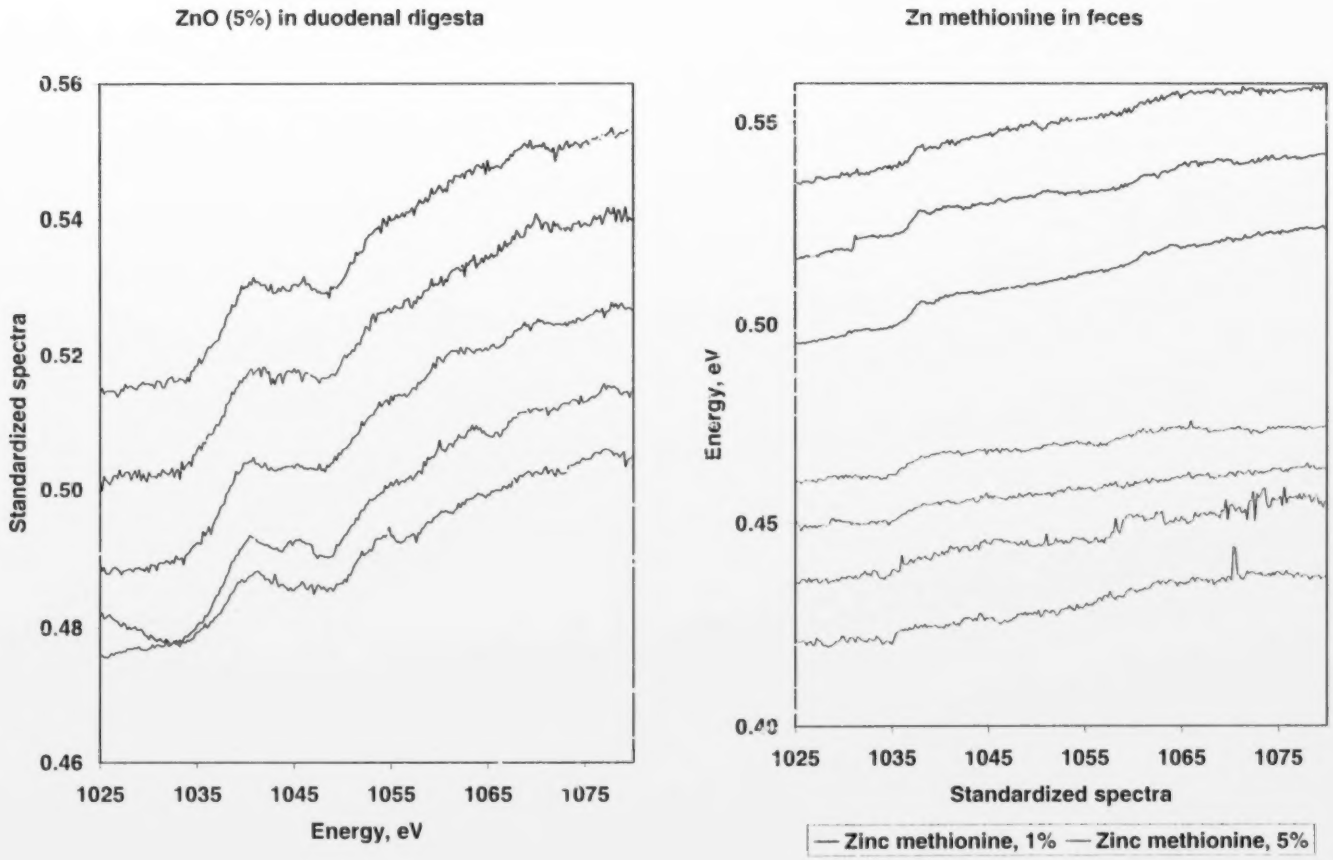

Figure 3. Standardized spectra for ZnO in duodenal digesta (at 5% Zn, left image) and Zn methionine in feces (at 1 or 5% Zn, right image). Some of the spectral features of ZnO are apparent, but with poor signal to noise ratio. Fewer features are apparent with the Zn methinione in feces (especially at 1% Zn) and with much poorer signal to noise. Baseline differences may be attributed to artifacts of sample thickness, etc.

Research Publications and Seminars

Yu, P. 2003. Synchrotron infrared microspectroscopy as an advanced bioanalytical microprobe for biological sciences. ANSC 813 - Monogastric Animal Nutrition, Dept. of Animal and Poultry Sciences, University of Saskatchewan, Saskatoon, SK, Canada, January 16 (Invited Lecture) (Synchrotron project).

Yu, P. 2004. Current synchrotron-based feed and nutrition related research. Research information update. VIDO Conference Centre, University of Saskatchewan, Saskatoon, SK, Canada. April 13-14, 2004. Seminar for livestock specialists in Saskatchewan.

Yu, P. 2004. Invited Lecture. Synchrotron analytical techniques. ANSC – 898.3. Advanced Laboratory Techniques. Dept. of Animal and Poultry Science, University of Saskatchewan, Saskatoon, SK. Canada, Dec 3, 2004 (Invited Lectures by Research Scientist Andrew Olkowski).

Yu, P., Christensen, C. R., Christensen, D. A., and McKinnon, J. J. 2005. Ultrastructural-chemical makeup of yellow- (Brassica rapa) and brown-seeded (Brassica napus) canola within cellular dimensions, explored with synchrotron reflection FTIR microspectroscopy. Canadian Journal of Plant Science. 85:533-541.

Yu, P., Christensen, D. A., Christensen, C. R., Drew, M. D., Rossnagel, B. G., and McKinnon, J. J. 2004. Use of synchrotron Fourier transform infrared microspectroscopy to identify chemical differences in barley endosperm tissue in relation to rumen degradation characteristics. Can. J. Anim Sci. 84:523-527.

Yu, P., J.J. McKinnon, C.R. Christensen, and D.A. Christensen. 2004. Quantify the α-Helix, β-Sheet and Their Ratio in Protein Secondary Structure of Various Feed Protein Sources at Ultra-Spatial Resolution and Relation to Protein Value. Proceeding of Canadian Light Source (CLS) 7th Annual Users' Meeting and Workshops 2004, University of Saskatchewan. November 17th - 21th, 2004. pp. 42.

Yu, P., McKinnon J. J., Christensen, C. R., and Christensen, D. A. 2004. Overview - current synchrotron-based feed and nutrition related research in our department. Dept. of Animal and Poultry Science, University of Saskatchewan, Saskatoon, SK, Canada, November 25 (Seminar for CLS and College of Agriculture).

Yu, P., McKinnon J. J., Christensen, C., and Christensen, D. A. 2003. Mapping plant composition with synchrotron infrared microspectroscopy and relation to animal nutrient

utilization. Proc. Canadian Society of Animal Science - Annual Conference. Saskatoon, SK, Canada, June 10-13, 2003 (Invited Article and Speaker: 20 pages).

Yu, P., McKinnon, J. J. and Christensen, D. A. 2003. Using advanced synchrotron infrared and X-ray techniques for animal feed research. Dairy Research Report, University of Saskatchewan, Saskatoon, SK, Canada.

Yu, P., McKinnon, J. J., and Christensen, D. A. 2003. Application of synchrotron IR microspectroscopy in biological sciences. Seminar. Dept. of Animal and Poultry Science, University of Saskatchewan, Saskatoon, SK, Canada. January 27, 2003.

Yu, P., McKinnon, J. J., Christensen, C .R., Rossnagel, B., Drew, M. D., and Christensen, D. A., 2003. Using synchrotron infrared microspectroscopy (SR-FTIR) to explore chemical difference in matrix of micro-endosperm tissue within cellular dimension between two barleys (Harrington vs. Valier) in relation to rumen degradation characteristics. Cellular and Molecular Biology. In Review (internal).

Yu, P., McKinnon, J. J., Christensen, C. R. Drew, M. D., and Christensen, D. A. 2002. Synchrotron Fourier transform infrared microspectroscopy as a novel bioanalytical microprobe for ultrastructural matrix of barley endosperm tissue. Proc. The 5th CLS Users Meeting and Synchrotron Workshop - Applications of Synchrotron Radiation in the Biological/ Life Sciences. Saskatoon, SK, Canada, November 15-16. pp. 30.

Yu, P., McKinnon, J. J., Christensen, C. R., and Christensen, D. A. 2003. Reveal spatially localized chemical functional groups and biological components of plant (feed) tissues using synchrotron FTIR microspectroscopy-U10B and U2b. The 6th Annual Synchrotron CLS Users' Meeting and Associated Synchrotron Workshops – WinXAS and Infrared. Proceeding of the 6th Annual Synchrotron CLS Users' Meeting and Associated Synchrotron Workshops. November 13-15, 2003. Saskatoon, SK, Canada. pp. 21.

Yu, P., McKinnon, J. J., Christensen, C. R., and Christensen, D. A. 2003. Synchrotron FTIR spectroscopic characteristics and chemical features of micro-structural matrix of cereal grains -wheat, corn, oats and barleys in relation to nutrient utilization and digestive behaviors in ruminants. The 6th Annual Synchrotron CLS Users' Meeting and Associated Synchrotron Workshops – WinXAS and Infrared. November 13-15, 2003. Saskatoon, SK, Canada. Pp. 22.

Yu, P., McKinnon, J. J., Christensen, C. R., and Christensen, D. A. 2004. Using synchrotron-based FTIR microspectroscopy to reveal chemical features of feather protein secondary structure: Comparison with other feed protein sources. Journal of Agricultural and Food Chemistry. 52:7353-7361.

Yu, P., McKinnon, J. J., Christensen, C. R., and Christensen, D. A. 2004. Imaging molecular chemistry of Pioneer corn. Journal of Agricultural and Food Chemistry. 52:7345-7352.

Yu, P., McKinnon, J. J., Christensen, C. R., and Christensen, D. A. 2004. Using synchrotron transmission FTIR microspectroscopy as a rapid, direct and non-destructive analytical technique to reveal molecular microstructural-chemical features within tissue in grain barley. Journal of Agricultural and Food Chemistry. 52:1484–1494.

Yu, P., McKinnon, J. J., Christensen, C. R., and Christensen, D. A. 2004. Use of synchrotron-based FTIR microspectroscopy to reveal chemical features of feather protein secondary structure and its relation to protein value. J. Anim.Sci. 82(Suppl.1)/J. Dairy Sci. 87(Suppl. 1)/Poult. Sci. 83(Suppl.1):220.

Yu, P., McKinnon, J. J., Christensen, C. R., Christensen, D. A., Marinkovic, N. S., and Miller, L. M. 2003. Chemical imaging of micro-structures of plant tissues within cellular dimension using synchrotron infrared microspectroscopy. Journal of Agricultural and Food Chemistry. 51:6062-6067.

Yu, P., McKinnon, J. J., Christensen, C., and Christensen, D. A. 2003. Possibility of using synchrotron based analytical technique (SR-FTIR) as a research tool for plant breeding. 1st Canadian Plant Genomics Workshop. August 23-26, 2003. Saskatoon, SK, Canada.

Yu, P., McKinnon, J. J., Christensen, C., Drew, M., and Christensen, D. A. 2003. Structural and chemical difference between two barley tissues measured by synchrotron infrared microspectroscopy. Canadian Journal of Animal Science. 83(3) (Abstract):657 [Proceeding of The Canadian Society of Animal Science - Annual Conference, 10-13 June 2003, University of Saskatchewan, Saskatoon, Canada (Abstract R81) pp 61].

Yu, P., McKinnon, J. J., Christensen, C., Drew, M., Rossnagel, B.G., and Christensen, D.A. 2003. Using synchrotron infrared microspectroscopy to probe molecule chemical difference between two types of barley with distinguished biodegradation behaviors in ruminants. J. Anim. Sci. 81.(Suppl. 1):267-268.

Yu, P., McKinnon, J. J., Christensen, D. A. 2003. Structural characterization of low lignin (AC

Assinobia) and high lignin (normal) of oat hulls by diffuse-reflectance Fourier transform vibrational infrared spectroscopic analysis. The British Society of Animal Science, Annual Meeting, University of York, UK. March 24-26, 2003. Summary of paper – Ref. No. 128.

Yu, P., McKinnon, J. J., Christensen, D. A., and Christensen, C. R. 2004. Applications of synchrotron technology (SR_FTIR) to feed analysis and utilization: A novel approach. Proceeding of the 25th Western Nutrition Conference - Nutrient Requirement and Ingredient Evaluation in 21st Century. Saskatoon, SK, Canada, Sept 28-30, 2004. pp. 98-112.

Yu, P., McKinnon, J. J., Newkirk, R. W., Christensen, C. R., and Christensen, D. A. 2004. Ultrastructural-chemical makeup of canola seed tissues explored with synchrotron reflection FTIR microspectroscopy: A preliminary study. J. Anim.Sci. 82(Suppl.1)/J. Dairy Sci. 87(Suppl. 1)/Poult. Sci. 83(Suppl.1):329.

Yu, P., Van Kessel, A. G., Drew, M., McKinnon, J.J., Christensen, C., and Christensen, D. A. 2003. Investigation of chemical composition in basement membrane of villi epithelium in gastrointestinal tract using synchrotron infrared microspectroscopy: Conventional vs. germ free animal. The 39th International Union of Pure and Applied Chemistry (IUPAC) Congress and 86th Conference of the Canadian Society for Chemistry, Aug 10-15, 2003. Ottawa, ON, Canada. Abstract CE-SP-OR.